

UNCLASSIFIED

AD NUMBER: ADB000132

LIMITATION CHANGES

TO:

Approved for public release; distribution is unlimited.

FROM:

Distribution authorized to US Government Agencies only; Test and Evaluation; 1 Apr 1974. Other requests shall be referred to Air Force Flight Dynamics Laboratory, Wright-Patterson AFB, OH 45433.

AUTHORITY

AFFDL ltr dtd 29 Dec 1978

THIS REPORT HAS BEEN DELIMITED
AND CLEARED FOR PUBLIC RELEASE
UNDER DOD DIRECTIVE 5200.20 AND
NO RESTRICTIONS ARE IMPOSED UPON
ITS USE AND DISCLOSURE.

DISTRIBUTION STATEMENT A

APPROVED FOR PUBLIC RELEASE
DISTRIBUTION UNLIMITED.

✓
AFFDL-TR-74-64

AD B 0 0 0 1 3 2

LABORATORY TESTS OF AN AIR CUSHION RECOVERY SYSTEM FOR THE JINDIVIK AIRCRAFT

Interim Report for Period February 1973 - November 1973

APRIL 1974



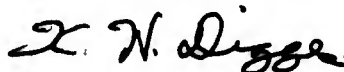
Distribution limited to U.S. Government agencies only; test and evaluation; statement applied April 1974. Other requests for this document must be referred to AF Flight Dynamics Laboratory, (FEM), Wright-Patterson AFB, Ohio 45433.

AIR FORCE FLIGHT DYNAMICS LABORATORY
AIR FORCE SYSTEMS COMMAND
WRIGHT-PATTERSON AIR FORCE BASE, OHIO 45433

NOTICES

When Government drawings, specifications, or other data are used for any purpose other than in connection with a definitely related Government procurement operation, the United States Government thereby incurs no responsibility nor any obligation whatsoever; and the fact that the Government may have formulated, furnished, or in any way supplied the said drawings, specifications, or other data, is not to be regarded by implication or otherwise as in any manner licensing the holder or any other person or corporation, or conveying any rights or permission to manufacture, use, or sell any patented invention that may in any way be related thereto.

This technical report has been reviewed and is approved.



KENNERLY H. DIGGES
Chief, Mechanical Branch
Vehicle Equipment Division

Copies of this report should not be returned to the Air Force Flight Dynamics Laboratory, FEM, unless return is required by security considerations, contractual obligations, or notice on a specific document.

UNCLASSIFIED

SECURITY CLASSIFICATION OF THIS PAGE (When Data Entered)

| REPORT DOCUMENTATION PAGE | | READ INSTRUCTIONS BEFORE COMPLETING FORM |
|--|-----------------------|--|
| 1. REPORT NUMBER AFFDL-TR-74-64 | 2. GOVT ACCESSION NO. | 3. RECIPIENT'S CATALOG NUMBER |
| 4. TITLE (and Subtitle) LABORATORY TESTS OF AN AIR CUSHION RECOVERY SYSTEM FOR THE JINDIVIK AIRCRAFT | | 5. TYPE OF REPORT & PERIOD COVERED INTERIM (FEB 73-NOV 73) |
| | | 6. PERFORMING ORG. REPORT NUMBER |
| 7. AUTHOR(s) JOHN C. VAUGHAN, III JAMES T. STEIGER DAVID J. POOL SHADE CAMPBELL | | 8. CONTRACT OR GRANT NUMBER(s) |
| 9. PERFORMING ORGANIZATION NAME AND ADDRESS AFFDL (FEM) WRIGHT-PATTERSON AFB, OHIO 45433 | | 10. PROGRAM ELEMENT, PROJECT, TASK AREA & WORK UNIT NUMBERS 62201F-1369-02-02 |
| 11. CONTROLLING OFFICE NAME AND ADDRESS AFFDL (FEM) WRIGHT-PATTERSON AFB, OHIO 45433 | | 12. REPORT DATE APRIL 1974 |
| | | 13. NUMBER OF PAGES 88 |
| 14. MONITORING AGENCY NAME & ADDRESS (if different from Controlling Office) | | 15. SECURITY CLASS. (of this report) UNCLASSIFIED |
| | | 15a. DECLASSIFICATION/DOWNGRADING SCHEDULE |
| 16. DISTRIBUTION STATEMENT (of this Report) Distribution limited to U.S. Government agencies only; test and evaluation; statement applied April 1974. Other requests for this document must be referred to AF Flight Dynamics Laboratory, (FEM), Wright-Patterson AFB, Ohio 45433. | | |
| 17. DISTRIBUTION STATEMENT (of the abstract entered in Block 20, if different from Report) APPROVED FOR PUBLIC RELEASE; DISTRIBUTION UNLIMITED | | |
| 18. SUPPLEMENTARY NOTES | | |
| 19. KEY WORDS (Continue on reverse side if necessary and identify by block number) AIR CUSHION LANDING SYSTEM (ACLS), DRONE RECOVERY, AIR CUSHION, AIR CUSHION RECOVERY SYSTEM (ACRS), REMOTELY PILOTED VEHICLE (RPV) RECOVERY. | | |
| 20. ABSTRACT (Continue on reverse side if necessary and identify by block number) Full-scale static tests and vertical drop tests were made with an air cushion recovery system (ACRS) installed on the Australian Jindivik drone. The actual aircraft fuselage and wing were used, while the jet engine and other equipment were simulated with inert weights. These laboratory tests were exploratory and the results were used to determine a final design. The air supply system components were varied to determine their effect on hover conditions, brake drag, three static and dynamic spring coefficients, three damping ratios and frequencies, and the vertical energy absorption. Twelve configurations were tested using combinations of these components: ejector, tip turbine fan, trunk pressure relief valve, and wing tip roll thrusters. The roll stiffness decreased from 70 down to 36 ft-lb/degree as cushion flow was added. The dynamic heave stiffness was 40% higher than the static heave stiffness. The damping ratio was 0.25 in heave, 0.065 in roll, and only 0.046 in pitch. The trunk coefficient of friction decreased from 0.6 (no air flow) to 0.4 (1 lb m/sec) and then to 0.15 (6 lb m/sec) due to an air lubricity effect. The recovery system had a 50% stroke efficiency. The ACRS trunk assembly weighed 55 lbs. A complete ACRS would weigh an estimated 87 lbs or 2.4% of the takeoff gross weight. | | |

SUMMARY

Full-scale static tests and vertical drop tests were made with an air cushion recovery system (ACRS) installed on the Australian Jindivik drone. The actual aircraft fuselage and wing were used, while the jet engine and other equipment were simulated with inert weights. These laboratory tests were exploratory and the results were used to determine a final design.

The air supply system components were varied to determine their effect on hover conditions, brake drag, three static and dynamic spring coefficients, three damping ratios and frequencies, and the vertical energy absorption. Twelve configurations were tested using combinations of these components: ejector, tip turbine fan, trunk pressure relief valve, and wing tip roll thrusters.

The roll stiffness decreased from 70 down to 36 ft-lb/degree as cushion flow was added. The dynamic heave stiffness was 40% higher than the static heave stiffness. The damping ratio was 0.25 in heave, 0.065 in roll, and only 0.046 in pitch. The trunk coefficient of friction decreased from 0.6 (no air flow) to 0.4 (1 lb m/sec) and then to 0.15 (6 lb m/sec) due to an air lubricity effect.

The recovery system had a 50% stroke efficiency. The ACRS trunk assembly weighed 55 lbs. A complete ACRS would weigh an estimated 87 lbs or 2.4% of the takeoff gross weight.

PREFACE

This exploratory development work was performed under Program 1369, Task 02, Work Unit 02, Air Cushion Landing System Technology. The tests were conducted by USAF personnel at Wright-Patterson AFB between February and November 1973. This effort is part of a program to develop and demonstrate air cushion systems for the takeoff and recovery of jet-powered drones. The Mechanical Branch of the Vehicle Equipment Division of the AF Flight Dynamics Laboratory has primary responsibility for this program.

The trunk assembly was made by B.F. Goodrich, the air supply system ejectors and tip fans were made by Tech Development, and the test tower and pressure relief valve were made by Centro Corp. The preliminary design of the test trunk was made by Sandaire under USAF Contract No. F33615-72-C-1769. This preliminary trunk design was modified by B.F. Goodrich and AFFDL for installation on the Jindivik fuselage. The Australian Government Aircraft Factories provided the drone shell for these tests. Lockheed Aircraft Company loaned the Tech Development ejectors. The Air Force Institute of Technology provided test data for the ejector and tip turbine fan at various back pressure conditions. Chandler Evans, Inc. designed and fabricated the wing tip roll control thrusters.

TABLE OF CONTENTS

| | PAGE |
|--|------|
| SUMMARY | 1 |
| PREFACE | 2 |
| LIST OF ILLUSTRATIONS | 4 |
| LIST OF TABLES | 5 |
| 1. INTRODUCTION | 6 |
| A. Background | 6 |
| B. Objectives | 6 |
| 2. APPARATUS | 7 |
| A. Jindivik Aircraft | 7 |
| B. Air Cushion Recovery System | 7 |
| 1. Design | 7 |
| 2. Trunk Assembly | 10 |
| 3. Air Supply System | 16 |
| 4. Relief Valve | 16 |
| 5. Roll Control Thrusters | 20 |
| 6. Air Cushion Configuration | 20 |
| C. Test Equipment | 25 |
| 1. Test Tower | 25 |
| 2. Primary Air Supply Source | 27 |
| 3. Instrumentation and Data Recording | 27 |
| 3. TEST PROGRAM | 31 |
| A. Text Matrix | 31 |
| B. Types of Tests | 31 |
| 4. TEST RESULTS | 40 |
| A. Static Hover | 40 |
| B. Static Heave Stiffness | 41 |
| C. Static Pitch Stiffness | 49 |
| D. Static Roll Stiffness | 53 |
| E. Pull Tests | 55 |
| F. Roll Damping | 59 |
| G. Pitch Damping | 59 |
| H. Heave Damping Drop Tests | 61 |
| I. Pitch and Heave Damping Drop Tests | 70 |
| 5. CONCLUSION | 73 |
| 6. RECOMMENDATIONS | 76 |
| 7. REFERENCE MATERIAL | 77 |
| List of References | 77 |
| Appendix A - Test Checklist | 78 |
| Appendix B - Sample Calculation for Damping Data | 80 |
| List of Symbols and Abbreviations | 81 |
| Subscripts | 83 |
| Distribution List | 84 |

LIST OF ILLUSTRATIONS

| Figure No. | Legend | Page |
|------------|---|------|
| 1. | Test Aircraft Weight Distribution | 8 |
| 2. | 1/10 Scale Jindivik (equipped with an Air Cushion System and Launch Supports) | 11 |
| 3. | ACRS Trunk Assembly Drawing | 12 |
| 4. | Brake Tread and Nozzles | 13 |
| 5. | Side Trunk 2-D Shape Versus P_c/P_t | 14 |
| 6. | Location of Side Trunk Ground Tangent | 15 |
| 7. | Pressure-Flow Characteristics of Three Different Air Supply Systems | 17 |
| 8. | Tip Turbine Fan and Ejector | 18 |
| 9. | Trunk Pressure Relief Valve | 19 |
| 10. | Relief Valve Vent Area Versus Stroke | 21 |
| 11. | Wing Tip Roll Control Thruster | 22 |
| 12. | Roll Thruster Vertical Thrust | 23 |
| 13. | Air Cushion Components | 24 |
| 14. | Test Tower and ACRS Equipped Jindivik | 26 |
| 15. | Primary Air Supply System | 28 |
| 16. | Data Recording Equipment | 29 |
| 17. | Instrument Locations On Test Aircraft | 30 |
| 18. | Longitudinal Location of Trunk's Center of Force, x_t | 34 |
| 19. | Side Location of Trunk's Center of Force, y_t | 36 |
| 20. | Static Heave Stiffness | 42 |
| 21. | Trunk Pressure Increase With Load | 44 |
| 22. | Cushion Pressure Increase With Load | 45 |
| 23. | A_t Increase With Stroke | 46 |
| 24. | Cushion and Trunk Heave Stiffness | 48 |
| 25. | Graphical Estimate of IGE Heights | 50 |
| 26. | Static Pitch Stiffness | 51 |
| 27. | x_t Shift With Pitch Angle | 52 |
| 28. | Roll Stiffness | 54 |
| 29. | Trunk Drag Versus Cushion Pressure | 56 |
| 30. | Trunk Drag Versus Cushion Flow | 57 |
| 31. | Roll Damping Improvement Using Thrusters | 60 |
| 32. | Peak Load-Stroke Conditions Versus Sink Speed | 64 |
| 33. | Pressure Relief Valve Response | 66 |
| 34. | Load-Stroke Curve | 67 |
| 35. | Drop Test Visicorder Record, 0.40 ips | 68 |
| 36. | Drop Test Visicorder Record, 10 ips | 69 |
| 37. | Combined Pitch and Heave Damping | 72 |
| 38. | Balance of Moments at Impact | 72 |

LIST OF TABLES

| Table No. | Heading | Page |
|-----------|---|------|
| 1. | Comparison of Jindivik ACRS with Previous ACLS Designs | 9 |
| 2. | Twelve Air Cushion Configurations | 25 |
| 3. | Instrumentation Channels | 27 |
| 4. | Test Matrix | 32 |
| 5. | Summary of Static Hover Conditions | 40 |
| 6. | Static Heave Stiffness Data | 43 |
| 7. | Pitch Stiffness Data (Test 72, Vent Open) | 53 |
| 8. | Pull Test Data | 58 |
| 9. | Peak Acceleration at CG During Drop Tests (max. g_{CG} reading) | 61 |
| 10. | Summary of Heave Damping Drop Test Results (Load - Stroke Data) | 63 |
| 11. | Heave Damping Data | 70 |
| 12. | Summary of Test Results | 75 |

1. INTRODUCTION

1.A. Background

The motivation behind this work is the belief that air cushion systems will prove to be the best way to takeoff and recover large jet-powered drones. This belief is based on several in-house and contracted studies^{1, 2, 3, 4, 5}. Small drones can be simply launched using rocket assist and simply recovered using parachutes. As the drone size increases to a weight comparable to small manned aircraft however, the rockets and parachutes become more expensive and less reliable than conventional aircraft landing systems, and also create a more burdensome field logistics problem. Alternative solutions using launch aircraft or recovery helicopters are considered much too expensive for large numbers of drone flights. Although self-powered takeoff and remotely controlled landings with wheeled gear on paved runways appear attractive for certain fixed or small operations, the requirement for a paved drone runway is not desirable for many anticipated tactical operations.

This work is part of a program to apply air cushion technology to the problem of drone takeoff and recovery, and to develop and demonstrate the technology on a currently available aircraft – the Australian Jindivik drone⁶. The Jindivik program has 3 specific objectives to develop: (1) the technology base necessary to adapt air cushion to jet-powered drones, (2) an air cushion recovery system (ACRS) and, (3) a complete air cushion system for takeoff, recovery, taxi, and parking. The program plan consists of 30 separate efforts. The laboratory tests described in this report are one of these efforts and are part of the accomplishment of the specific objective to develop an ACRS.

The basic ACRS design originated from a Sandaire study⁷. Although the shape and dimensions of the test trunk were approximately the same as the Sandaire design, several design improvements and new concepts were introduced by B.F. Goodrich and AFFDL. Three basic air supply system approaches were tested (ejector, tip fan, and direct bleed plus relief valve) in different trunk and cushion flow combinations. A unique roll control thruster was also tested to simply obtain some baseline data. The full scale system was tested in a typical landing weight configuration to determine the system response to various input conditions.

1.B. Objectives

The objective of these tests was to gather full scale performance data on a basic ACRS design with several air supply configurations. The test results would then be used to select a final ACRS design for demonstration on the Jindivik aircraft. This objective was accomplished, and the final design components are being fabricated in 1974.

-
1. "Recovery of Unmanned Aircraft, ASD Technology Needs", TN-ASD-4-72-526, 19 Dec 1972.
 2. Digges, K. H. and Vaughan, J. C., "Drone Launch and Recovery Using Air Cushion Systems", AFFDL/FEM Briefing Brochure, April 1973.
 3. Ryken, J. M., "A Study of an Air Cushion Landing System for Recovery of Unmanned Aircraft", AFFDL-TR-72-87, July 1972. (AD 758789)
 4. Sinfield, L. S., "RPV ACLS Applications Study", AFSC Contract F33615-73-C-4140, Teledyne Ryan Aeronautical TR ASD/XR 73-22, 15 Dec 73. Secret.
 5. Gardner, L. H. and Milns, P., "Air Cushion Landing System Applications Study", AFSC Contract F33615-73-C-4169, Boeing TR ASD/XR 73-21, Jan 74. Secret
 6. Vaughan, J. C., "The Jindivik Program to Develop Air Cushion Technology for Drones – A progress report". Paper presented at the 16th meeting of TTCP Sub-Group H-TP-1, Targets and Drones, 24-25 Sep 73, U.S. Army Missile Command, Huntsville, Ala.
 7. McCudden, H. B., et al, "Conceptual Design of an Air Cushion Landing System for an Unmanned Aircraft", AFFDL-TR-72-155, 3 January 1973.

2. APPARATUS

2.A. Jindivik Aircraft

The Australian Jindivik drone aircraft was selected from the preliminary designs^{3, 7} as being the best aircraft on which to demonstrate air cushion capabilities for future remotely piloted vehicles (RPVs). The Australian Government Aircraft Factories loaned the AFFDL a Jindivik shell for use in these initial tests.

Modifications were necessary to make the aircraft shell closely resemble the weight and inertia of a fully-equipped aircraft in the landing configuration (Figure 1). The 66 lb forward fuselage hood was removed for all tests in order to open up a convenient location to mount test equipment. The 125 lb landing skid and fairing were also removed. This left a bare airframe weighing 915 lbs. This included the large Mk 7 wing tips pods and 40 inch wing tip extension. The ACRS test equipment weighed approximately 122 lbs including trunk assembly, on board air supply components, structural modifications, ducting, and on board instrumentation. The drop cradle weighed 30 lbs. Finally, weights were added at various positions to simulate the proper landing weight and inertia. A 653 lb metal block was installed in the aft fuselage to simulate the engine, and 550 lbs of ballast were installed in the forward fuselage to simulate the internal equipment and the 66 lb hood. Lead shot bags weighing 200 lbs total were loaded near the center of gravity to simulate the fuel that is normally in the fuselage tank at landing. The total test aircraft weighed 2470 lbs at the start of the tests.

A good description of the capabilities and operation of the basic unmodified Jindivik drone aircraft can be found in References 7, 8, and 9. Reference 8 shows that Jindivik is a cost effective target in comparison to the BQM-34A target. Reference 9 is a study of a Bell Aerospace Co. ACRS design to give the Jindivik a soft field landing capability.

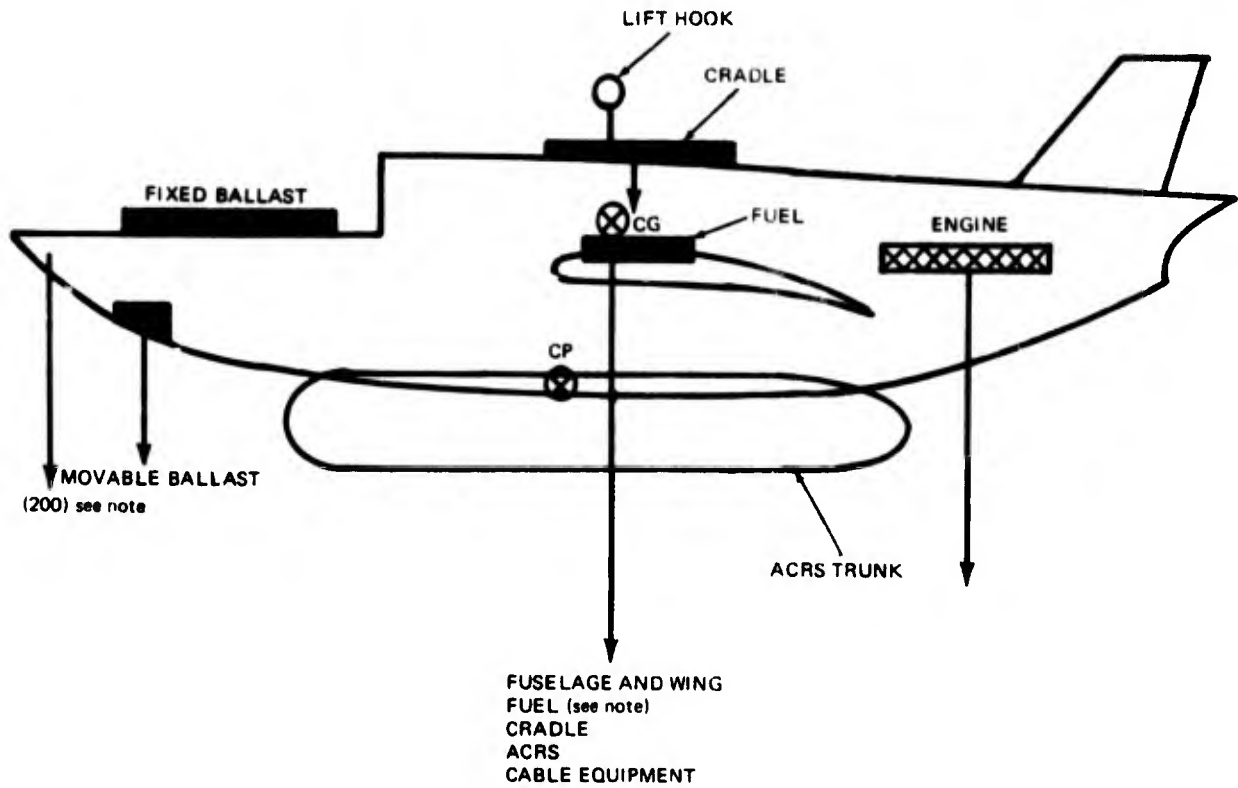
2.B. Air Cushion Recovery System

2.B.1. DESIGN. The air cushion design selected for these initial tests was an AFFDL and B.F. Goodrich modification of the Sandaire design⁷. The main characteristics of this Jindivik ACRS design are shown in Table 1 along with comparisons with the only two ACLS aircraft flown to date - the LA-4 and the CC-115 (short trunk configuration).

The Jindivik ACRS is designed for the recovery of a high speed, high density jet aircraft; while the LA-4 and CC-115 ACLS designs are for takeoff and landing of low speed, low density, propeller aircraft. There are several inherent differences between these two air cushion systems. These differences will not change significantly as the final Jindivik design is developed. There are four features that are noticeably different: (1) trunk and cushion pressures, (2) cushion volume, (3) flight and landing speed, and (4) total airflow used for landing.

The In-Ground Effect (IGE) trunk pressure of the Jindivik is almost twice as large as the scaled trunk pressure of previous ACLS designs. This pressure is still less than 2 psig, and therefore will not create any known problems. Operations over water at below hump speed, however, do not appear practical at these pressures and sizes. Although the cushion pressure is usually half the trunk pressure for ACLS designs, the possibility of landing with no cushion pressure will be examined during these ACRS tests.

8. Moten, J. M., "Cost Effectiveness Study of the Jindivik MK.303A Target", prepared for CINC PAC FLT, 4 Aug 1967.
9. Ryken, J. M., "Design of an Air Cushion Recovery System for the Jindivik Drone Aircraft", AFFDL-TR-74-38, March 1974.



WEIGHT SUMMARY

| | |
|-------------|--|
| 915 | FUSELAGE AND WING (HOOD AND SKID REMOVED) |
| 653 | ENGINE |
| 410 | FIXED BALLAST FOR FORWARD EQUIPMENT AND HOOD |
| 140 | MOVABLE BALLAST TO BALANCE AIRCRAFT AT LIFT HOOK |
| 200 | LEAD SHOT BAGS SIMULATING FUEL LEFT AT LANDING |
| 30 | DROP CRADLE |
| 122 | AIR CUSHION TEST EQUIPMENT (ACRS) |
| <u>2470</u> | LBS TOTAL WEIGHT (AT START OF TESTS) |
| 30 | CABLE EQUIPMENT ADDED AFTER TEST 68 |
| <u>2500</u> | LBS (AFTER TEST 68) |

NOTE: FOR THE HEAVE DAMPING DROP TESTS, 200 LBS WAS MOVED 8.8 FEET FORWARD FROM THE WING TO THE NOSE TO SHIFT THE CG TO APPROXIMATELY ABOVE THE TRUNK CP (0.5 INCHES AFT OF CP).

Figure 1. Test Aircraft Weight Distribution

Table 1. Comparison of Jindivik ACRS with Previous ACLS Designs.

| Quantity | Units | Symbol | Jindivik ACRS | LA-4 | Scale Factor | CC-115 (Short Trunk) $\lambda = 0.41$ Scale |
|---------------------------|----------------------|-----------|---------------|-------|-----------------|---|
| Aircraft Landing Weight | lb _m | W_a | 2470 | 2110 | λ^3 | 2700 |
| Aircraft Wing Span | ft | — | 20.75 | 38 | λ | 39.4 |
| Max. True Airspeed | kts. | — | 540 | 110 | $\lambda^{0.5}$ | 157 |
| Touchdown Speed | mph | — | 150 | 60 | $\lambda^{0.5}$ | 52 |
| Aircraft Pitch Inertia | slug ft ² | I_{yy} | 1810 | | λ^5 | 3260 |
| Aircraft Roll Inertia | slug ft ² | I_{xx} | 1190 | | λ^5 | 2600 |
| Aircraft Yaw Inertia | slug ft ² | I_{zz} | 2840 | | λ^5 | 4680 |
| Ground Tangent length/dia | — | — | 3.1 | 3.1 | 1 | 2.9 |
| Cushion Area | in ² | A_c | 2346 | 6000 | λ^2 | 5570 |
| Cushion Volume | ft ³ | V_c | 3.1 | | λ^3 | 16.5 |
| Cushion Perimeter | ft | — | 21.2 | 32. | λ | 26. |
| Hover Cushion Pressure | psig | P_c | 0. | 0.416 | λ | 0.486 |
| Hover Trunk Pressure | psig | P_t | 1.71 | 0.972 | λ | 0.972 |
| Pressure Ratio | — | P_c/P_t | 0.0 | 0.43 | 1 | 0.5 |
| Trunk Volume | ft ³ | V_t | 39.1 | | λ^3 | 75.2 |
| Max. Brake Area | in ² | A_b | 2220 | 690 | λ^2 | 252 |
| Landing Air Flow | lb m/sec | \dot{m} | 1.4 | 14. | $\lambda^{2.5}$ | 16. |
| Air Horse Power | hp | — | 8.5 | 65 | $\lambda^{3.5}$ | 46.8 |
| Hover Structural Height | in | hcg | 12. | | λ | 16.6 |
| CP Forward of CG | in | x_{cp} | 9. | | λ | 12.3 |

The cushion volume of the Jindivik is only one-fifth that of a CC-115 design scaled down to the same weight. This may result in poorer rough field takeoff performance for an air cushion Jindivik but the overall effect is not clearly known at this time. For landing, however, the cushion pressure can be zero and therefore the small cushion volume will have no effect.

The landing and flight speeds of the Jindivik are much higher than the previous ACLS aircraft. The landing speed of the Jindivik is three times that of the LA-4 and scaled CC-115. This creates a more difficult braking problem and has resulted in a new brake system design which better distributes the energy. The much higher flight speed (Mach 0.86) is 5 times faster than the LA-4 and presents a more difficult design problem with respect to stowage and drag.

The Jindivik ACRS design will use less than one-tenth the air flow during landing and slide out than that used by the previous ACLS designs. One goal of the Jindivik program is to determine what minimum amounts of air flow are required during recovery. Basic research has only been directed at the takeoff flow requirements^{10, 11}.

10. Rogers, J. R., "Two-Dimensional Air Cushion Landing System Peripheral Jet Configuration Study", AFFDL-TR-73-5, November 1973.

11. Carreras, E. M., "Static Performance of a Cushion Fed Air Cushion Landing System", AFIT Thesis, GAW/AE/74-1, Dec 73 (AFFDL-TM-74-56-FEM).

The scaling factors used for air cushion systems have not been completely satisfactory. Some differences have been noted between the performance of the 1/4 scale and 1/10 scale models of the CC-115^{12, 13}. Most of these differences are believed due to the inability to easily scale the air supply system. For this reason it is fortunate that full-scale testing of the Jindivik system can be economically done during the design phase. Scale model testing has already proven valuable however, even in a 1/10 Jindivik model weighing only 3 lbs¹⁴ (Figure 2).

2.B.2. TRUNK ASSEMBLY. The trunk assembly design was a modification of the Sandaire design⁷. AFFDL added the feature of an integral pressure vessel trunk. AFFDL added ejectors to the design and changed the trunk dimensions slightly to remove the "hat section". AFFDL also added the capability to separately control the cushion airflow – which enables the ACTS/ACRS design concept to takeoff and land with different airflow rates rather than the same flow rate inherent with the ACLS design. B.F. Goodrich developed the trunk fabrication methods including trunk and brake material selection, stitching, layup, and bonding. A lightweight trunk attachment method was also devised by B.F. Goodrich and pressure zippers were installed along both sides of the trunk to aid in drilling the nozzles and in inspecting, repairing, or modifying the design. Features of the trunk assembly are shown in Figures 3 and 4. The change in side section shape with P_c/P_t ration is shown in Figure 5 and 5, as calculated by a two-dimensional method¹⁵

The trunk was fabricated from neoprene coated nylon fabric (10 oz/yd² coated weight). The girt was made from the same type material, but a heavier weight (22 oz/yd²). The brake tread was made from tire tread rubber that was 3/8 inches thick. The entire trunk assembly, including attachment hardware (rivnuts and bead clamp) and ejector connections, weighed approximately 55 lbs – including the brake tread which weighed 35 lbs.

The trunk nozzles were drilled through the brake tread at a 45° inward injection angle. The inward angle was used because two-dimensional trunk flow studies^{10, 11} show that inward injection is clearly better for hover performance and therefore possibly could be better for all-around performance.

The cushion area of the trunk was measured during a static hover test with airflow only into the trunk. The outer tread line encircled an area of 4565 square inches on the floor. The inner tread line was 9 inches inboard and enclosed an area of 2346 square inches. This smaller area was found to be the effective area over which the cushion pressure acted. This cushion area roughly consisted of a rectangle 70 inches by 26-1/4 inches and two half-circles of 12-inch radius (aft) and 13-3/8 inch radius (forward). For a brake tread width of 9 inches the maximum brake footprint is about 2220 square inch.

The trunk was mounted on the fuselage such that the trunk's center of force (CF) and cushion's center of pressure (CP) were at FS 121.25. The present skid CP is approximately at FS 119 extended (supporting no weight) and FS 127 static. Other ACRS designs for Jindivik have located the cushion CP at FS 126.25 and FS 120.27^{7, 9}. The center of gravity (CG) of the unmodified aircraft can vary between FS 127.9 and FS 130.8 (16 and 22% MAC), depending on fuel weight and configuration⁹. For these static tests, the weights were adjusted to place the CG at FS 130.25 (directly below the top lifting hook). For the heave damping drop tests, the weights were adjusted to place the CG approximately 0.5 inch aft of the cushion CP (see Figure 1).

12. Vaughan, J. C., et al. "Static Drop Tests of a Quarter Scale Model of the CC-115 Aircraft Equipped with an Air Cushion Landing System", AFFDL-TM-72-01-FEM, Sep 1972.

13. Rodrigues, A., "Drop and Static Tests on a Tenth Scale Model of an Air Cushion Landing System (ACLS)", AFFDL-TR-73-46, Sep 1973.

14. Parker, P. M., "Landing Simulation of a 1/10 Scale Jindivik Drone Equipped with an Air Cushion Landing System", AFIT Thesis, GAM/AE/73A-15, Nov 72 (AFFDL-TM-74-58-FEM).

15. Digges, K. H., "Theory of an Air Cushion Landing System for Aircraft", AFFDL-TR-71-50, Jun 1971.

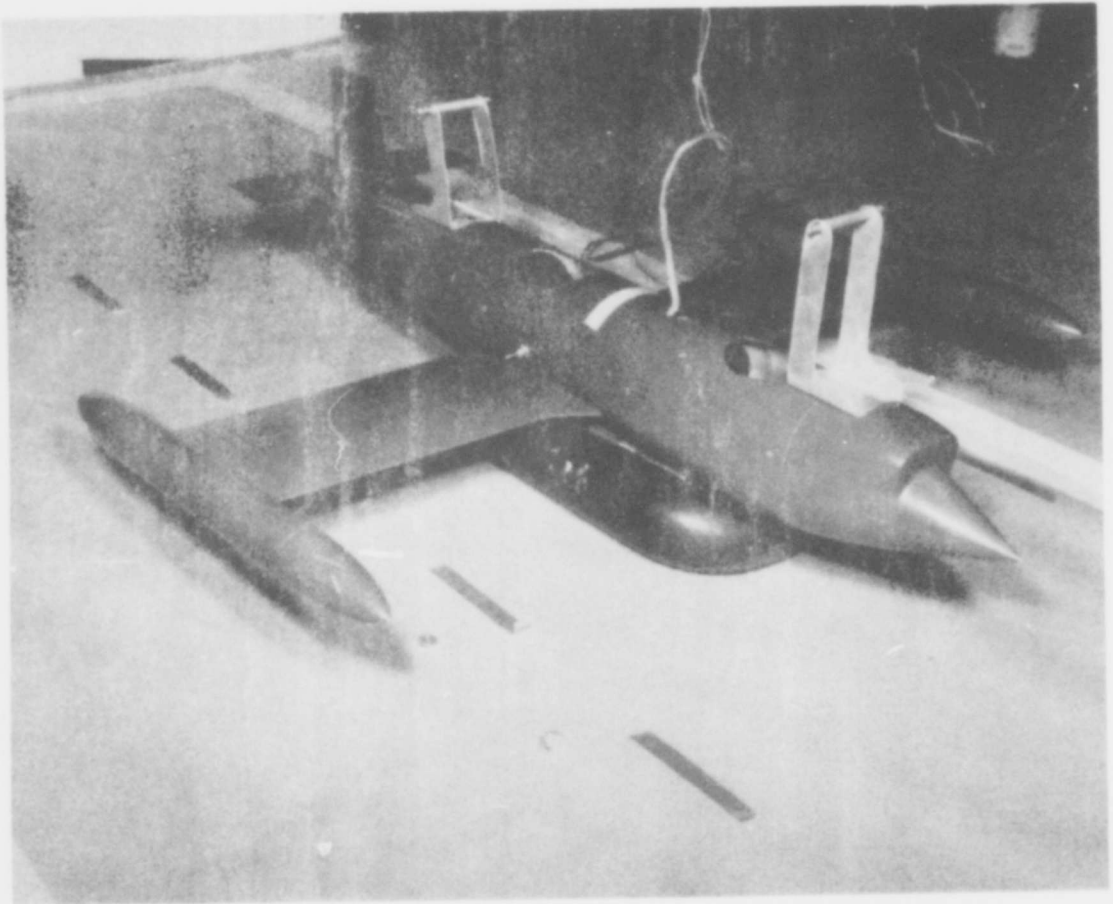


Figure 2. 1/10 Scale Jindivik (equipped with an Air Cushion System and Launch Supports).

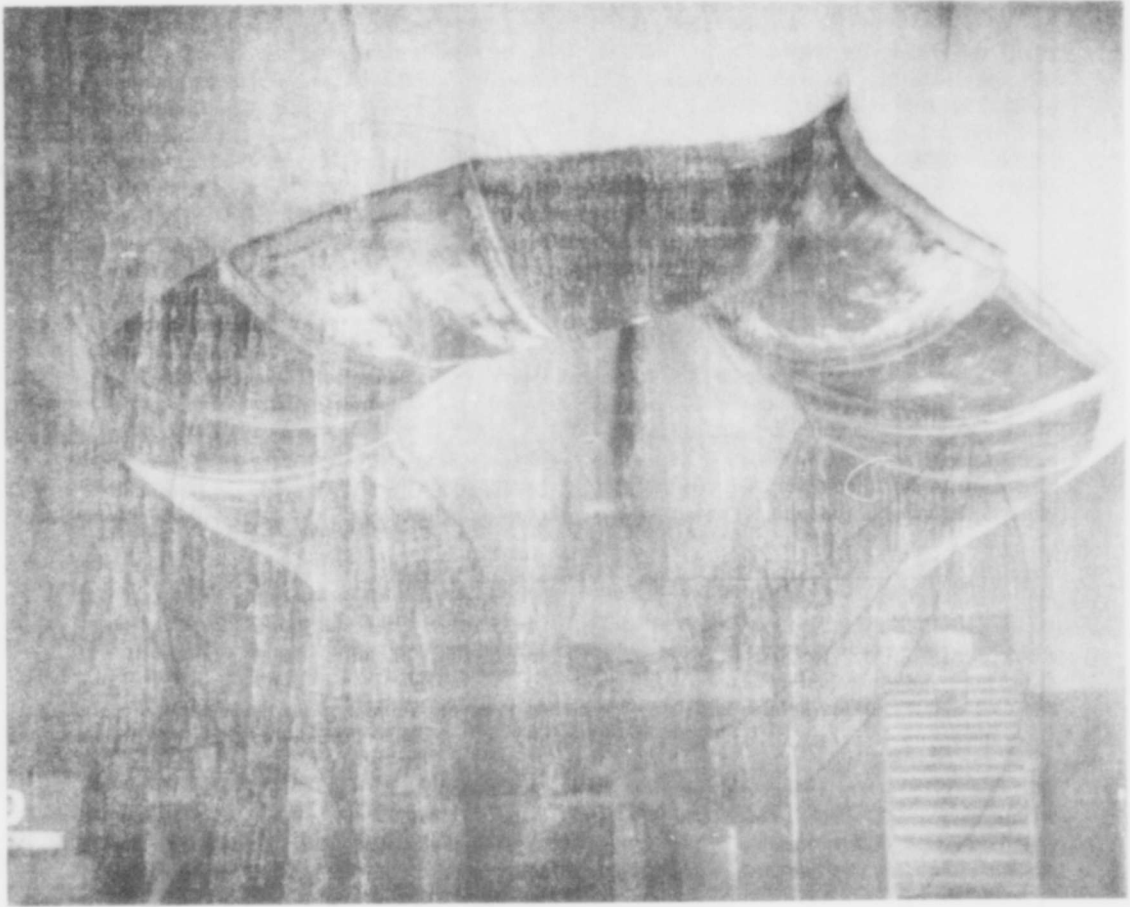


Figure 4. Brake Tread and Nozzles.

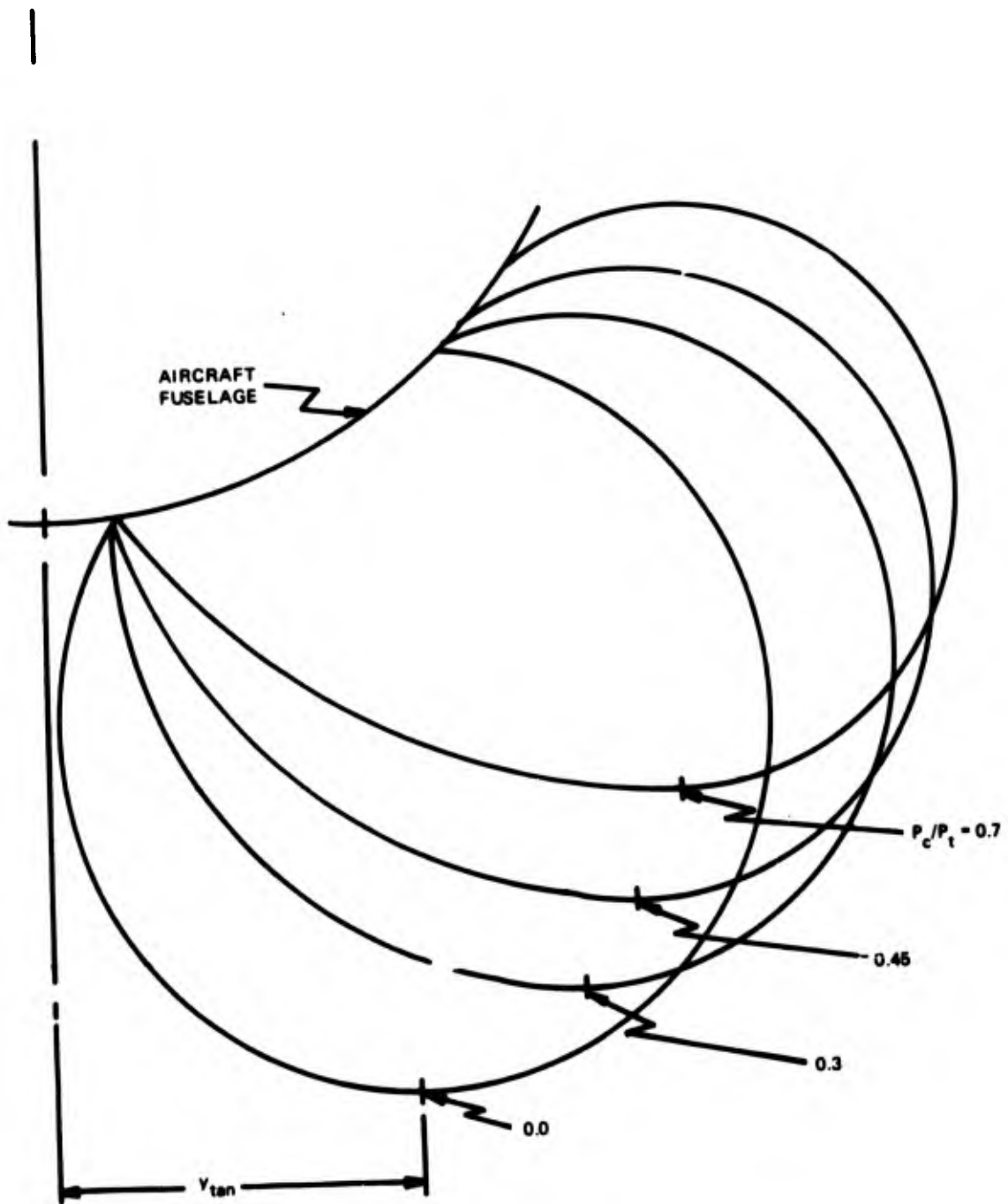


Figure 5. Side Trunk 2-D Shape Versus P_c/P_t

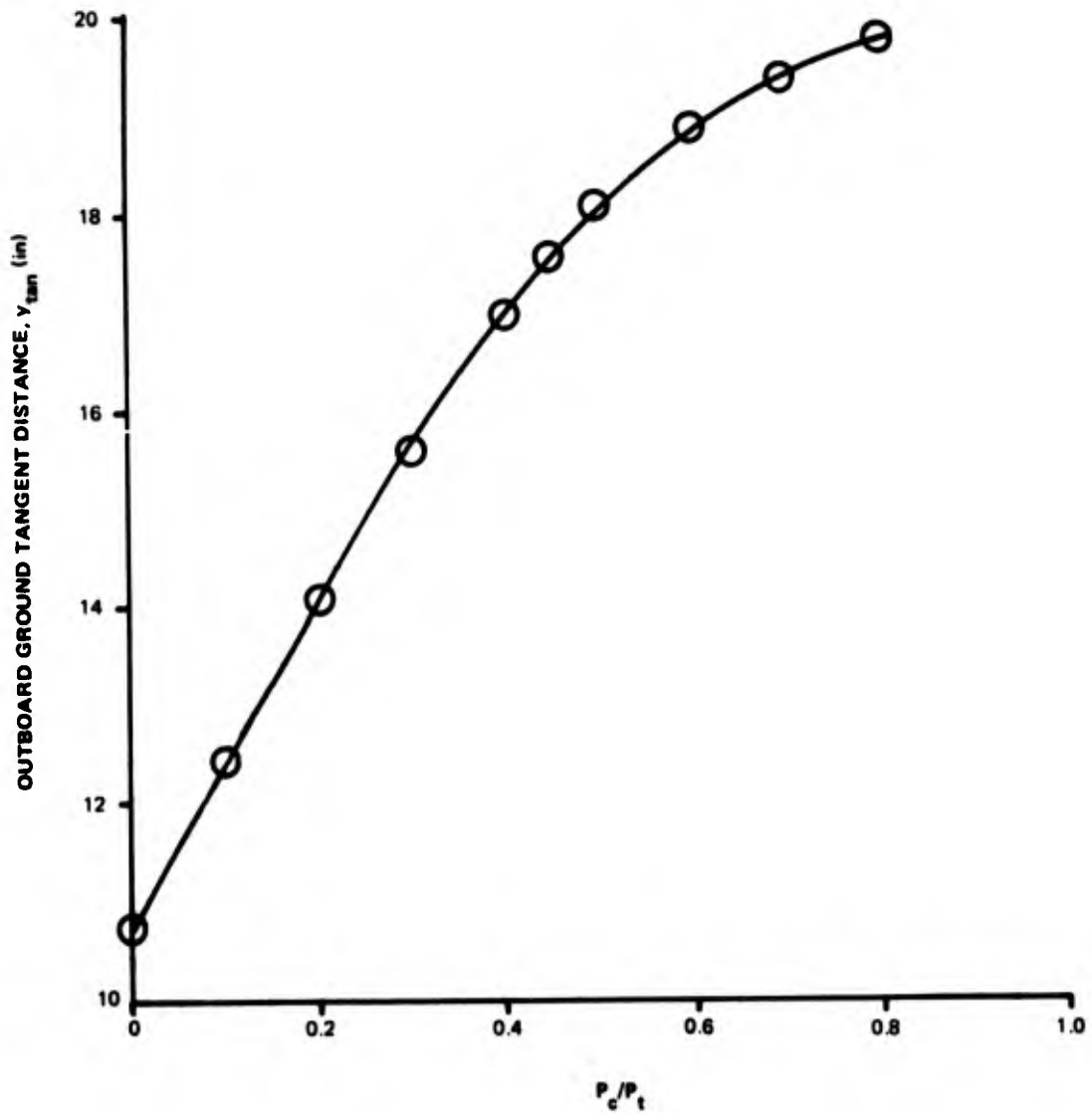


Figure 6. Location of Side Trunk Ground Tangent.

The only trunk damage occurred during the first inflation when the trunk ripped approximately 18 inches along a stitch line in the forward cushion area where the trunk attaches to the girt. The tear was easily repaired by using the heavier girt material in this region of concentrated stitching and load. No other damage occurred to the trunk assembly throughout the test series.

2.B.3. AIR SUPPLY SYSTEM. The preliminary designs^{7,9} indicated that air could best be supplied to the trunk or cushion by using the jet engine compressor bleed air as a prime source. This primary air could be used in three different ways: (1) direct bleed, (2) augmented using an ejector, or (3) augmented using a tip turbine fan. All three of these air supply methods were evaluated during these tests.

Two previous studies had shown what type of augmentation performance could be expected. An analysis has shown that tip fans are much more efficient than ejectors¹⁶. Static component tests have measured the flow versus back pressure for a typical ejector and tip fan¹⁷. A comparison of the flow characteristics of these three types of air supply systems is shown in Figure 7.

The direct bleed system is the simplest system since it only consists of a duct running directly from the on-off valve at the engine bleed port to the trunk. The performance is low however, since the augmentation ratio is 1.0 (no secondary air). Also the pressure relief is very stiff -- thus requiring a separate trunk pressure relief valve to prevent excessive loads during impact. Finally, for aircraft with higher performance jet engines than Jindivik (i.e., higher compressor bleed temperatures and pressures), direct bleed would be unacceptable because the primary air temperatures would be too high for the trunk material.

An ejector is a simple device that can be added to both lower the air temperature entering the trunk and to reduce the bleed air requirements by providing part of the required air flow from secondary air. The ejector can provide augmentation ratios higher than 3, and can possibly eliminate the need for a trunk pressure relief valve.

Tip turbine fans are more complicated and costly devices than ejectors, but they also provide good pressure relief and very high performance or augmentation ratios. High performance is needed for an air cushion takeoff system (ACTS), because a high volume rate of flow is needed. For landing-only systems such as ACRS however, the high performance of a tip fan is not required. A tip fan was evaluated during these tests, however, since a combination ACTS plus ACRS would have a tip fan on board which could provide air to the cushion during recovery (if desired) or for a taxi capability following recovery.

The ejector and tip turbine fan used for these exploratory Jindivik tests are shown in Figure 8.

A 3.5 inch long transition section was used to duct the fan flow into the 21 square inch rectangular cutout in the trunk girt. The flow losses in this duct were not measured, therefore the cushion airflow from the tip fan could only be estimated.

2.B.4. RELIEF VALVE. A trunk pressure relief valve was required when the direct bleed air supply system was used. The relief valve was not essential when the trunk air was supplied from an ejector or fan -- but the effect of the valve plus an ejector or fan was investigated.

The relief valve (Figure 9) was designed and fabricated by Centro Corp. The valve was spring loaded and designed to mount on the fuselage so that it vented the trunk air into the forward fuselage equipment

16. Vaughan, J. C., "Performance of Jet Ejectors", ASD/XR 72-5, 15 Feb 1972. (AD 759671)

17. Kundstadt, E., "Study of Reverse Flow Characteristics of a Tip Fan and an Ejector", AFFDL-TR-73-73, Sep 1973.

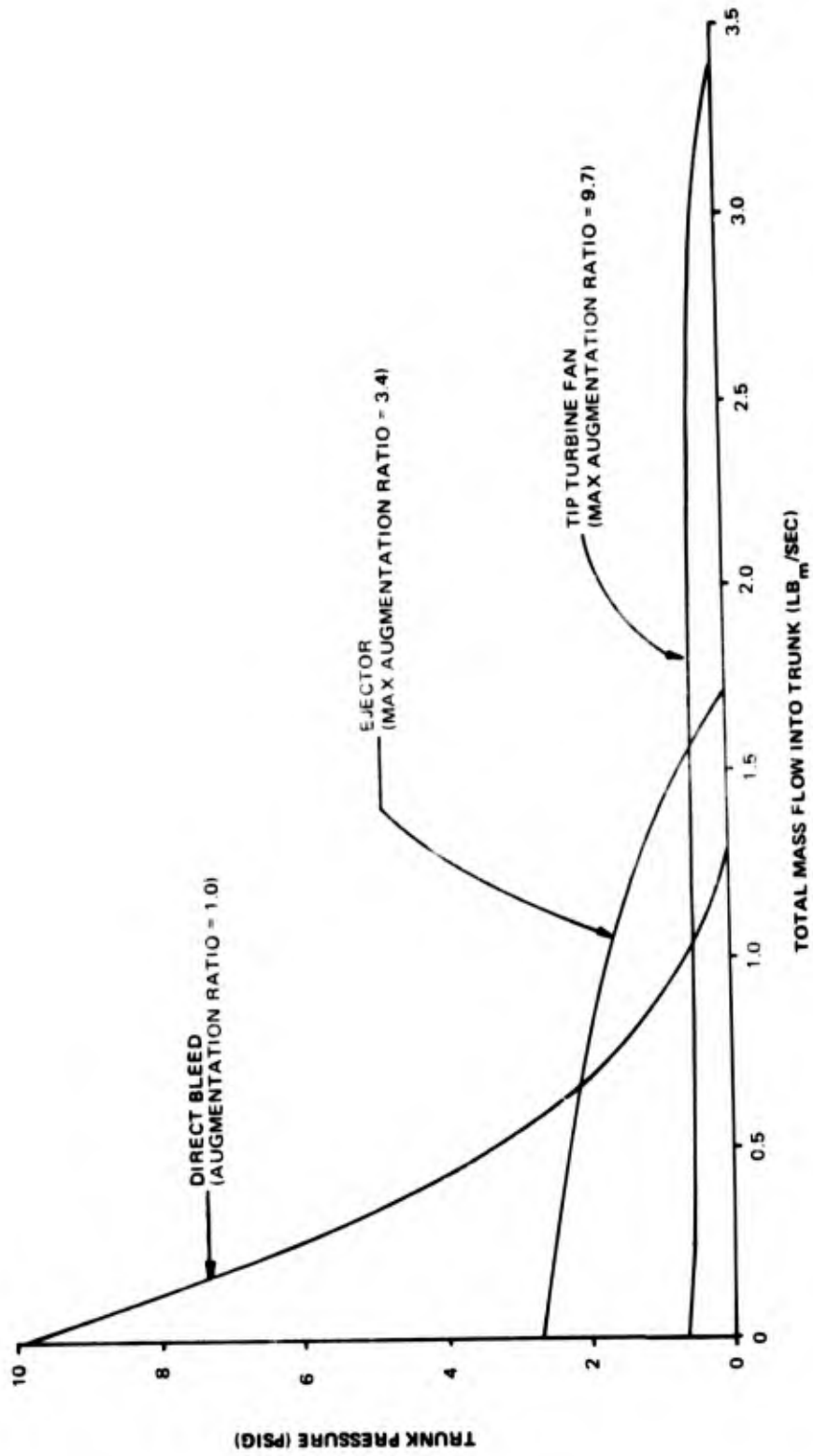


Figure 7. Pressure-Flow Characteristics of Three Different Air Supply Systems.

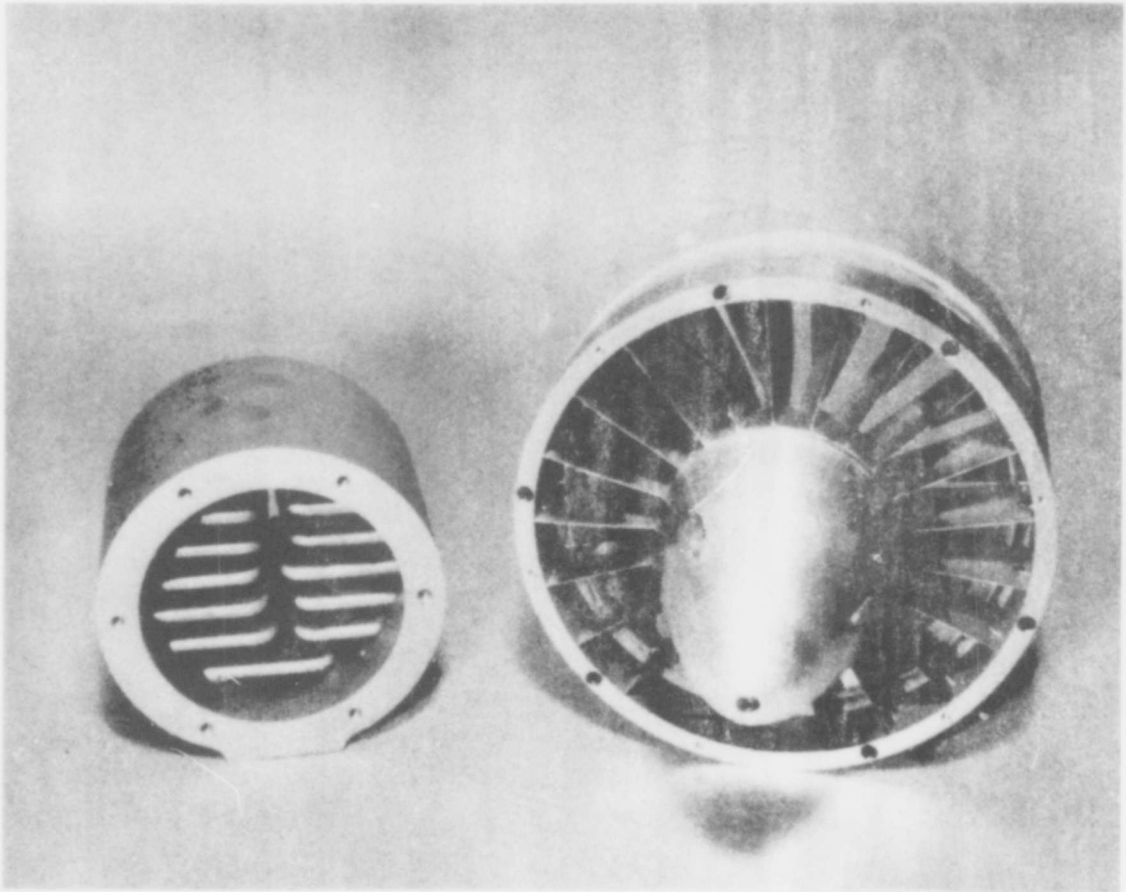


Figure 8. Tip Turbine Fan and Ejector.

SPECIFICATIONS

| | |
|-----------------------------|--|
| Orifice Diameter | 7.24 inches |
| Orifice Clearance Full Open | 2.0 inches |
| Full Open Orifice Area | 45.4 square inches |
| Overall Diameter | 9.25 inches |
| Overall Height | 5.69 inches |
| Weight | 4 pounds |
| Cracking Pressure | 246 psf \pm 15 psf Adjustable |
| Full Open Pressure | 366 psf |
| Construction: | Black Anodized Aluminum Except Steel Spring |

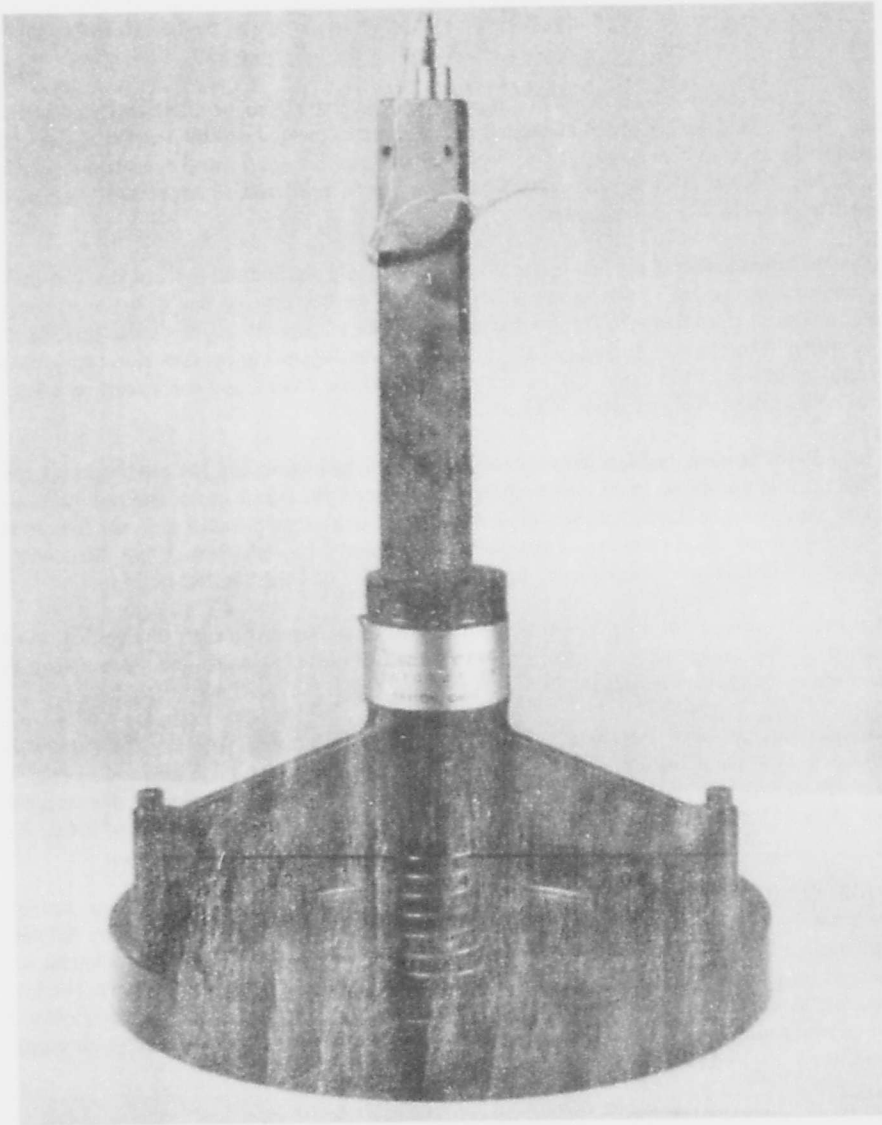


Figure 9. Trunk Pressure Relief Valve.

bay. The orifice plate moves up between the three vertical columns and is guided by its shaft passing through the spider assembly on top. A stop is provided to prevent over-stressing the spring. An "O" ring in the base plate seals the valve when it is closed.

The construction of the valve resulted in an unusual vent area versus valve stroke curve (Figure 10). The plate was placed 0.75 inches inside the housing, and this restricted the flow until the plate moved above the housing. If the orifice plate were mounted on the top of the housing, then the relief area would increase linearly with stroke (area = circumference x stroke).

2.B.5. ROLL CONTROL THRUSTERS. Since the present skid-equipped Jindivik aircraft has no rudder, it is directionally controlled during landing slideout by roll-induced yaw. The present Jindivik does not taxi, and is directionally controlled during take-off by nosewheel steering of the takeoff trolley that it is mounted on.

There are several methods by which an air cushion equipped Jindivik can be directionally controlled during landing, takeoff, and taxi. During landing, the same control method can be used for ACRS as is presently used for the skid. At high speeds, the ailerons provide direct roll control and indirect roll-induced yaw control. At very low speeds at the end of slideout there is no effective roll or yaw control – although roll protection is provided by the wing tip skids.

During an air cushion takeoff run, the ailerons can again supply roll and roll-induced yaw control at high speeds. Some additional roll control and roll-induced yaw control may be useful, however, during three particular modes of operation: (1) the low speed start of the takeoff run, (2) low speed taxi and (3) operations over water. Therefore a wing tip roll control thruster was designed to operate from engine bleed air and was evaluated as part of this exploratory test program. Alternate control approaches such as a direct yaw thruster or differential braking were not evaluated.

These wing tip roll control thrusters were conceived, designed, and fabricated by Chandler Evans, Inc. (Figure 11). One thruster was mounted on each wing tip 9.8 feet from the aircraft center line and the thrust (flow) from each unit could be directed either up or down. Both units were installed to thrust downward unless a roll control torque was directed from the position command electronic control unit. The control unit could be operated manually or in a feedback mode using the wing tip height as a signal.

The thrusters are unique due to the simple method used to vector the thrust. The system uses a solenoid actuated shutter which exposes one wall of the two dimensional nozzle to the ambient air pressure. This pressure then acts to deflect the flow to the opposite side.

The manufacturer measured the thrust versus supply pressure for each thruster. The units were designed for 43 psig, at which point they each delivered 18.2 lbs thrust and used 0.5 lb m/sec of air (125°F air through a nozzle throat area of 0.4 sq. in.). The vertical thrust was found to vary linearly for pressures between 3 and 45 psig (Figure 12). Each thruster weighed 0.7 lbs and had overall dimensions of 5.4 by 1.6 by 2.8 inches.

2.B.6. AIR CUSHION CONFIGURATION. Although a large number of different air cushion configurations were used during the 9 months of testing, the variations can be summarized by defining twelve configurations (Table 2). Most of the configurations use a different combination of components such as an ejector, tip fan, direct bleed, cushion vent orifice plate, relief valve, or roll thrusters. The first four configurations use the same ejectors for both the trunk and the cushion, but the cushion ejector is operated with different primary drive pressures. The general location of each trunk and cushion air supply component is shown in Figure 13.

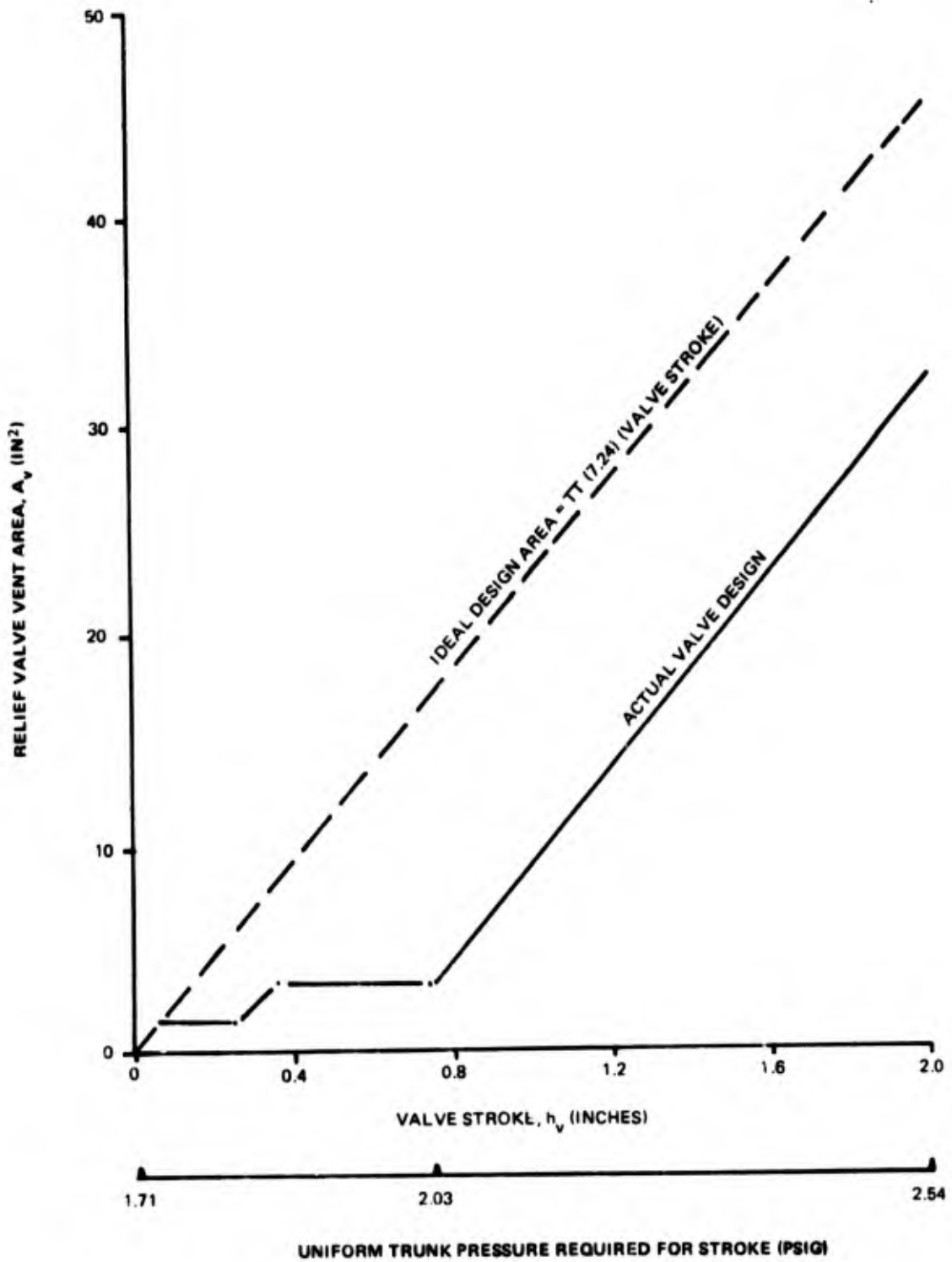


Figure 10. Relief Valve Vent Area Versus Stroke.

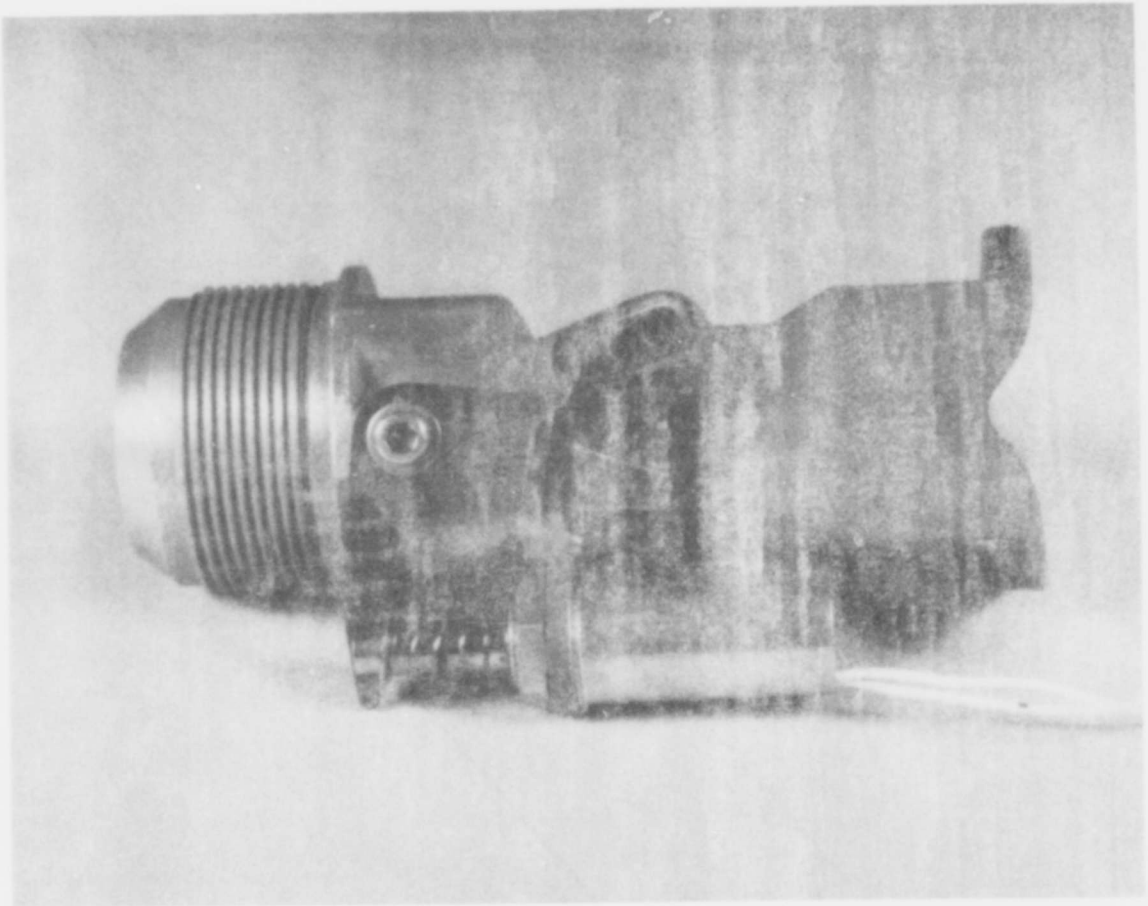


Figure 11. Wing Tip Roll Control Thruster.

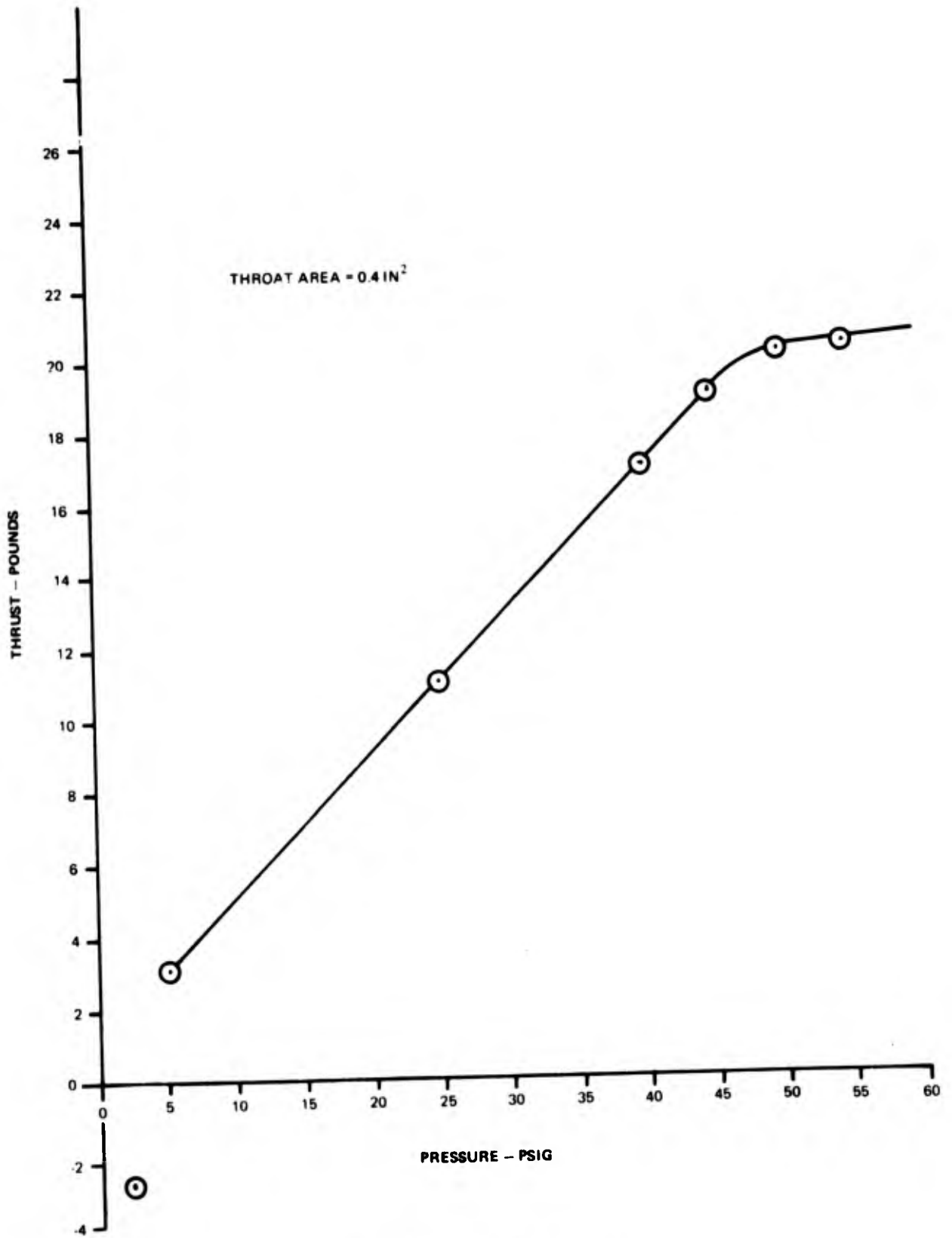


Figure 12. Roll Thruster Vertical Thrust.

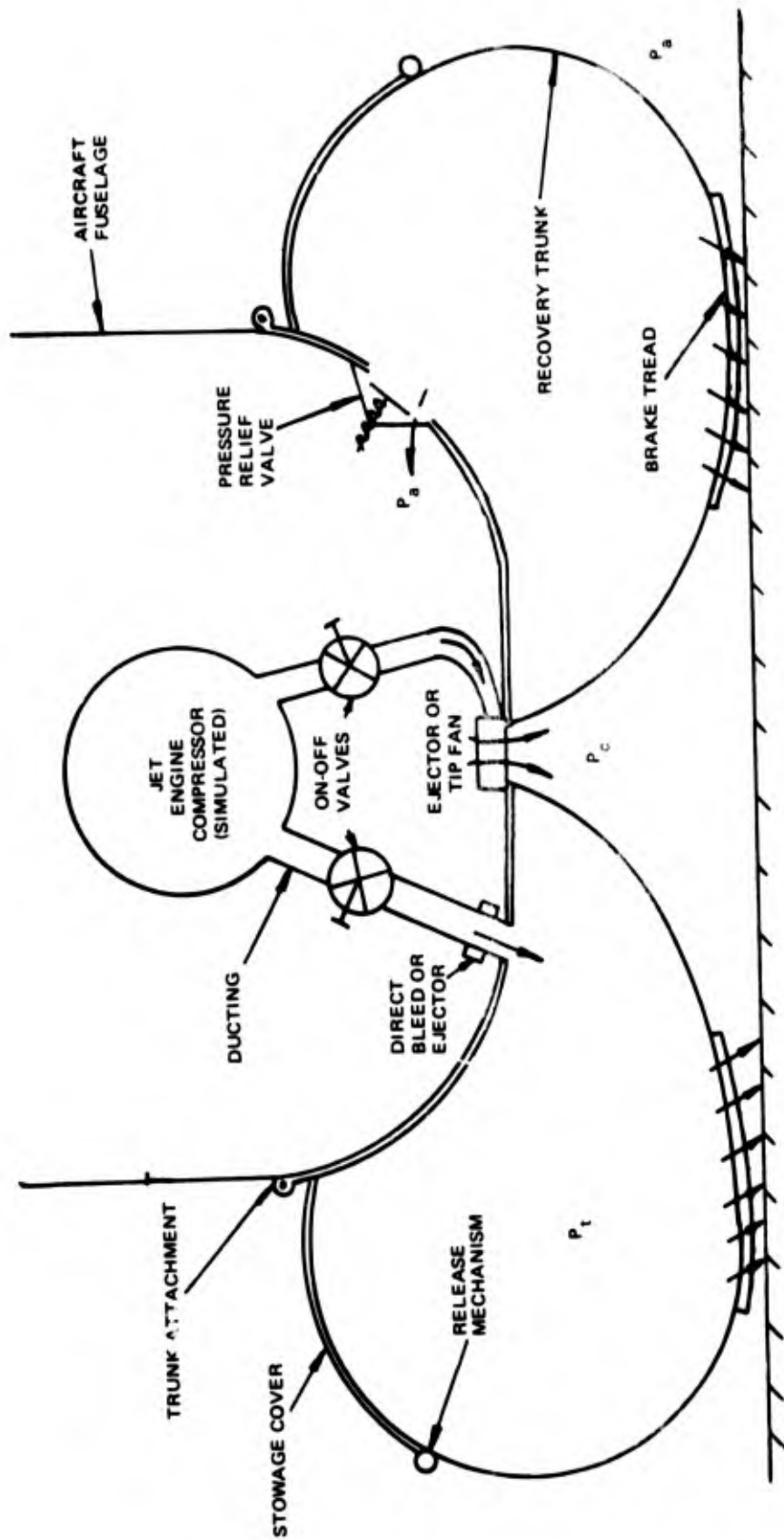


Figure 13. Air Cushion Components.

Table 2. Twelve Air Cushion Configurations.

| Configuration No. | Trunk Air Supply System | | | | Cushion Air Supply System | | | CG | Wing Tip |
|-------------------|--------------------------------------|--|-------------------------|------------------------|---------------------------|-------------------------|------------------------------|----------|----------------------------|
| | Nozzle Area A_n (in ²) | Relief Valve Max Area A_v (in ²) | Air Source | | Air Source | | Vent Area (in ²) | Location | Roll Thruster P_p (psig) |
| | | | Ejector P_{tp} (psig) | Direct P_{tp} (psig) | Ejector P_{cp} (psig) | Tip Fan P_{cp} (psig) | | | |
| 1 | 14.5 | N/A | 35 | N/A | 0 | N/A | 4.6 | 9.05 | N/A |
| 2 | 14.5 | N/A | 35 | N/A | 0 | N/A | 0.0 | 9. | N/A |
| 3 | 14.5 | N/A | 35 | N/A | 12.5 | N/A | N/A | 9.05 | N/A |
| 4 | 14.5 | N/A | 35 | N/A | 30.4 | N/A | N/A | 9.05 | N/A |
| 5 | 14.5 | N/A | 35 | N/A | -22 to +21 | 0-240 | 0-47 | 9. | N/A |
| 6 | 14.5 | 32.4 | 35 | N/A | N/A | 0. | 0.0 | 0.5 | N/A |
| 7 | 14.5 | N/A | 35 | N/A | N/A | 104 | N/A | 0.5 | N/A |
| 8 | 14.5 | 32.4 | 35 | N/A | N/A | 104 | N/A | 0.5 | N/A |
| 9 | 7.25 | 32.4 | N/A | 10 | N/A | 104 | N/A | 0.5 | N/A |
| 10 | 0.0 | 32.4 | N/A | 10 | N/A | 0 | 0.0 | 9. | N/A |
| 11 | 7.25 | 32.4 | N/A | 10 | N/A | 0 | 0.0 | 9. | 0-32 |
| 12 | 7.25 | 32.4 | N/A | 10 | N/A | 0 | 21.0 | 9. | 0-34 |

Note: 1) Cushion vent area is approximate.
 2) A_v and A_n do not include discharge coefficients.
 3) N/A (not applicable) denotes that the component was not installed.
 4) Negative P_{cp} value indicates ejector was reversed to create a negative P_c .

2.C. Test Equipment.

2.C.1. TEST TOWER. All of the ACRS tests were conducted in the high bay of Building 255 in Area B of Wright-Patterson AFB (Figure 14). The primary facility test equipment consisted of: (1) a test tower, (2) an air supply source, and (3) the instrumentation and data recording equipment.

The test tower and aircraft cradle were designed and fabricated by Centro Corporation. The cradle fits on top of the test aircraft and can be used to hold the aircraft at non-level pitch or roll angles for drop tests. The aircraft is raised up by its ground lifting hook which is inserted into the top fuselage above the center of gravity. A two-ton mechanical hoist was used to raise the aircraft, and a bomb shackle was used to release the aircraft for drop tests. Four trailer jacks were also used for added safety when working under the aircraft. The test tower height was adjusted to achieve a variety of vertical drop speeds.

The original tower was modified by AFFDL and Centro personnel during the course of these tests in order to achieve a forward pulling force through the aircraft center of gravity and a pure nose-down pitching moment. For the pulling force, a two-ton capacity fence stretcher was used to pull two cables attached to a cross bar through the center of gravity. A pure nose-down moment was achieved by pulling forward on a ten foot vertical beam that was attached to the rear of the aircraft in place of the 39 lb tail ballast section. The cable was attached to the top of the beam and was routed over the top of the tower and then vertically down to the anchored fence stretcher.

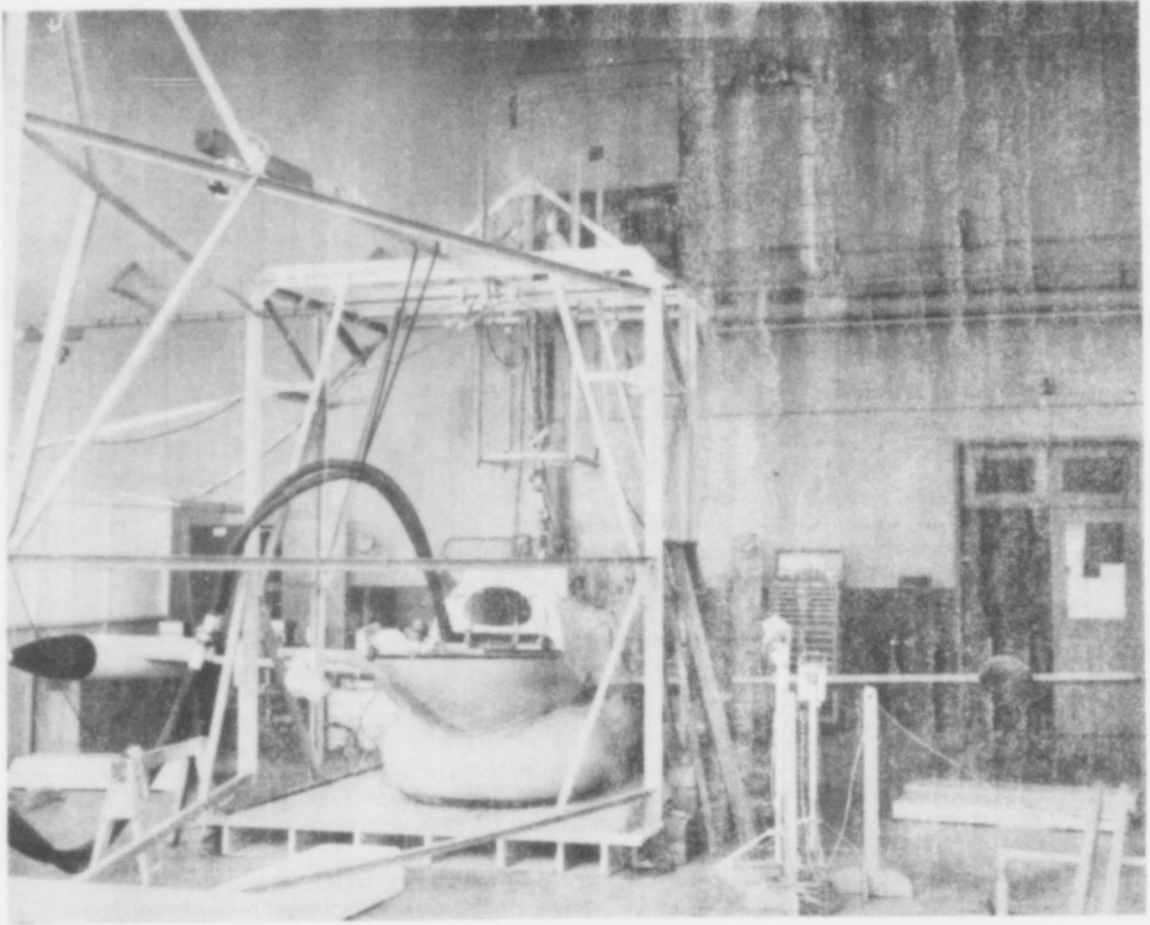


Figure 14. Test Tower and ACRS Equipped Jindivik.

An eight-inch raised plywood floor was used to support the aircraft during static and drop tests. Styrofoam blocks eight inches high were also used below the wing tips, nose, and tail of the test aircraft.

2.C.2. PRIMARY AIR SUPPLY SOURCE. The air source came from a mobile, high pressure gas storage bottle cart. The bottles were pressurized by a mobile air compressor. Both of these units were standard USAF flightline inventory items. The twelve cylinder air trailer was a Type MD-1 and the bottles were rated at 3500 psi. When the bottles were pressurized to the usual 2100 psig used for tests, they contained 218 lb_m of air in 20.4 ft³. The air was usually bled down to 900 psig which provided 124.5 lb_m of air, or up to a 200-second run time for normal flow configurations. Between tests the air bottles were repressurized with a 15 ft³/min. capacity, electric motor driven, type MB-1 air compressor.

The air flow was controlled through a system which is schematically shown in Figure 15. The air flow could be independently controlled to the cushion and to the trunk.

2.C.3. INSTRUMENTATION AND DATA RECORDING. The primary components of the data recording system were a Bell and Howell tape recorder (Model VR 3700B), signal conditioners, a Honeywell visicorder (Model 906A), and galvanometers (Figure 16).

The particular parameters that were measured varied with each type of test. The trunk and cushion pressures and three vertical heights were recorded for all tests. The vertical accelerations were recorded at three locations during drop tests. The primary drive pressures for the cushion and trunk were usually recorded in order to calculate the exact flow rates. The weight of the aircraft and the pulling force or pitching moment were measured with load cells when necessary. Real time color movies and black and white high speed films were taken for a few representative tests.

Table 3 lists the instrumentation channels and the sensitivities that were used during the majority of the tests and Figure 17 shows the location of the instruments on the test aircraft. Galvanometer type M400-120 was used for channels 1-3, and type M1000 was used for channels 4-8.

Table 3. Instrumentation Channels.

| Channel Number | Symbol | Parameter | Visicorder Value Per Inch Deflection |
|----------------|---------------|---|--|
| 1(drop) | g_{cg} | Acceleration at CG | 2g |
| 2(drop) | g_w | Acceleration at Starboard Wing Tip | 2g |
| 3(drop) | g_n | Acceleration at Forward Nose | 2g |
| 1(static) | L, F_{pull} | Lift from load cell, or cable pull (drag) | 500, or 250 lb. |
| 2(static) | P_{tp} | Trunk Primary Pressure | 10 psig |
| 3(static) | P_{cp} | Cushion Primary Pressure | 10 or 50 psig |
| 4 | h_{fus} | Structural Height Above Floor at FS146.75 | 10 inches |
| 5 | h_n | Height of nose pitot boom above floor | 10 inches |
| 6 | h_w | Height of starboard wing tip above floor | 10 inches |
| 7 | P_t | Trunk Pressure | 1.0 psig (drop tests) 0.5 psig (static tests) |
| 8 | P_c | Cushion Pressure | 0.5 psig (drop tests) 0.25 (static tests) |

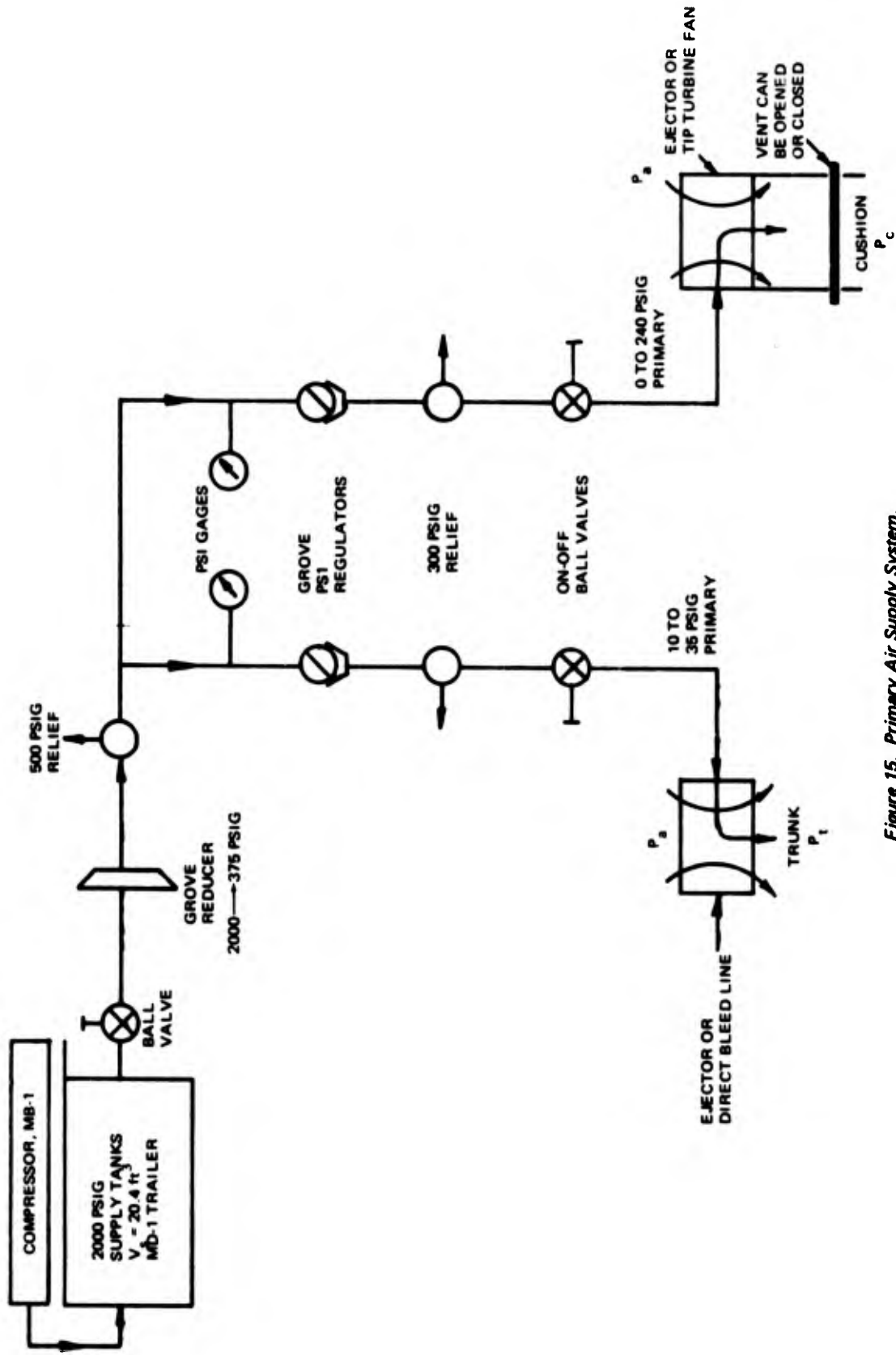


Figure 15. Primary Air Supply System.

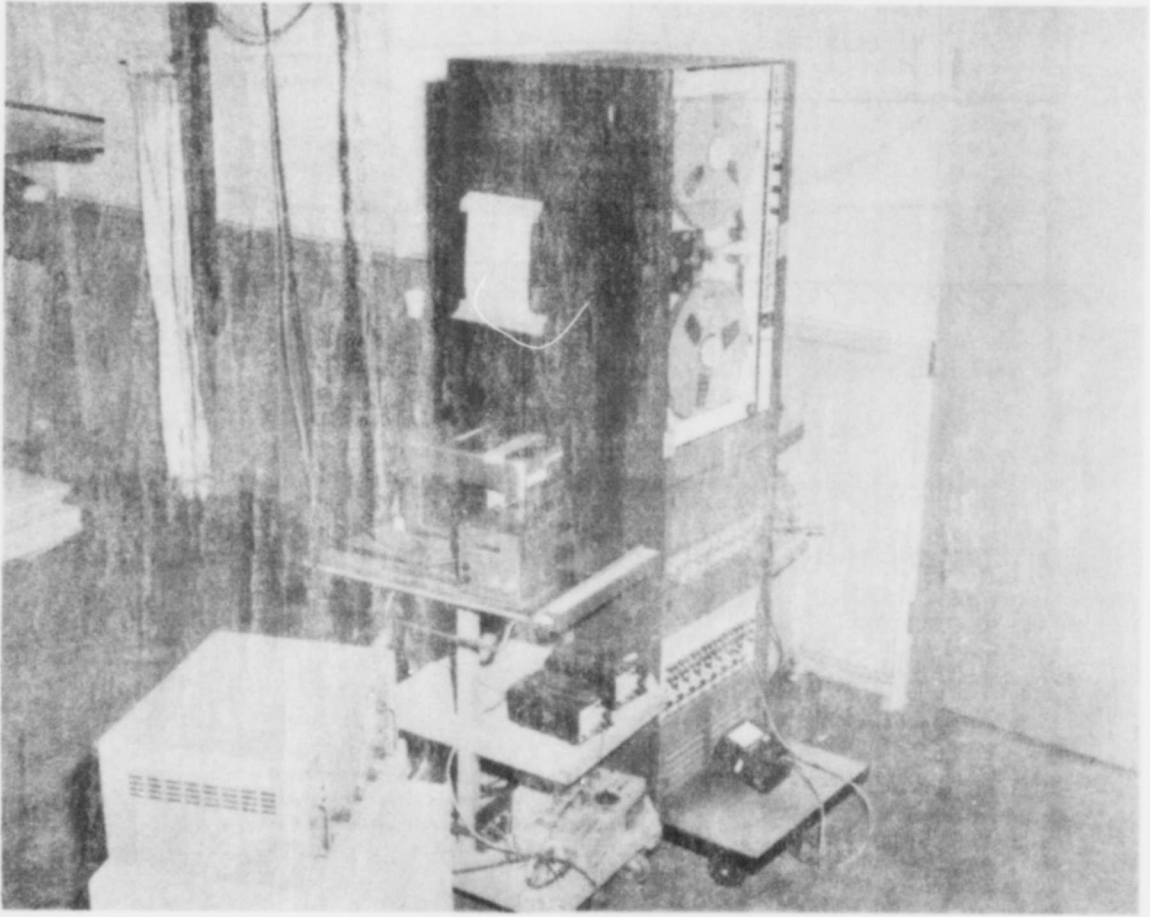
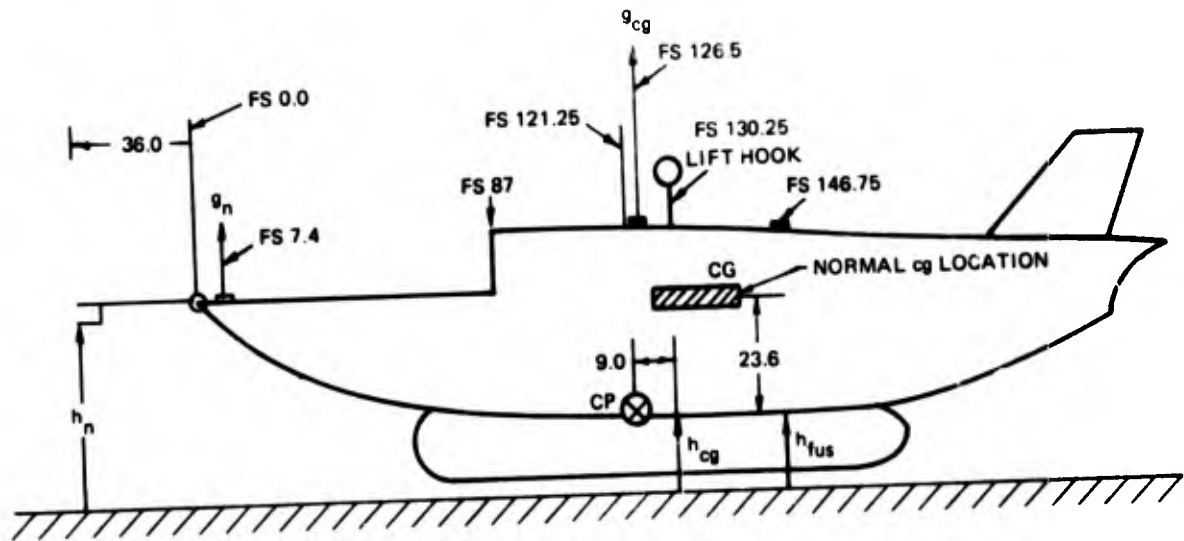


Figure 16. Data Recording Equipment.



The instrument pickups for g_w and h_w were placed on the starboard wing tip opposite FS 141 and FS 131, respectively. Both were positioned 164.75 inches outboard of the aircraft centerline. For configurations 10, 11, and 12; h_w was moved to a position 156 inches outboard of the centerline.

Figure 17. Instrument Locations On Test Aircraft.

3. TEST PROGRAM

3.A. Test Matrix

Nine types of static and dynamic ground tests were conducted on twelve different configurations. The forward speed of the aircraft was zero during all of these laboratory tests. The test results were used to determine a final ACRS design for Jindivik and will serve as a data baseline for other air cushion application studies. The static and dynamic stiffnesses and damping ratios measured in these tests can also be used to develop models of the air cushion system for use in aircraft equations of motion simulations. Certainly flight test and ground tests with forward speed would better test the design configurations, but these expensive methods were not considered warranted at this time until the design is further refined.

The nine types of tests can be classified as: (a) static hover, (b) static stiffness (heave, pitch, and roll), (c) pull tests, (d) damping (roll, pitch and heave), and (e) combined pitch and heave damping. Drop tests were needed to measure pure heave damping and combined pitch and heave damping.

A total of 194 tests were conducted. There were nine different categories of tests and twelve different air cushion configurations used, but each configuration was not subjected to every type of test. The following test matrix (Table 4) shows which tests were conducted on each air cushion configuration. The 194 chronological run numbers are categorized by type of test and air cushion configuration. An initial test series of 42 tests was conducted from 27 Feb to 29 Mar 1973. Following these preliminary tests, a more complete and accurate test series (43-194) was then conducted. The test checklist procedures used for static and drop tests are given in Appendix A.

3.B. Types of Tests

STATIC HOVER. The hover conditions are those equilibrium conditions which are present when the aircraft is hovering over a particular surface with no forward speed. For all of these laboratory tests the hover conditions were measured over a smooth plywood floor. During hover it was assumed that the vertical support was provided entirely by the trunk and the cushion (this assumes that jet thrust is negligible). Therefore a vertical force balance reduced to:

$$\begin{aligned}W_{ct} &= W_a \\W_{ct} &= W_t + W_c \\W_{ct} &= P_t A_t + P_c A_c\end{aligned}$$

Since the cushion area (A_c) of inextensible trunks has been found to be approximately constant, the trunk's footprint area can be calculated from measured data:

$$A_t = (W_{ct} - P_c A_c) / P_t$$

The aircraft's upward pitch angle, and the structural clearance below the aircraft's CG (lift hook) were calculated from measured data:

$$\Theta = \sin^{-1} \{ (h_n - (h_{fus} + 14.3)) / 182.75 \}$$

$$h_{cg} = h_{fus} + 16.25 \sin \Theta + 23.6 (1 - \cos \Theta)$$

except for heave damping tests, where

$$h_{cg} = h_{fus} + 24.7 \sin \Theta + 23.6 (1 - \cos \Theta)$$

Table 4. Test Matrix.

| Configuration Type of Test | 1 Vent Open | 2 Vent Closed | 3 $\dot{m}_c =$ 0.5 \dot{m}_t | 4 $\dot{m}_c =$ \dot{m}_t | 5 Vary Flow | 6 Valve Vent Closed | 7 Fan | 8 Valve, Fan | 9 Valve, Fan, Direct | 10 Valve, Closed Trunk | 11 Thruster, Vent Closed | 12 Thruster, Vent Open |
|--|--|--|---|-----------------------------------|---|------------------------------|-------------------------------|--------------------|-------------------------------|---------------------------------|--|---|
| 1. Static Hover | <u>74,77,</u> <u>78,80,</u> <u>81,87</u> | <u>74,77,</u> <u>78,80,</u> <u>81,87</u> | <u>74,77</u> <u>78,80,</u> <u>81,87</u> | <u>88</u> | | <u>128,130</u> | <u>138</u> | <u>141</u> | <u>154</u> | <u>165</u> | <u>174</u> | <u>182</u> |
| 2. Static Heave Stiffness | <u>4-11,</u> <u>26,51</u> | <u>12-18,</u> <u>27,39,</u> <u>50</u> | <u>53</u> | | | | | | | | | |
| 3. Static Pitch Stiffness A. Add Weight | <u>21-24,</u> | <u>29,30,</u> <u>36,37,</u> <u>70,71</u> | | | | | | | | | | |
| B. Pure Moment | <u>72</u> | <u>69</u> | <u>73</u> | | | | | | | | | |
| 4. Static Roll Stiffness | <u>25,57</u> | <u>28,38,</u> <u>54</u> | <u>58</u> | | | | | | | <u>163</u> | <u>166,171,</u> <u>173-</u> <u>174</u> | <u>175-</u> <u>180,</u> <u>182,192</u> |
| 5. Pull Tests A. Smooth Floor | <u>83,91</u> | <u>82,90</u> | <u>84,94</u> | <u>96</u> | <u>92,93,</u> <u>95,97,</u> <u>98,105,</u> <u>106,109,</u> <u>149</u> | | | | | | | <u>181,185,</u> <u>186,188-</u> <u>191,193,</u> <u>194</u> |
| B. Corrugated Floor | | | | | <u>101-104</u> | | | | | | | |
| 6. Roll Damping | <u>56</u> | <u>38,55</u> | <u>58</u> | <u>85,88</u> | | | | | | | | |
| 7. Pitch Damping | <u>59</u> | <u>60</u> | <u>61</u> | <u>86,89</u> | | | | | | | | |
| 8. Heave Damping Drop Tests | <u>123</u> | | <u>122</u> | <u>121</u> | <u>129-134</u> | <u>136-140</u> | <u>141-147,</u> <u>150</u> | <u>154-159</u> | | | | |
| 9. Pitch & Heave Damping Drop Tests | <u>110-120</u> | <u>31-35,</u> <u>40,</u> <u>63-68</u> | <u>115-117</u> | <u>110-114,</u> <u>124-126</u> | | | | | | | | |
| 10. Calibration Tests | | <u>46</u> | <u>45,47,</u> <u>49</u> | <u>19,20,</u> <u>48</u> | <u>52</u> | | <u>135</u> | | <u>151-</u> <u>153</u> | <u>161-</u> <u>162,164</u> | <u>172</u> | |
| 11. Incomplete Data | <u>1-3</u> <u>76,79</u> | <u>41,75,</u> <u>79,127</u> | <u>62,79</u> | <u>42</u> | <u>99,100</u> <u>107,108</u> <u>148</u> | | | | | <u>160</u> | | <u>187,183,</u> <u>184</u> |

NOTE: Results from underlined test numbers are used in this report.

This data correction of h_{fus} to h_{cg} was necessary since h_{fus} was measured at FS 146.75 instead of at the aircraft's CG which was at FS 120.25 (or FS 121.75 for the heave damping tests).

STATIC HEAVE STIFFNESS During previous tests of scale model ACLS aircraft, the static heave stiffness or spring coefficient (lb/inch deflection) was measured by adding weights to the aircraft CG. For the 1/10 scale CC-115, the spring coefficient was found to be approximately constant for weights from nearly zero up to 5 times the aircraft weight¹³. For the 1/4 scale CC-115 the axial flow fans had sharp stall points and the spring coefficient was found to be constant only up to the trunk pressure level which caused the fans to stall abruptly¹².

For these full scale Jindivik tests, the static heave stiffness was only measured from zero load up to the aircraft weight (2470 lbs). This was accomplished by lowering and raising the aircraft slowly in and back out of ground effect, thereby transferring the aircraft weight from the fuselage lift hook to the ACRS and back again. No additional weights were added above the aircraft weight, but the static stiffness can be assumed to remain relatively constant since the fan, ejector, and direct bleed line used to supply air to the trunk have smooth, monotonic flow characteristics in backflow (Figure 7) rather than an abrupt stall point like the 1/4 scale CC-115 model fans.

The vertical balance of forces during a heave stiffness test is:

$$W_a = W_{ct} + F_j + L$$

The vertical jet thrust, F_j is less than 1% of W_a for an ACRS, but may be 10% W_a for a high flow ACLS¹⁵. The jet thrust is a sum of the cushion thrust from the ejector or tip fan plus the thrust from the 45° trunk nozzles:

$$F_j = F_{jc} + (\dot{m}_t)^2 \cos 45^\circ / (\rho C_d A_n g_c)$$

The lift, L , applied to hold the aircraft is equal to W_a when the air flow is zero, decreases by the value of F_j when the air is turned on out of ground effect, and decreases to zero as the aircraft is lowered into the hover position.

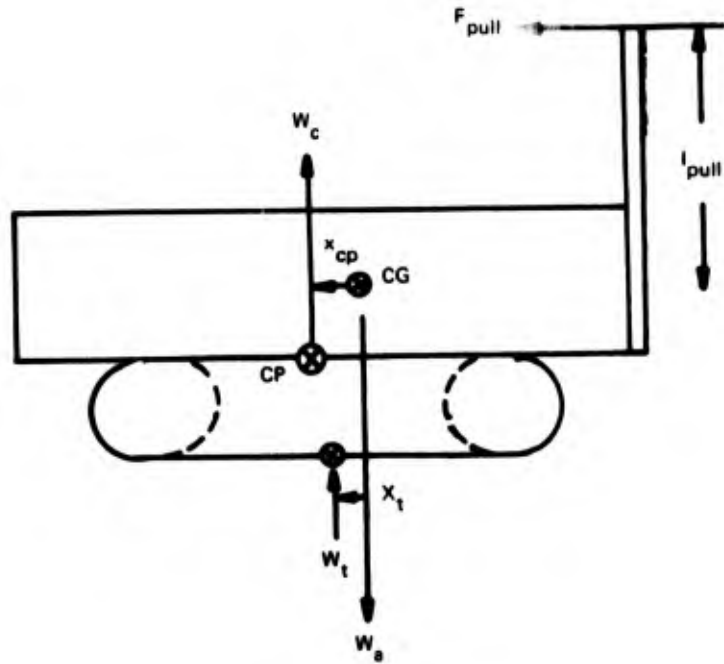
Static heave stiffness can also be referenced to as load-stroke, but load-stroke usually refers to the *dynamic* response of an energy absorption system.

STATIC PITCH STIFFNESS. The static pitch stiffness or spring coefficient (ft. lb/degree) was determined by applying a known pitch moment to the hovering aircraft and measuring the amount of pitch rotation. The pitch moment was applied in two different ways.

One way was to apply a pure pitch moment by pulling horizontally from the top of a vertical beam mounted behind the vertical stabilizer. The second method was to apply a pitch moment by adding weights forward of the CG. This second method had the additional effect however, of increasing the aircraft weight and moving the center of gravity forward. Therefore the first method is considered a more acceptable method of measuring pitch stiffness.

Once the vertical beam was added on the tail to apply a pure moment (tests 72, 69, and 73), additional weights were added in the nose to balance the aircraft. W_a increased from 2470 to 2562 lbs for these tests.

Figure 18 shows the balance of forces and moments for the pitch stiffness tests using a pure moment. By assuming a zero aerodynamic lift (laboratory tests), a small pitch angle, and a negligible F_j ; the location



EQUILIBRIUM VERTICAL FORCE BALANCE (ZERO LIFT AND THRUST)

$$W_a - W_t - W_c = 0$$

SUM OF PITCH MOMENTS ABOUT CG (SMALL ANGLE Θ)

$$W_c x_{cp} + W_t x_t - F_{pull} l_{pull} = 0$$

SOLVING FOR THE X AXIS LOCATION OF THE TRUNK'S CENTER OF FORCE:

$$x_t = \frac{F_{pull} l_{pull} - W_c x_{cp}}{W_t}$$

Figure 18. Longitudinal Location of Trunk's Center of Force, x_t

of the trunk's center of force can be expressed in terms of a moment arm about the aircraft CG.

$$x_t = \frac{F_{\text{pull}} l_{\text{pull}} - W_c x_{cp}}{W_t}$$

Figure 18 can also be used to show that if the CP is offset from the CG, then the aircraft weight cannot be fully supported by the cushion. The maximum P_c can be calculated from:

$$P_{c \text{ max}} = \frac{W_a}{A_c} \left(\frac{x_t}{x_t - x_{cp}} \right)$$

where x_t must have a negative value (be located aft of the CG) if the CP is forward of the CG. The maximum absolute value of x_t is one half the trunk ground tangent length. For this ACRS trunk design with $x_{cp} = 9$ inches, the maximum aft location of x_t is: $9 - 107.7/2 = -44.85$ inches. Therefore, W_c cannot exceed about 63% of W_a during hover conditions.

STATIC ROLL STIFFNESS. The roll stiffness or spring coefficient (ft-lb/degree) was determined by applying a known roll moment near the wing tip of the hovering aircraft and measuring the change in roll angle. The roll angle, ϕ , was calculated as follows:

Test 1-159

$$\phi = \sin^{-1} \frac{[(h_{cg} + 17.6) - h_w]}{164.75}$$

Test 160-194

$$\phi = \sin^{-1} \frac{[(h_{cg} + 17.8) - h_w]}{156.0}$$

The second equation was needed for the roll thruster tests because the wing pods were removed and the $h_{\text{starboard}}$ transducer was relocated.

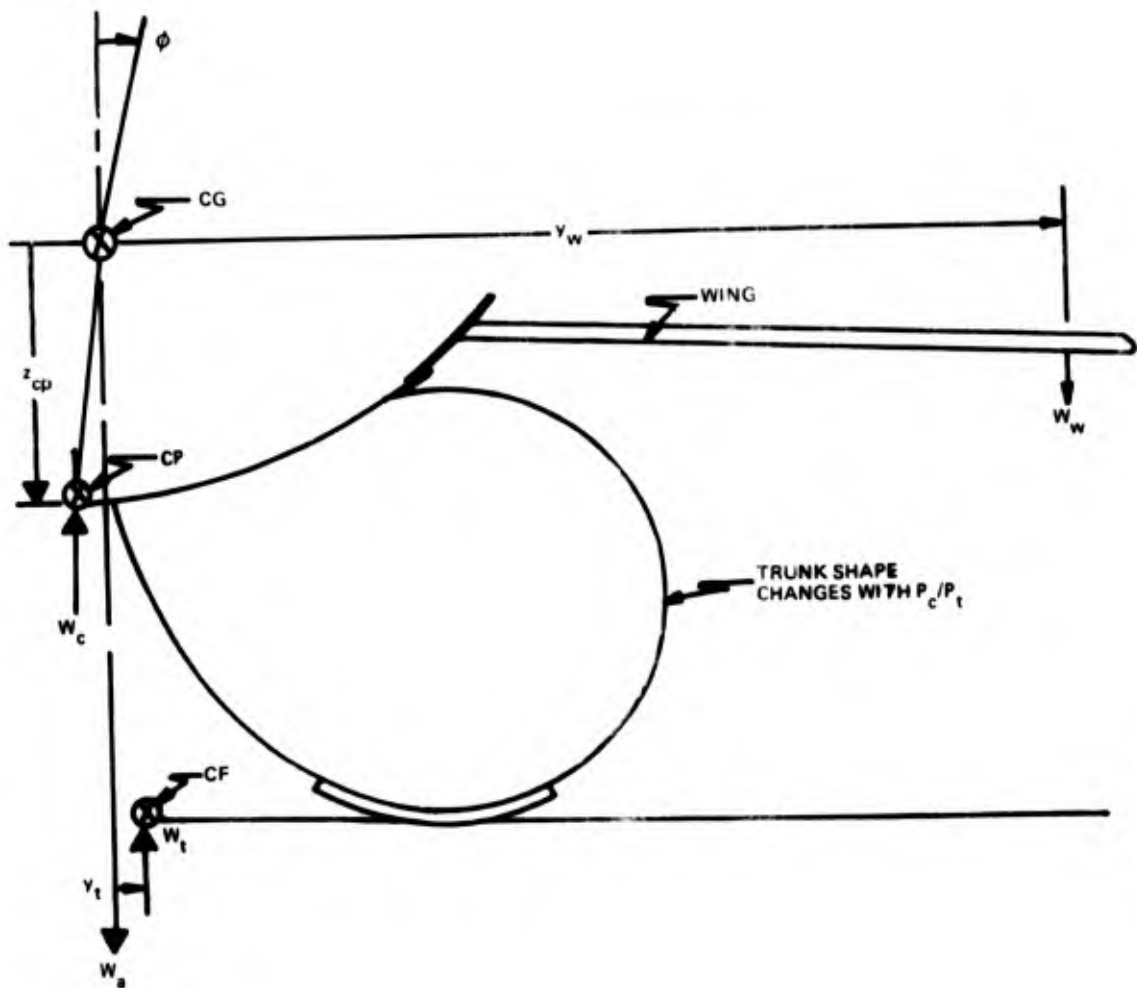
Figure 19 shows the balance of roll moments for tests where the weight used to create the roll moment is small compared to W_a . By also assuming zero lift and thrust and that the aircraft fuselage rolls but the trunk remains fixed; the side location of the trunk's center of forces can be calculated from:

$$y_t = \frac{W_c z_{cp} \sin \phi + W_w y_w}{W_t}$$

PULL TESTS. The brake drag was determined by measuring the horizontal pull force necessary to start the aircraft moving forward. The force was measured by a load cell which was connected by cables to a steel bar which ran through the center of the fuselage just aft of the cg. The force was applied by a two-ton fence stretcher.

The ACRS trunk used in these tests had brake tread installed all around the trunk ground tangent perimeter (Figure 4). Therefore, the brake tread area was much greater than an ACLS design using pillow brakes. The principle of lowering the cushion pressure to increase the brake drag is the same for both brake concepts, but the mechanisms are entirely different¹⁸. The ACLS cushion pressure is vented by

18. Vaughan, J. C., "The Jindivik Drone Program to Demonstrate Air Cushion Launch and Recovery", paper presented at First Conference on ACLS, Miami Beach, Florida, December 12-14, 1972, Proceedings published by UTSI, March 1973.



EQUILIBRIUM VERTICAL FORCE BALANCE (ZERO LIFT, $W_m/W_a \rightarrow 0$)

$$W_a - W_t - W_c = 0$$

SUM OF ROLL MOMENTS ABOUT CG (SMALL ANGLE ϕ)

$$W_c z_{cp} \sin\phi + W_w y_w - W_t y_t = 0$$

SOLVING FOR y_t :

$$y_t = \frac{W_c z_{cp} \sin\phi + W_w y_w}{W_t}$$

Figure 19. Side Location of Trunk's Center of Force, Y_t

mechanically distorting the trunk on each side of the brake pillows. The ACRS cushion pressure is reduced by decreasing, turning off or reversing the air flow into the cushion.

There are three different coefficients of friction (μ) that are of interest in evaluating an air cushion aircraft system. The brake tread has a certain material coefficient of friction (μ_m) between itself and any given surface.

The effect of air flow through the tread is to increase the air lubrication and therefore decrease the friction coefficient. Therefore, a second coefficient is calculated by dividing the horizontal drag by the vertical load which is supported by the ACRS trunk ($\mu_t = F_{\text{pull}}/W_t$). This equation is only true for an ACRS design, where the load supported by the trunk is equal to the load on the brake skids. The assumption is also made here that the trunk coefficient is the same all around the ground tangent. This will not be true for later ACRS designs which have lower friction coefficients for the forward trunk.

A third coefficient of friction can be calculated by dividing the brake drag by the aircraft weight ($\mu_a = F_{\text{pull}}/W_a$). This aircraft coefficient of friction is lower than μ_t if the wing lift or the cushion pressure is above zero. This coefficient is also the component of the horizontal deceleration rate (g's) due to the brakes.

Any of the 3 friction coefficients measured on one surface can be quite different when the aircraft is operated on a different surface. Rough surfaces will usually increase the aircraft friction coefficient because they can add the effect of obstacle drag and also further vent the cushion pressure – which puts more weight on the brakes. The vertical load on the brakes is also effected by the amount of wing lift.

ROLL DAMPING. The roll damping tests were conducted by loading down the starboard wing tip of the hovering aircraft until the wing tip (or wing tip skid if installed) touched the ground, and then suddenly removing the wing tip load. The change in wing tip height, h_w was then measured versus time. The amount that this height varied from its average value was noted at the beginning and end of each cycle (h_i and h_{i+2} respectively) and this data was used to calculate the following damping parameters:

$$\text{damped natural frequency, } f_d \text{ (cps)} = \frac{\text{no. cycles during test}}{\text{test time, sec}}$$

$$\text{damping ratio, } \zeta = d/\sqrt{4\pi^2 + d^2}$$

$$\text{where } d = \ln(h_i/h_{i+2})$$

$$\text{dynamic roll stiffness, } k_\phi \text{ (ft lb/deg)} = \frac{0.689fd^2 I_{xx}}{(1 - \zeta^2) g_c}$$

$$\text{roll damper coefficient, } C_\phi \frac{\text{(ft lb/sec)}}{\text{deg}} = \frac{\zeta \sqrt{1 - \zeta^2}}{\pi f_d} (k_\phi)$$

When the damping ratio, ζ , is small the damped natural frequency, f_d , is just slightly slower than the undamped natural frequency, f_n , since: $f_n = f_d/\sqrt{1 - \zeta^2}$.

A dynamic model of the ACRS Jindivik has been studied using linear springs and dampers, and the necessary spring and damper coefficients (k and C) were calculated¹⁹.

19. Bauer, F. C., "Air Cushion Landing System; Drop Dynamics Theory (Mechanical)", AFIT Thesis, GAM/AE/73A-1, Dec 73. (AFFDL-TM-74-57-FEM)

The wing tip roll thrusters were operated using several different feedback signals (non-optimized) in an effort to evaluate the ability of the thrusters to increase the roll damping ratio. The feedback signal was simply proportional to the distance from wing level height and did not differentiate between whether the aircraft was moving away from or towards a wing level position.

PITCH DAMPING. The initial pitch oscillation was created by manually rocking the tail of the hovering aircraft until the pitch motions were approximately 3 degrees to either side of the equilibrium position. The change in height of the nose extension, h_n , was measured versus time. The data was reduced in a similar way to the roll damping data. The damped natural frequency and damping ratio (f_d and ζ) were calculated first. Then the dynamic pitch stiffness (k_Θ) was calculated using the pitch moment of inertia (I_{yy}). Finally the pitch damper coefficient (C_Θ) was calculated using K_Θ . A sample of the calculation procedure used to reduce all the damping data is given in Appendix B.

HEAVE DAMPING DROP TESTS. Drop tests were conducted to determine pure heave dynamic characteristics, isolated from other degrees of freedom²⁰. To accomplish this isolation, the aircraft CG was moved forward to approximately coincide with the trunk CP. A total of 200 lbs was moved forward 8.8 ft from the original aircraft CG (located below the lifting hook). This had the effect of moving the aircraft CG 8.5 inches forward. Since the trunk CP was 9.0 inches forward of the original CG, this placed the new CG an estimated 0.5 inches aft of the trunk CP. This offset was small enough to isolate the heave dynamics, although very small pitch oscillations did occur during the aircraft motions following impact.

One goal of the ACRS designer is to position the trunk on the fuselage such that there is a minimum pitching moment introduced by the landing impact. To accomplish this, the trunk CP is located a small distance forward of the nominal cg so that the nose down pitching moment created by the horizontal surface drag during initial impact is balanced by the nose up pitching moment of the upward ACRS forces acting forward of the CG. The balance can never be exact for all situations however, since the CG position can vary from approximately 2.5 inches forward to 0.3 inches aft of the lifting hook during flight. The change in lift with angle of attack at impact can also change the resulting pitching moments during initial impact. Further, the ACRS drag can vary with landing surface conditions. A well designed system however, will minimize the resultant moment about the CG and the aircraft motions will be similar to those observed during these heave damping tests.

The aircraft was released from various drop heights in order to achieve representative sink speeds, v_{sink} (ft/sec) at the time of impact. The approximate drop height clearance ($h_{\text{cg drop}}$) needed to achieve a desired peak sink speed can be calculated by assuming a constant 1g acceleration during drop.

$$h_{\text{cg drop}} = 12 (v_{\text{sink}})^2 / 2g_c$$

It has been observed during laboratory drop tests however, that the sink speed continues to increase after the ACRS first comes into ground effect (until the acceleration passes through zero). Therefore another term must be added to the above constant acceleration equation. At the start of these ACRS tests, it was assumed that the system entered ground effect at 15 inches and reached zero acceleration when $h_{\text{cg}} = 11$ inches.

If the force buildup is linear during this four inch stroke, then the sink speed increases an additional 0.8 ft/sec after entering ground effect. Therefore, for these tests the necessary drop height was calculated from:

$$h_{\text{cg drop}} \text{ (inches)} = 15 + \frac{12}{2g_c} (v_{\text{sink}} - 0.8)^2$$

20. Vaughan, J. C. and Steiger, J. T., "Vertical Energy Absorption Analysis of an Air Cushion Landing System", AFFDL-TM-72-03-FEM, August 1972.

For example, to achieve 8 ft/sec peak sink speed, the aircraft was released from an h_{cg} of 24.65 inches.

The peak sink speed can also be estimated from the visicorder record after the test. At release the aircraft accelerates at $-1g$ for a certain time (Δt_1) and then changes from $-1g$ to zero g during another time interval, Δt_2 .

$$v_{\text{sink}} = g_c (\Delta t_1 + 0.5 \Delta t_2)$$

Since no wing lift mechanism was used, the aircraft was in free fall from release to touch. This situation causes two unrealistic conditions: (1) the aircraft is accelerating downward instead of being at a constant sink speed when it hits, and (2) the wing assembly instantaneously loses its support from the center of the aircraft at the moment of release. This step function change in the center support loading of the flexible wing causes it to start oscillating near its undamped natural frequency as the aircraft falls. Therefore instead of the wings uniformly supporting the aircraft weight at the moment of impact, the wings are unloaded and oscillating.

In addition to measuring the heave damping response of the ACRS, these drop tests also gave valuable information about the *load-stroke characteristics* and the peak aircraft loads. Since these laboratory drop tests did not use a simulated wing lift mechanism, the aircraft hit with a $-1. g$ downward acceleration instead of the normal zero g condition with wing lift equal to aircraft weight. The only upward forces acting on the aircraft weight (W_a) were from either the cushion or the trunk. The sum of the cushion and trunk forces must build up to the aircraft weight before any deceleration starts to occur. The ACRS is loaded to $1g$ when the CG accelerometer is passing through zero. The load response of the ACRS is best measured by the term $g_{cg} + 1.$, and the non-equilibrium force balance for this vertical energy absorption condition is:

$$(g_{cg} + 1.) W_a = P_c A_c + P_t A_t$$

The stroke efficiency is a term used to measure the effectiveness of an energy absorption system. The term is defined in MIL-L-8552C as the area under the load-stroke curve divided by the product of the max load and the max stroke. Therefore a system with a rectangular load stroke curve has 100% stroke efficiency while a triangular-shaped curve denotes a 50% efficient system.

PITCH & HEAVE DAMPING DROP TESTS. Additional vertical drop tests were made with the aircraft's CG moved back to the lift hook, 9.0 inches aft of the trunk's CP. Although the aircraft's CG was then located near its actual flight position, the impact dynamics were less realistic than for the heave damping tests where the pitching moments, $(W_t + W_c)x_{cp}$, were better balanced to simulate a brake drag, $\mu_t W_t$.

The purpose of these tests was to examine the dynamic characteristics which would occur in the extreme case where the resultant force from the ACRS passes 9.0 inches in front of the aircraft CG – rather than through the CG as in the ideal case. The effects of aerodynamic lift and drag, rapid flap retraction, and elevator control would also have to be considered in the complete case.

If the moments about the CG are balanced at impact, then (from Figure 38):

$$x_{cp} \left(1 + \frac{W_c}{W_t}\right) = \epsilon_t \mu_t$$

This simple relationship assumes: (1) uniform μ_t for all the tread, (2) no net moments created by lift, aerodynamic drag, or engine thrust, (3) no aerodynamic moment created by the elevators.

4. TEST RESULTS

4.A. Static Hover

A summary of the hover conditions for the twelve configurations is given in Table 5. In the first 4 configurations P_t decreased as P_c increased, and this caused the flow from the trunk ejector (\dot{m}_t) to increase. The flow into the trunk for direct bleed, however, is relatively independent of changes in P_c and P_t (configurations 9, 10, 11, 12). When the CG was moved forward for the drop tests (configuration 6-9), the aircraft hover height (h_{CG}) was increased slightly and the pitch angle was lowered to approximately 2 degrees.

The trunk airflow for configuration 10 was unusual. All of the trunk nozzles were blocked for this configuration and the trunk air was supplied using a direct bleed line from a 10 psig source. The trunk pressure was maintained by the relief valve since this was the only exit for air from the trunk. This configuration was tested since a "no flow" ACRS trunk design is a possible landing configuration. This would be similar to a landing air bag with a pressure relief device.

The equilibrium hover conditions for configuration 10 were unusual. A vertical oscillation was repeatedly obtained in the hover condition. The relief valve cycled open and closed between 0.03 and 0.55 inches stroke. This oscillation of the spring loaded relief valve followed a P_t oscillation between 1.6 and 1.7 psig and this in turn created an up and down motion of the aircraft ($h_{CG} = 11.9$ to 12.7 inches). The trunk pressure oscillation was also present when the aircraft was out of ground effect. Opening up the forward half of the trunk nozzles eliminated this oscillation (configurations 9, 11, and 12).

Table 5. Summary of Static Hover Conditions.

| Configuration No. | Description | Test No. | Hover Conditions | | | | | | |
|-------------------|-----------------------|----------|------------------|------------|----------------------|----------------------|-------------------|-------------------|-----------|
| | | | Pressures | | Flow Rates | | $\frac{P_c}{P_t}$ | $\frac{W_t}{W_B}$ | Hog in. |
| | | | P_t Psig | P_c Psig | \dot{m}_t lb m/sec | \dot{m}_c lb m/sec | | | |
| 1 | Vent Open | 51 | 1.93 | 0.05 | 0.8 | <0. | 0.03 | 0.95 | 11.4 |
| 2 | Vent Closed | 27 | 1.65 | 0.54 | 1.0 | 0.0 | 0.33 | 0.49 | 11.4 |
| 3 | $m_c = 0.5 m_t$ | 53,58 | 1.59 | 0.59 | 1.1 | 0.5 | 0.37 | 0.44 | 10.8 |
| 4 | $m_c = m_t$ | 88 | 1.52 | 0.67 | 1.1 | 1.3 | 0.44 | 0.39 | 10.5 |
| 5 | Variable Flow | - | - | - | - | - | - | - | - |
| 6 | Valve/Vent Closed | 130 | 1.54 | 0.54 | 1.1 | 0.0 | 0.35 | 0.49 | 12.0 |
| 7 | Fan | 138 | 1.43 | 0.61 | 1.2 | 1.0 | 0.43 | 0.43 | 12.0 |
| 8 | Valve/Fan | 141 | 1.39 | 0.61 | 1.3 | 1.0 | 0.44 | 0.43 | 12.3 |
| 9 | Valve/Fan/Direct | 154 | 1.50 | 0.76 | 0.8 | 0.3 | 0.51 | 0.29 | 11.7 |
| 10 | Valve/Closed Trunk | 165 | 1.6-1.7 | 0.02 | 0.8 | 0.0 | 0.01 | 0.98 | 11.9-12.7 |
| 11 | Thrusters/Vent Closed | 174 | 1.61 | 0.42 | 0.8 | 0.0 | 0.26 | 0.61 | 10.7 |
| 12 | Thrusters/Fan Vented | 182 | 1.70 | 0.0 | 0.8 | <0. | 0.00 | 1.00 | 10.5 |

NOTE: CG placed over CP for configurations 6-9.

Several attempts were made to change from configurations 2 to 1 and then to 3 during one continuous hover test (tests 74, 77, 78, 80, 81, and 87). The first change was made by removing the cushion ejector cover plate and the second change was made by supplying drive air to the cushion ejector. The normal hover height was not achieved, however, for configuration 1. The hover height, h_{cg} , decreased during test 81 from 11.3 to 10.7 inches as the aircraft was changed from configuration 2 to configuration 1. Therefore although the pressures and areas were the same as the normal hover conditions for configuration 1, the hover height was lower than that of configuration 2 instead of being higher. This difference was caused by the trunk's inability to move inward across the plywood floor. The low flow ACRS trunk was therefore "stuck" in the position for $P_c/P_t = 0.3$ (configuration 2) and could not move inward to assume its normal position for $P_c/P_t = 0.0$ (configuration 1). To achieve the necessary A_t to support the load, the aircraft had to move downward when the cushion was vented. This result makes it clear that an ACRS trunk can have different equilibrium positions or heights, depending on how it was loaded just prior to reaching the new equilibrium cushion pressure.

A review of the hover conditions shows that the aircraft weight can be supported either entirely by the trunk (configuration 12) or by a combination of the trunk and the cushion. For example, at the end of drop test 154, only 29% of W_a was supported by the trunk ($P_t A_t$). The entire aircraft weight can never be supported entirely by the cushion as long as the CG is aft of the CP, since this moment must be counteracted by some other force. For this ACRS design the weight on the trunk is also equal to the vertical load on the brake tread.

In general, as the amount of cushion flow was increased, P_c increased and more of the load was supported by the cushion. As \dot{m}_c was increased beyond approximately 1.5 lb m/sec (configuration 5), the trunk vibrated noticeably although the aircraft remained steady. This trunk flutter is considered acceptable for an ACRS since high \dot{m}_c would only be used during brief periods of taxi following a landing.

4.B. Static Heave Stiffness

The first three configurations were tested to determine their static heave stiffness response. Each configuration was identical except for the amount of flow in the cushion area. All three configurations were equipped with an ejector in the cushion area. The first configuration used an open cushion vent and the cushion ejector primary flow was turned off. Therefore, the cushion pressure remained nearly zero and the net cushion flow was actually *negative* since some of the trunk flow escaped through the open ejector vent. The second configuration used a plate to close the cushion vent and the cushion flow was *zero*. In the third configuration, the cushion ejector was supplied with a primary pressure so that the cushion flow was approximately *half the trunk flow*. Tests 51, 50 (or 27), and 53 tested the static heave stiffness of these three configurations respectively. Only the results from the first and third configurations will be reported and compared since the second configuration had a net cushion flow or pressure between the other two configurations and the results likewise were bracketed by tests 51 and 53.

Table 6 shows the basic data used to determine the effect of cushion flow on static heave stiffness. The jet thrust from the trunk was estimated to be a total of 9.4 lbs, or approximately 7 lbs downward. This was based on 1.1 lb/sec of unchoked air flowing through an effective area of 7.54 in² ($C_d = 0.52$) at a velocity of 275 ft/sec. The jet thrust from the cushion ejector was estimated to be 9 lbs based on manufacturer's data with a drive pressure of 12 psig.

Figure 20 shows that the static heave stiffness is linear and can be represented by a constant, k_h , except for the first 15 or 20% of the load where the stiffness is lower and non-linear. The vent open configuration had a linear system stiffness (k_h) of approximately 870 lb/inch, whereas the configuration with cushion flow added (50% more total flow) was 17% less stiff ($k_h = 725$ lb/inch). This decrease in k_h with increasing cushion pressure for the ACRS is opposite to the effect of cushion pressure for an ACLS.

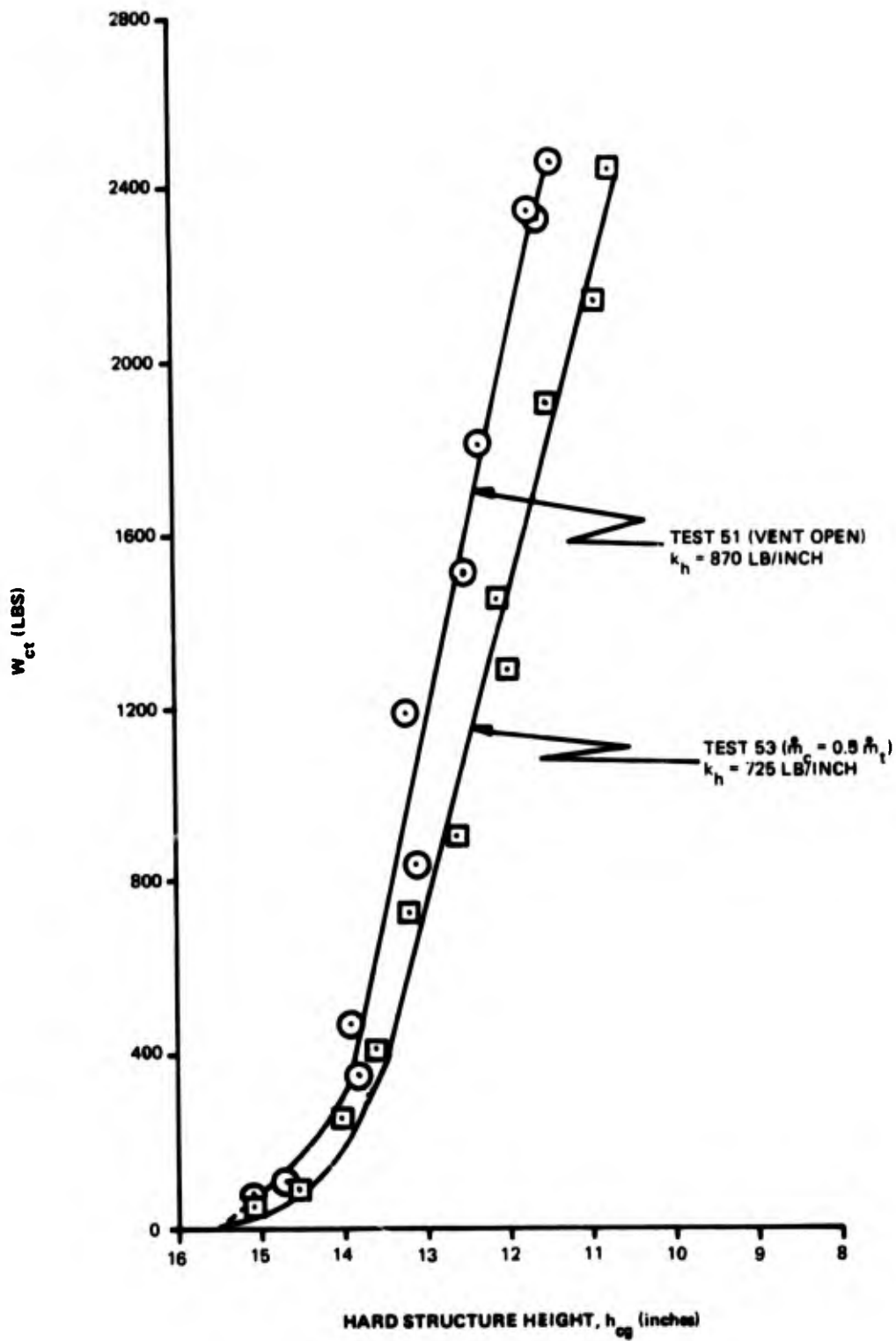


Figure 20. Static Heave Stiffness.

Table 6. Static Heave Stiffness Data.

| W_{ct} (lb) | h_{cg} (inches) | P_t (psig) | P_c (psig) | P_c/P_t | A_t (in ²) | $\frac{W_t}{W_{ct}}$ | Θ (deg) |
|--|----------------------|-----------------|-----------------|-----------|-----------------------------|----------------------|-------------------|
| Test 51 (Vent Open, $F_j = 7$ lb) | | | | | | | |
| 88 | 15.1 | 1.35 | 0.005 | 0.004 | 56 | 0.87 | 1.4 |
| 468 | 13.9 | 1.45 | 0.022 | 0.015 | 287 | 0.89 | 2.0 |
| 1193 | 13.2 | 1.63 | 0.037 | 0.023 | 679 | 0.93 | 2.3 |
| 1813 | 12.3 | 1.79 | 0.047 | 0.026 | 953 | 0.94 | 2.5 |
| 2353 | 11.7 | 1.89 | 0.047 | 0.025 | 1190 | 0.95 | 2.9 |
| 2463 | 11.4 | 1.93 | 0.047 | 0.024 | 1220 | 0.95 | 3.0 |
| 2333 | 11.6 | 1.89 | 0.050 | 0.026 | 1170 | 0.95 | 3.0 |
| 1513 | 12.5 | 1.62 | 0.075 | 0.045 | 795 | 0.88 | 2.4 |
| 838 | 13.1 | 1.52 | 0.065 | 0.043 | 450 | 0.82 | 2.4 |
| 348 | 13.8 | 1.39 | 0.042 | 0.030 | 179 | 0.72 | 1.8 |
| 108 | 14.7 | 1.35 | 0.017 | 0.013 | 50 | 0.63 | 1.6 |
| Test 53 ($\dot{m}_c = 0.5 \dot{m}_t$, $F_j = 16$ lb) | | | | | | | |
| 58 | 15.1 | 1.36 | 0.000 | 0.000 | 43 | 1.00 | 1.1 |
| 256 | 14.0 | 1.38 | 0.013 | 0.009 | 163 | 0.88 | 1.8 |
| 724 | 13.2 | 1.46 | 0.107 | 0.073 | 324 | 0.65 | 2.0 |
| 1294 | 12.0 | 1.46 | 0.285 | 0.20 | 428 | 0.48 | 2.4 |
| 1909 | 11.5 | 1.50 | 0.44 | 0.29 | 586 | 0.46 | 3.1 |
| 2454 | 10.7 | 1.57 | 0.547 | 0.35 | 748 | 0.48 | 3.6 |
| 2144 | 10.9 | 1.52 | 0.502 | 0.33 | 636 | 0.45 | 3.4 |
| 1454 | 12.1 | 1.47 | 0.325 | 0.22 | 470 | 0.48 | 2.8 |
| 909 | 12.6 | 1.41 | 0.195 | 0.14 | 320 | 0.50 | 2.3 |
| 416 | 13.6 | 1.37 | 0.067 | 0.049 | 189 | 0.62 | 1.9 |
| 95 | 14.5 | 1.34 | 0.010 | 0.007 | 53 | 0.75 | 1.7 |

This difference in stiffness is caused mainly by the effect of P_c on P_t . Since the ACRS trunk does not have air nozzles directed into the cushion area; when the cushion pressure builds up in an ACRS, the trunk pressure doesn't increase due to a nozzle back pressure effect (like for an ACLS). Instead the ACRS trunk pressure *decreases* as P_c increases. This is due to the weight being removed from the brake tread and therefore causing more air to escape from the trunk.

Figure 21 shows how P_t increased with load for both ACRS configurations. As mentioned before, for any given load, P_t for this ACRS design decreases as P_c increases.

There was also a difference noticed in the P_t variation with load depending on whether the aircraft was being lowered or raised. This is best shown on Figure 22, which shows that P_c was lower when the aircraft was being lowered onto the ACRS than it was when the aircraft was being raised. In other words, P_c was slow in building up as the aircraft was lowered; but once the full weight was supported by the ACRS, P_c remained higher as the aircraft was raised.

Figure 23 shows the calculated trunk contact area (A_t) based on the assumption that A_c is the same constant for both configurations. It is interesting to note from this graph that even though the trunk is

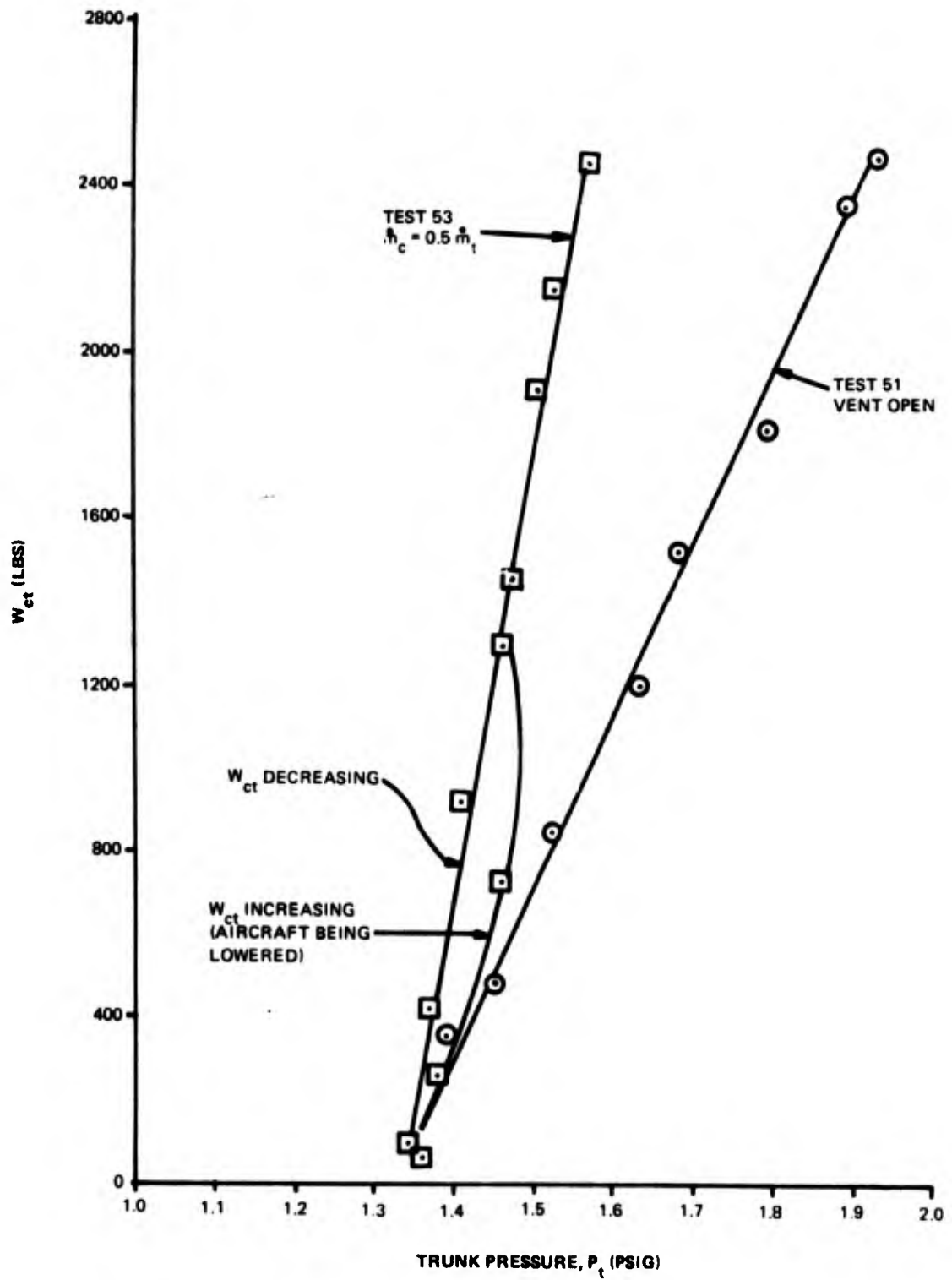


Figure 21. Trunk Pressure Increase With Load.

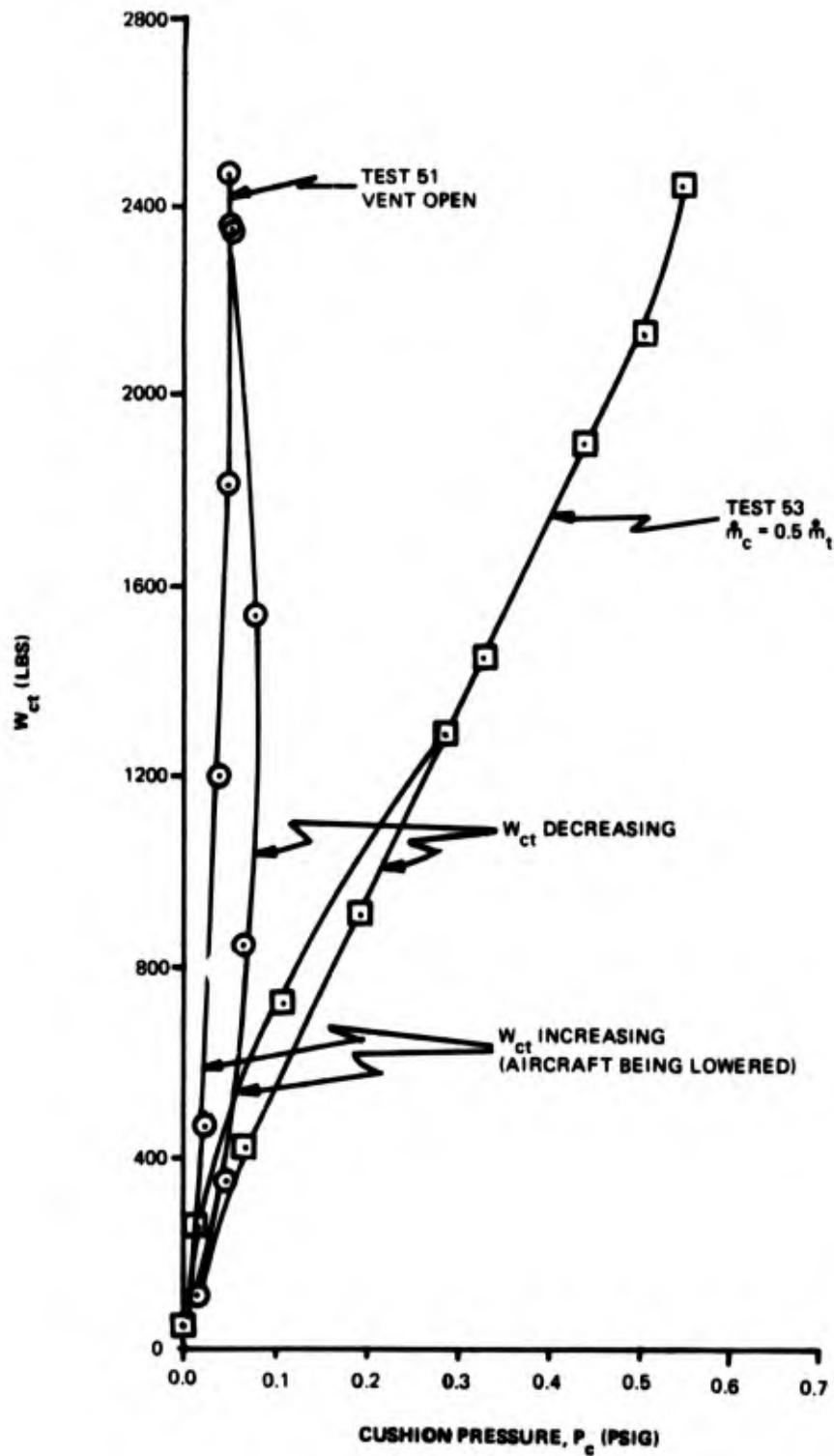


Figure 22. Cushion Pressure Increase With Load.

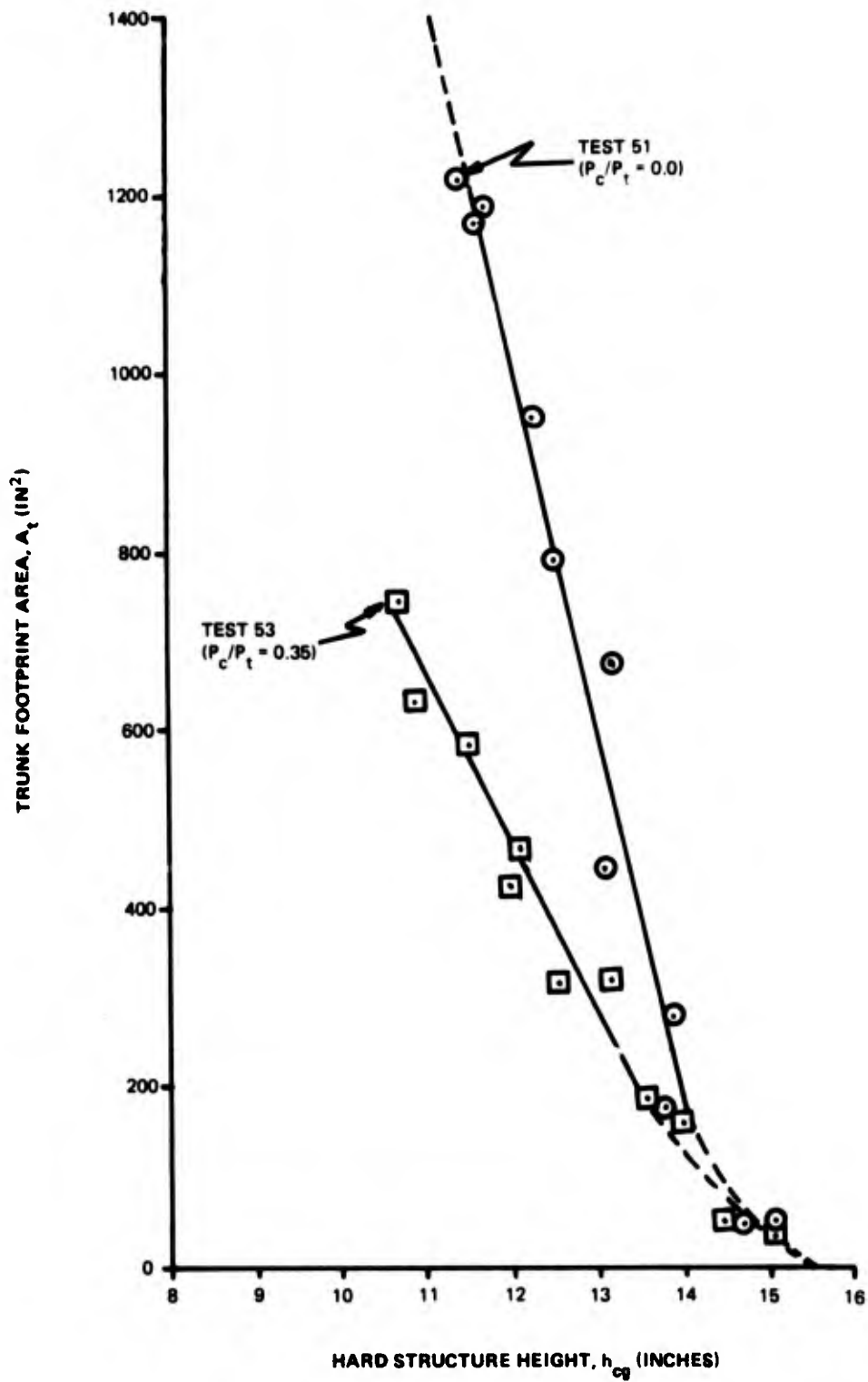


Figure 23. A_t Increase With Stroke.

identical for both configurations, the effective trunk footprint or contact area is considerably different at a given height. For example, at $h_{cg} = 12.5$ inches, A_t is 800 in^2 with the vent open and $A_t = 400 \text{ in}^2$ when cushion flow is added. The corresponding loads (W_{ct}) at 12.5 inches height are 1600 lbs and 1100 lbs. The corresponding P_c/P_t ratios are 0.03 and 0.15, respectively. Therefore at a given height, A_t and W_{ct} decrease as P_c or P_c/P_t increase. It has been shown in two-dimensional analysis that the trunk shape is pushed outboard as P_c/P_t increases. Therefore at a given height there is less flattened trunk area when the cushion pressure is high.

Figure 24 shows that even for this low flow ACRS, there are conditions where the cushion can support more weight than the trunk. Above 1200 lbs total load (W_{ct}) the vertical cushion support (W_c) exceeds the vertical trunk support (W_t). This result is not true for landing over rough surfaces where the cushion pressure will not build up significantly. For example, for test 51 with the cushion vent open the ratio W_c/W_{ct} never went above 0.37.

The results from these static heave stiffness tests show that the effect of cushion flow or cushion pressure is different for this low flow ACRS than it is for a high flow ACLS such as those previously tested¹². One difference is that the continuous brake tread can "stick" to the landing surface due to the small amount of air lubricity provided to the tread. Therefore, in these static tests the ACRS trunk sometimes stuck to the plywood floor in different equilibrium positions when the cushion pressure was low. A second difference of an ACRS from an ACLS is that P_t increases as P_c decreases. This in turn can cause the heave stiffness to increase as the surface roughness increases.

The results from these tests also show that the static heave stiffness was again found to be linear over the major portion of the load-stroke curve – just as has been observed in ACLS tests. A "hysteresis" or difference in P_t and P_c with load was noticed between when the aircraft is lowered and then when it was later raised. There was no noticeable hysteresis in the load-stroke response, but these results indicate that the aircraft should also be raised in order to measure the pressure response.

The ability to predict k_h for a given system requires the ability to predict how A_t varies with h_{cg} and with P_c/P_t for a given trunk. This problem was examined by Stuart²¹. If a relationship for A_t is known then k_h can be calculated from a sum of three different terms:

$$k_h = k_{h_{trunk}} + k_{h_{cushion}} + k_{h_{material}}$$

These three terms represent the contribution to the stiffness from the trunk footprint, cushion area, and trunk material. Only one design has been tested to date where the trunk material itself had a vertical stiffness even when unpressurized¹⁴.

By definition this equation for a linear k_h can be expressed as:

$$k_h = \left(\frac{A_{t_{ref}}}{h_t - h_{ref}} \right) P_{t_{ref}} + \left(\frac{A_c}{h_c - h_{hover}} \right) P_{c_{hover}} + k_{h_m}$$

21. Stuart, J.L., "An Experimentally Based Prediction of the Static Performance in the Vertical Direction of an Air-Cushion Landing System". AFFDL-TM-74-55-FEM, March 74.

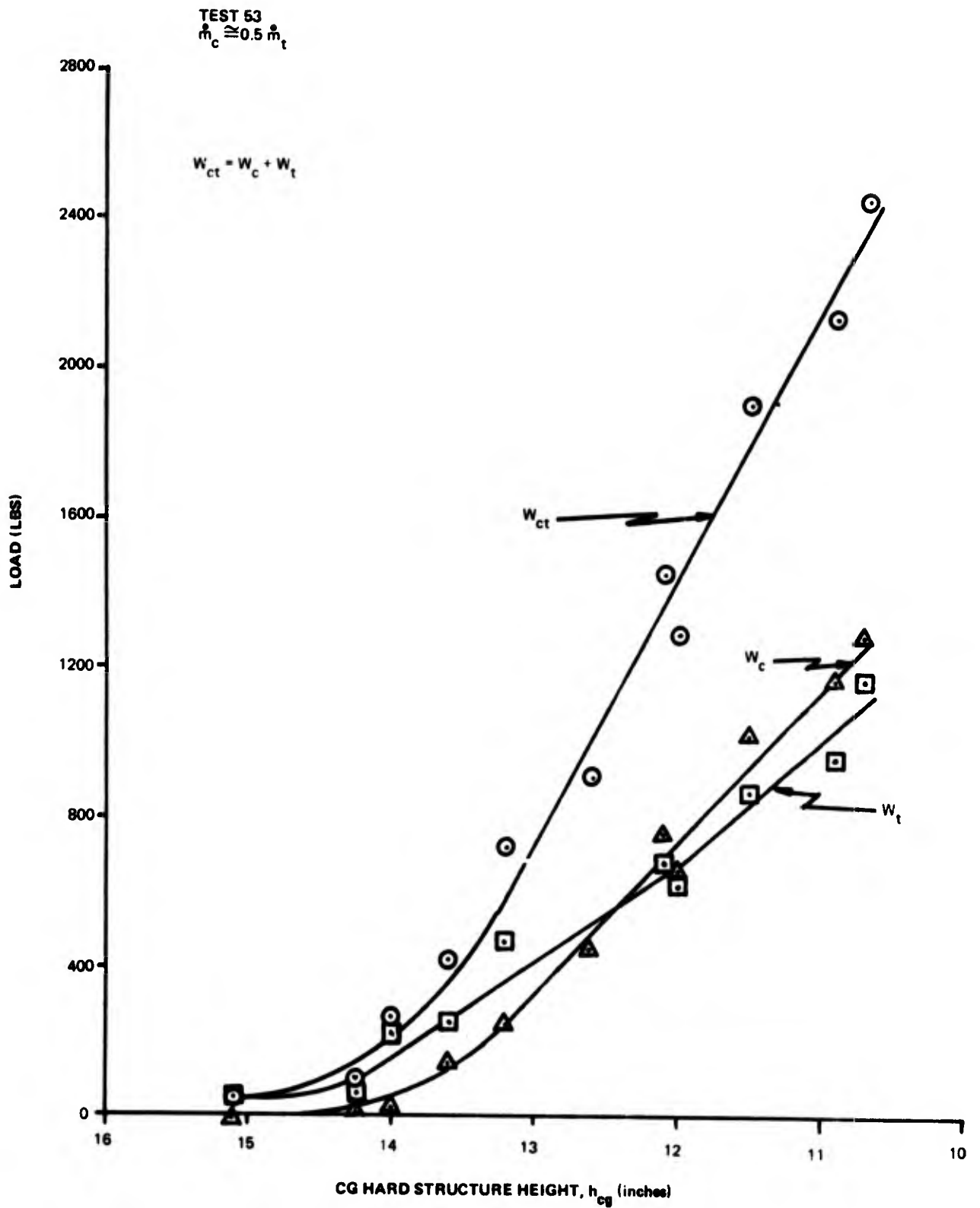


Figure 24. Cushion and Trunk Heave Stiffness.

This equation can be used to estimate k_h in the linear portion of the static load-stroke curve, disregarding the non-linear buildup period where the system is entering ground effect. The heights at which the trunk and cushion pressures can be assumed to start a linear buildup from their out of ground effect values are designated h_t and h_c , respectively. The reference condition for A_t , P_t , and h can be at hover or at some lower height if the entire load is supported by the cushion at hover.

This equation can be used to calculate the linear k_h for tests 51 and 53. The reference condition is taken as hover. The material stiffness is zero and all of the necessary data can be obtained from Table 6, except h_t and h_c . These heights can be determined graphically by plotting the sharpest pressure buildups for P_t and P_c versus height (Figure 25). The IGE and OGE lines intersect to give $h_t = 14.5$ and $h_c = 14.0$ inches.

$$k_h (\text{TEST 51}) = \left(\frac{1220}{14.5-11.4} \right) 1.93 + \left(\frac{2346}{14.0-11.4} \right) 0.047 + 0.0$$

$$= 760 + 43 = 803 \text{ lb/inch}$$

and

$$k_h (\text{TEST 53}) = \left(\frac{748}{14.5-10.7} \right) 1.57 + \left(\frac{2346}{14.0-10.7} \right) 0.547 + 0.0$$

$$= 309 + 386 = 695 \text{ lb/inch}$$

These calculated values of k_h are about 5% lower than the values determined from Figure 20.

4.C. Static Pitch Stiffness

The pitch stiffness or spring coefficient was measured for configurations 1, 2, and 3 and was found to be constant and approximately 980 ft lb/degree for each configuration (Figure 26). The stiffness decreased slightly for moments above 5000 ft lbs. The stiffness did not vary significantly with configuration, which showed that the static pitch stiffness for a given ACRS trunk installation is independent of cushion air flow and P_c/P_t ratio.

The longitudinal location, x_t of the trunk center of force, CF, had to shift from a position aft of the cushion CP to forward of the CP as the nose down pitching moment was increased (Figure 27). The data for configuration 1 (Table 7) shows that the trunk CF was 0.43 inch aft of CG during hover at $\Theta = 3.4^\circ$ and shifted to 24.5 inches forward of the CG when Θ reached -2.5° . The trunk footprint area, A_t , remained nearly constant during the test and the dependence on h_{cg} agreed closely with previous hover data for this configuration (Figure 23). Throughout the test the CF shifted approximately 4.6 inches for each degree of pitch.

The static pitch stiffness was also determined by a second method which involved applying a vertical force instead of a pure moment. The value of k_Θ was approximately 15% higher by this method. The aircraft weight, however, was increased by adding 400 to 1110 lbs at distances of 9 to 6 feet forward of the CG, respectively. This increase in W_a also had the effect of increasing W_t , which in turn can increase k_Θ .

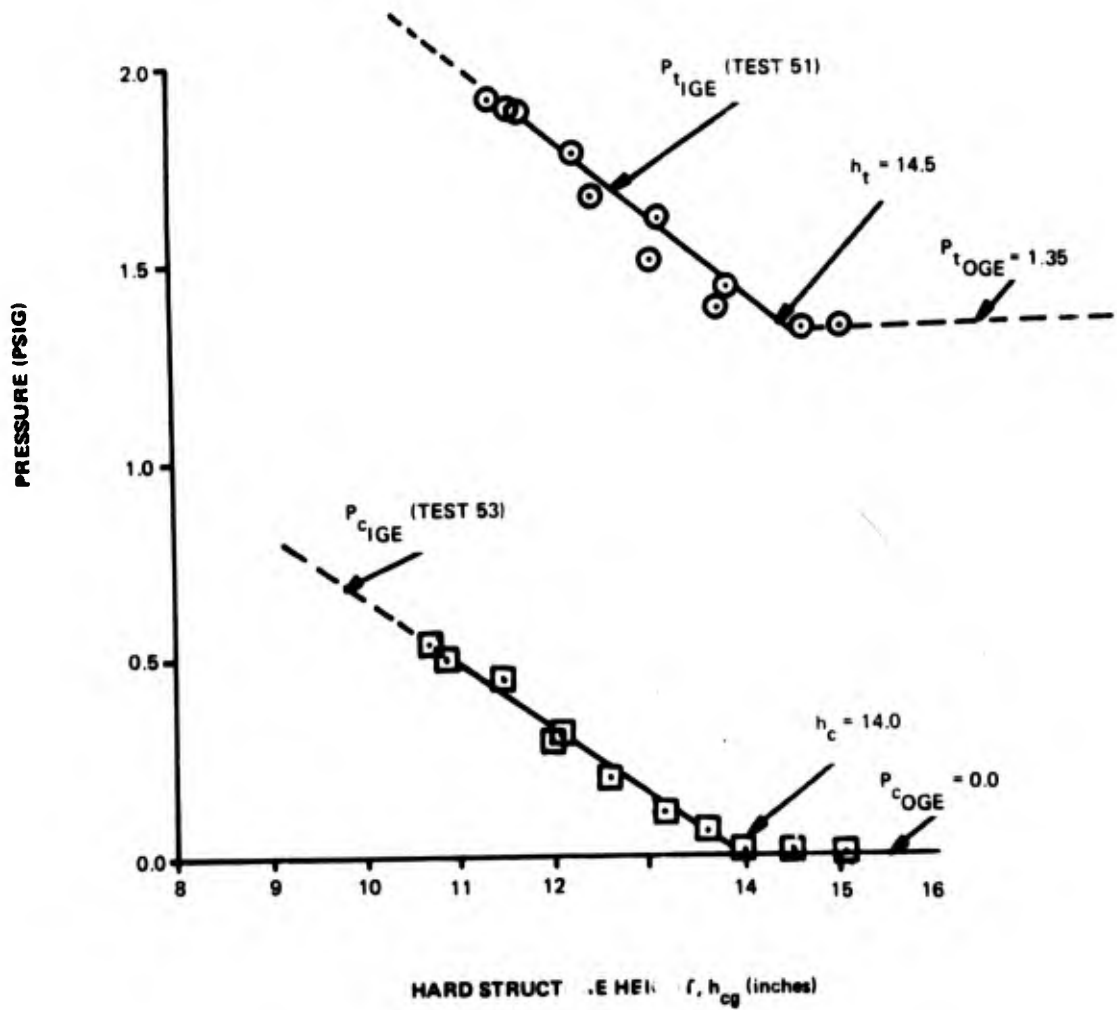
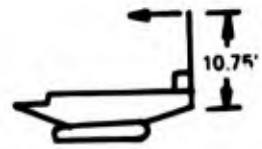


Figure 25. Graphical Estimate of IGE Heights.



- TEST 72 (VENT OPEN)
- TEST 69 (VENT CLOSED)
- △ TEST 73 ($\dot{m}_c = 0.5 \dot{m}_t$)

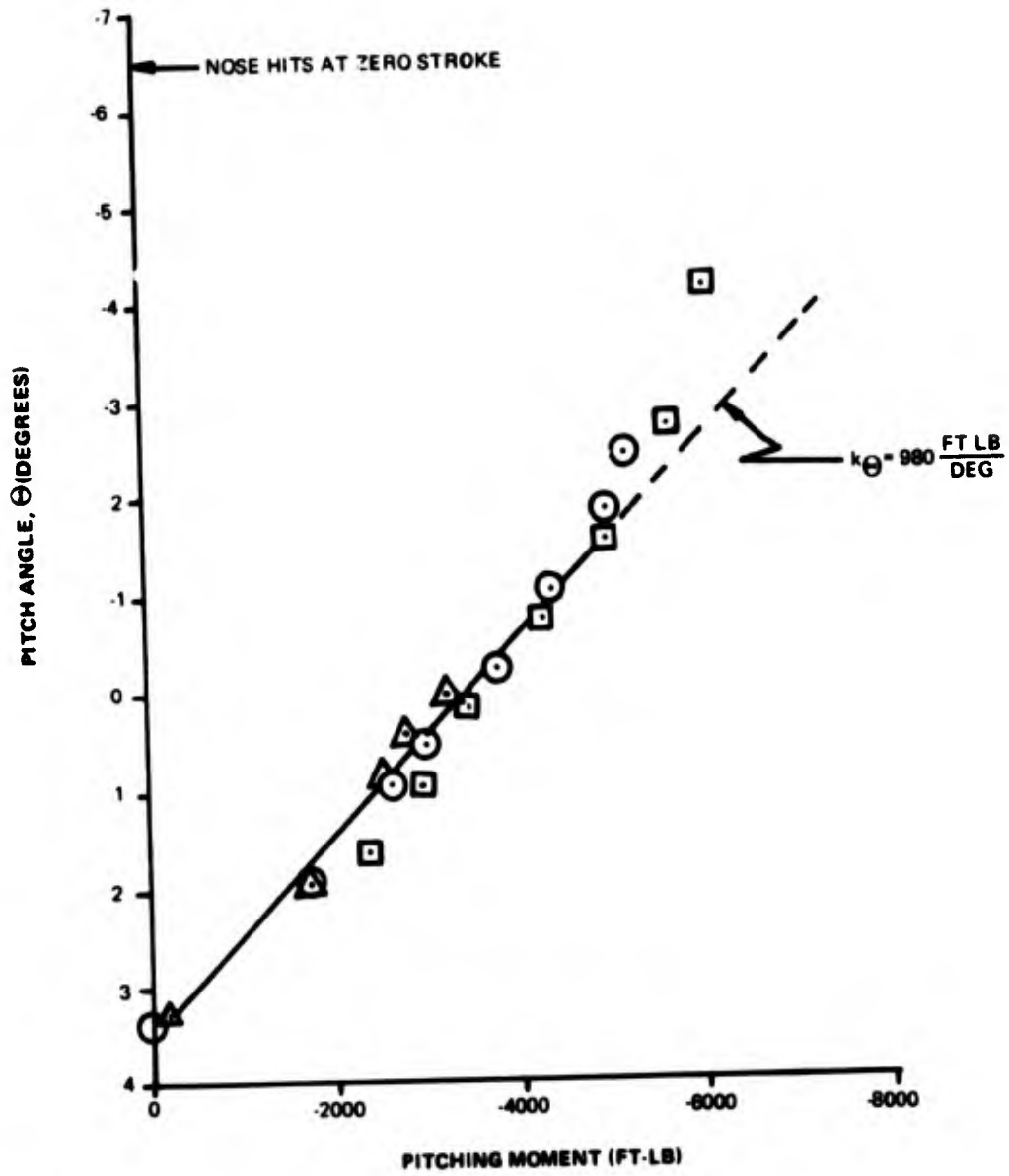


Figure 26. Static Pitch Stiffness.

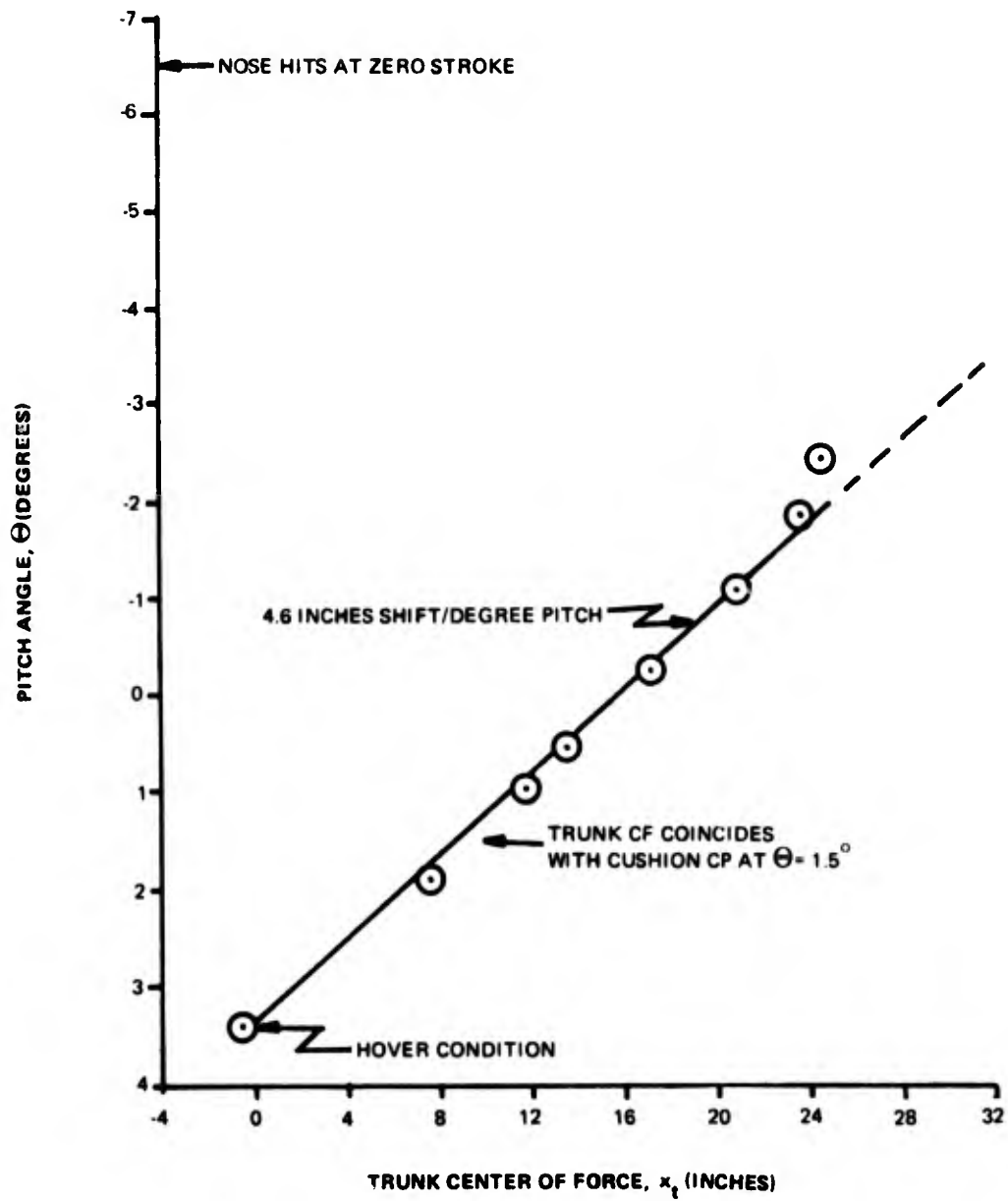


Figure 27. x_t Shift With Pitch Angle.

Table 7. Pitch Stiffness Data (Test 72, Vent Open).

$$W_a = 2562 \text{ lbs}$$

$$A_c = 2346 \text{ in}^2$$

$$l_{\text{pull}} = 124 \text{ inches}$$

$$x_{cp} = 9.0 \text{ inches}$$

$$x_t = \frac{F_{\text{pull}} l_{\text{pull}} - W_c x_{cp}}{W_t}$$

| F_{pull} (lbs) | Θ (deg) | P_t (psig) | P_c (psig) | W_c (lbs) | $W_a - W_c$ (lbs) | x_t (in.) | A_t (in ²) | h_{cg} (in) |
|----------------------------|-------------------|-----------------|-----------------|----------------|----------------------|----------------|-----------------------------|------------------|
| 0.0 | 3.4 | 2.03 | 0.05 | 117 | 2445 | -0.43 | 1200 | 10.9 |
| 160 | 1.9 | 2.04 | 0.03 | 70 | 2492 | +7.7 | 1720 | 11.3 |
| 245 | 0.9 | 2.02 | 0.03 | 70 | 2492 | +11.8 | 1232 | 11.7 |
| 278 | 0.5 | 2.01 | 0.03 | 70 | 2492 | +13.6 | 1239 | 11.6 |
| 352 | -0.3 | 2.00 | 0.03 | 70 | 2492 | +17.2 | 1246 | 11.6 |
| 407 | -1.1 | 1.98 | 0.10 | 235 | 2327 | +20.8 | 1178 | 11.6 |
| 460 | -1.9 | 1.95 | 0.10 | 235 | 2327 | +23.6 | 1195 | 11.8 |
| 482 | -2.5 | 1.95 | 0.08 | 188 | 2374 | +24.5 | 1218 | 11.9 |

4.D. Static Roll Stiffness

Configurations 1, 2, 3, and 12 were tested and the static roll stiffness, k_ϕ , was found to be approximately constant for a given configuration (k_ϕ independent of roll angle). The roll stiffness was found to vary directly with P_t and inversely with P_c . When the flow to the cushion was increased, P_c and W_c increased – which in turn caused P_t and W_t to decrease. An increase in P_c/P_t ratio pushed the side trunk outward and created a larger moment arm for W_t (see Figure 6).

The roll moment was applied by adding weights in 10 lb increments to the wing tip. The moment arm, y_w , was 11.3 ft for configurations 1-3 and 9.0 ft for configuration 12. Since the initial hover angle was usually a fraction of a degree from zero, the data was graphically adjusted to force the roll moment to be zero when the roll angle was actually zero.

The roll moment-angle curves for configurations 1, 2, and 3 are shown in Figure 28. The roll stiffness decreased ($k_\phi = 67, 53, \text{ and } 49 \text{ ft lb/deg}$) as the trunk pressure decreased ($P_t = 1.93, 1.60, \text{ and } 1.57 \text{ psig}$ respectively, in hover). An empirical relation for roll stiffness for these 3 configurations is: $k_\phi = 25 P_t^{1.5}$.

Configuration 12 however, did not follow this relationship. For this configuration, the trunk pressure was prevented from rising above 1.7 psig by the pressure relief valve, and k_ϕ was found to be 46 ft lb/degree. The roll stiffness is therefore not just a function of P_t .

Since an increase in P_c/P_t causes the side trunk to push outward, the moment arm, y_t , for the trunk restoring force, $P_t A_t$, was located further outboard when P_c/P_t was high. For configurations 1, 2, 3, and 12 the respective moment arms when $\phi = 5^\circ$ were: 1.8, 4.8, 5.3, and 1.1 inches (assuming $x_{cp} = 23.6$ inches). Therefore the side trunk footprint for configuration 12 was further inboard than configuration 1, even though the P_c/P_t ratio was the same. The reason for this smaller y_t may have been either the lower P_t or the reduced trunk nozzles. In either case the effect of a smaller y_t is to further reduce k_ϕ for configuration 12 below that of configuration 1.

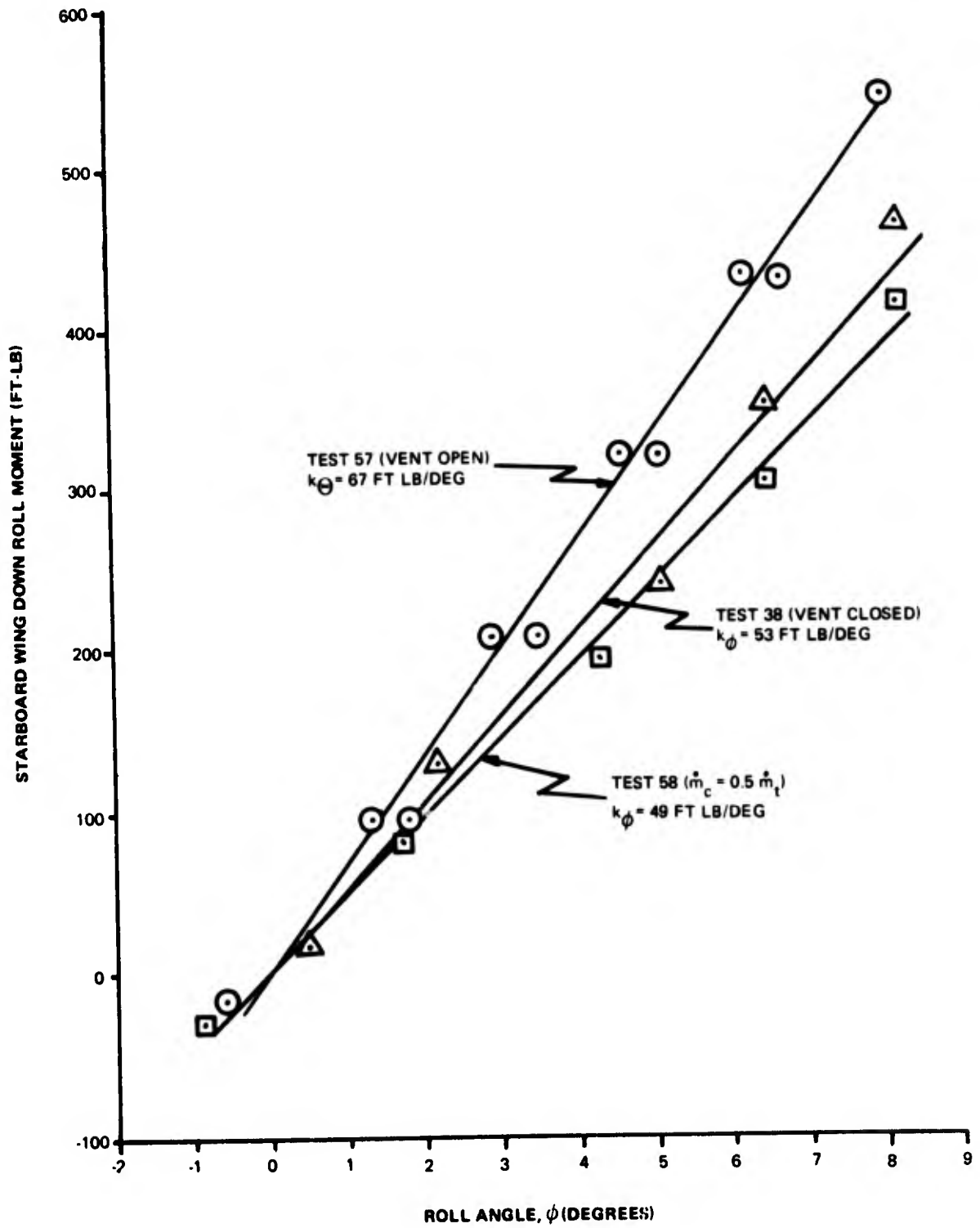


Figure 28. Roll Stiffness.

4.E. Pull Tests.

The majority of tests were conducted over a smooth plywood floor. The air flow into the cushion was varied from positive to negative values. The cushion flow was supplied by either an ejector or a tip turbine fan. The trunk flow was supplied by an ejector. Although the primary drive pressure for the trunk ejector was held constant, the total trunk flow decreased slightly as the trunk load increased.

The brake tread rubber material was tested on the plywood surface without airflow and the material coefficient of friction (μ_m) was measured to be 0.6. When about 0.7 lbm/sec of air was fed through the brake tread nozzles, the trunk coefficient of friction was reduced to approximately 0.4 due to an "air lubricity" effect.

The pulling force varied from as low as 122 lbs to as high as 1950 lbs. The aircraft coefficient of friction therefore varied from 0.05 to 0.78 as \dot{m}_c was varied.

Figure 29 shows the variation of pulling force or aircraft drag with cushion pressure, P_c . The change in P_c is also a direct indication of the change in W_c and W_t . The graph shows that the tip turbine fan data points do not fall on the curve. Since the fan was usually delivering more flow (\dot{m}_c) at a given cushion pressure, this lack of correlation indicates that the drag may be more a function of cushion flow than cushion pressure.

Figure 30 shows how drag varied with cushion flow, \dot{m}_c . This time the fan and ejector points correlate. Only the high flow fan points were used on the graph. The lower fan flow points do not contradict the ejector data, but the amount of flow rate uncertainty makes these few points of no value for this curve (see Table 8).

Since drag is a function of \dot{m}_c rather than P_c , the trunk coefficient of friction was a function of \dot{m}_c and was lower when the fan was used. The aircraft coefficient of friction varies similarly. The drag variation versus \dot{m}_{total} (instead of \dot{m}_c) would give similar effects since \dot{m}_t remained near 0.8 lb m/sec (± 0.3) for all the tests.

During the low flow ejector tests, the cushion pressure was observed to build up as the pulling force was increased up to the breakaway value. For example, during test 90 (configuration 2) the cushion pressure was 0.57 psig at hover ($F_{pull} = 0$) and then increased to 0.68 psig when F_{pull} was 393 lbs.

Four additional pull tests (101-104) were made over 2 inch wide plywood slats attached to the plywood floor. Seventeen slats were placed at two inch intervals. The slats were 0.69 inches high and were placed crosswise under the straight section of the trunk. The effective vent area between the slats was 46.8 in². The load supported by the cushion was 4 to 14% of the aircraft weight despite the large vent area. The average trunk coefficient of friction was 0.64, which is very close to the "non-lubricated" μ_m of 0.61 measured without air blowing through the tread. This indicates that the air lubricity effect can be lost over extremely rough or unusual surfaces.

The F_{pull} versus \dot{m}_c curve changes slope abruptly near the point where \dot{m}_c is zero. When the cushion flow was negative, a small addition to \dot{m}_c caused a large decrease in drag. Once the cushion flow became positive, a much larger amount of flow was required to reduce the drag a corresponding amount. The ACRS trunk also started to flutter shortly after \dot{m}_c became positive. Since this trunk was not designed for high flow, it was not equipped with flutter suppression devices.

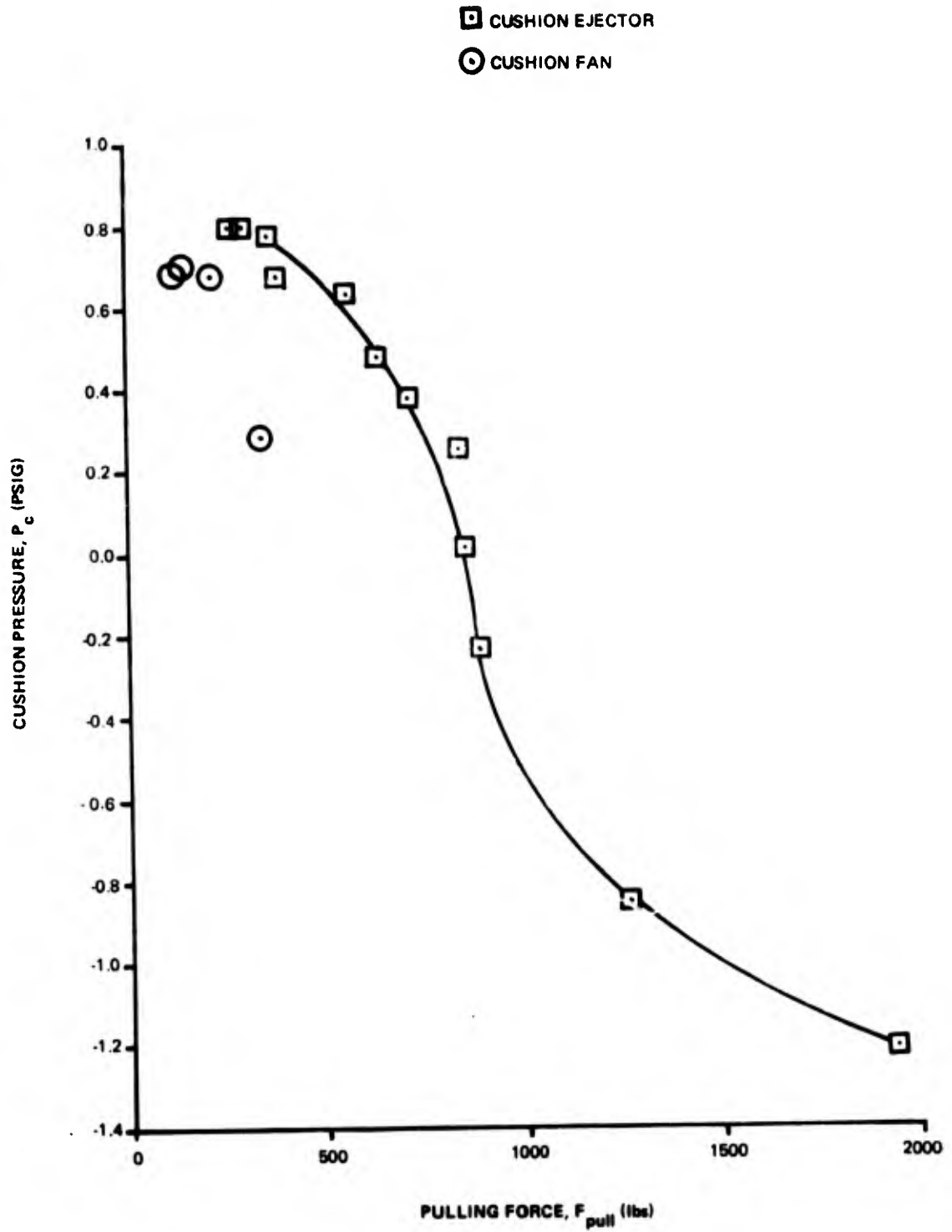


Figure 29. Trunk Drag Versus Cushion Pressure.

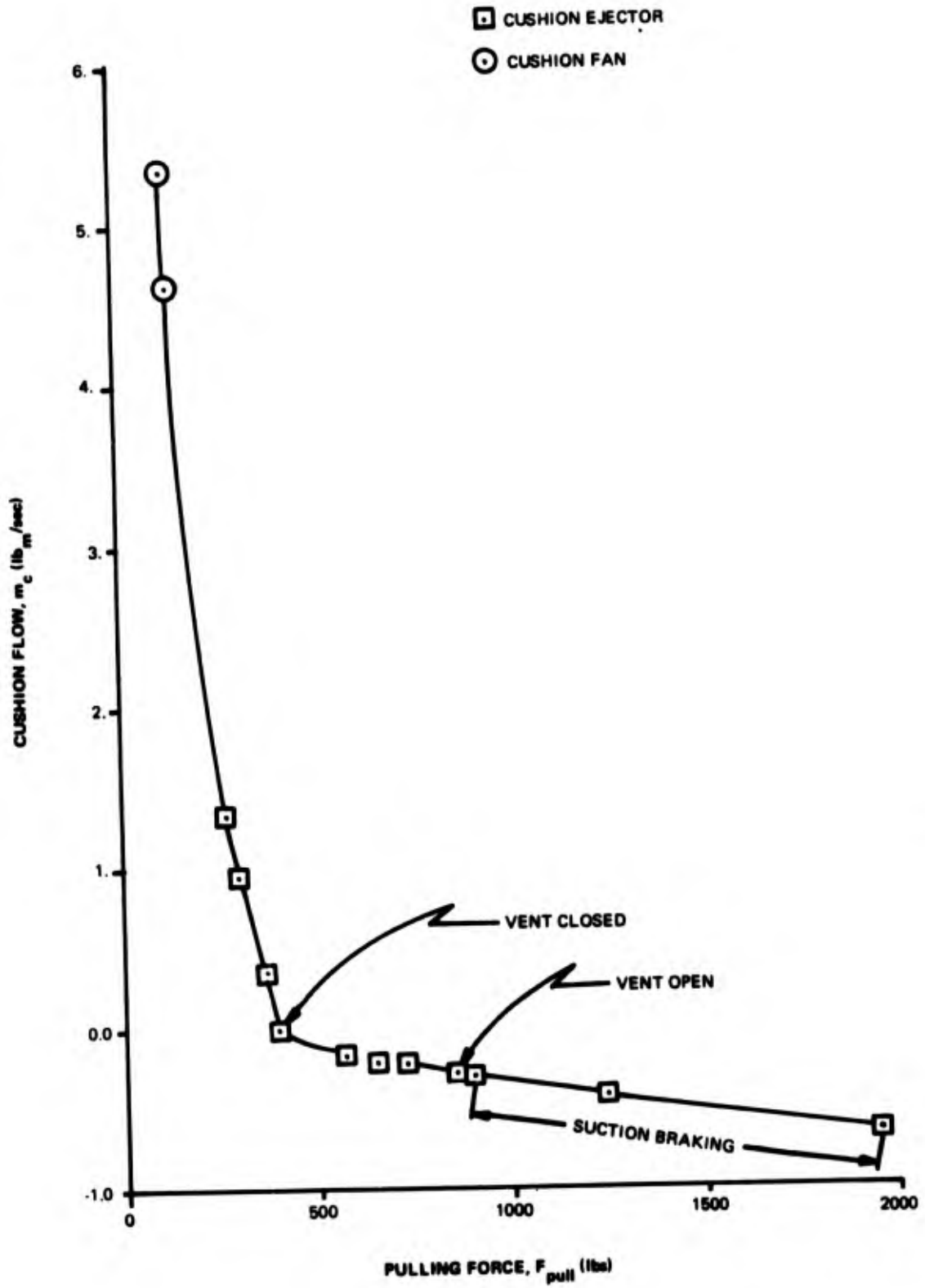


Figure 30. Trunk Drag Versus Cushion Flow.

Table 8. Pull Test Data.

| Test No. | Measured Data | | | | Calculated Data | | | | |
|---------------------------------------|---|------------------|---------------|---------------|---------------------------|---------------------------|-------------------|--------------------------------|--------------------------------|
| | Pull Force F_{pull} lb _f | P_{cp} psig | P_c psig | P_t psig | $\frac{m_c}{lb_m}$ sec | $\frac{m_t}{lb_m}$ sec | $\frac{W_t}{W_a}$ | $\mu_t = \frac{F_{pull}}{W_t}$ | $\mu_a = \frac{F_{pull}}{W_a}$ |
| Cushion Ejector Over Smooth Floor | | | | | | | | | |
| 109 | 1950 | -22. | -1.21 | 2.3 | -0.65 | 0.47 | 2.1 | 0.37 | 0.78 |
| 106 | 1270 | -14. | -0.85 | 2.3 | -0.42 | 0.44 | 1.8 | 0.28 | 0.51 |
| 105 | 900 | -4.8 | -0.23 | 2.2 | -0.30 | 0.55 | 1.2 | 0.30 | 0.36 |
| 91 | 965 | open | 0.02 | 2.0 | -0.28 | 0.72 | 0.98 | 0.35 | 0.35 |
| 92 | 850 | 1.9 | 0.26 | 1.9 | -0.27 | 0.80 | 0.76 | 0.45 | 0.34 |
| 97 | 725 | 3.4 | 0.38 | 1.7 | -0.22 | 0.95 | 0.64 | 0.45 | 0.29 |
| 98 | 650 | 4.2 | 0.48 | 1.7 | -0.20 | 0.98 | 0.55 | 0.47 | 0.26 |
| 93 | 568 | 6.0 | 0.64 | 1.7 | -0.15 | 1.01 | 0.40 | 0.57 | 0.23 |
| 90 | 393 | closed | 0.68 | 1.7 | 0.00 | 1.00 | 0.36 | 0.44 | 0.16 |
| 94 | 373 | 12. | 0.78 | 1.6 | 0.37 | 1.06 | 0.27 | 0.56 | 0.15 |
| 95 | 300 | 20. | 0.80 | 1.6 | 0.97 | 1.07 | 0.25 | 0.48 | 0.12 |
| 96 | 268 | 29. | 0.80 | 1.6 | 1.34 | 1.06 | 0.25 | 0.43 | 0.11 |
| Cushion Fan Over Smooth Floor | | | | | | | | | |
| 149 | 345 | 51. | 0.29 | 1.6 | 0.0-1.8 | 0.9 | 0.73 | 0.19 | 0.14 |
| 149 | 225 | 100. | 0.67 | 1.5 | 0.0-2.9 | 1.0 | 0.37 | 0.24 | 0.09 |
| 149 | 155 | 144. | 0.69 | 1.4 | 2.7-4.2 | 1.05 | 0.35 | 0.18 | 0.06 |
| 149 | 135 | 193. | 0.68 | 1.4 | 4.2-4.9 | 1.05 | 0.36 | 0.15 | 0.05 |
| 149 | 122 | 241. | 0.68 | 1.4 | 5.1-5.6 | 1.05 | 0.36 | 0.13 | 0.05 |
| Cushion Ejector Over Floor With Slats | | | | | | | | | |
| 104 | 1580 | closed | 0.05 | 1.8 | 0.0 | 0.92 | 0.95 | 0.66 | 0.63 |
| 101 | 1520 | open | 0.05 | 1.8 | <0. | 0.99 | 0.95 | 0.64 | 0.61 |
| 103 | 1400 | 27. | 0.14 | 1.8 | 1.4 | 0.95 | 0.87 | 0.64 | 0.56 |
| 102 | 1360 | 13. | 0.11 | 1.8 | 0.9 | 0.93 | 0.90 | 0.61 | 0.54 |

- NOTES: 1. $W_a = 2500$ lb.
 2. $A_c = 2346$ sq. in.
 3. $\mu_m = 0.61$
 4. Negative values of P_{cp} indicate ejector was reversed.

The minimum possible W_t for the drag configurations tested ($x_{cp} = 9.0$ inches and $x_t = -44.85$ inches) is $0.20 W_c$. Therefore $W_{t_{min}}$ is 16.7% of W_a or 417 lbs. The corresponding maximum P_c is 0.89 psig for the 2500 lb aircraft ($A_c = 2346$ sq. in.). The minimum W_t calculated from the pull test data was 625 lbs and the corresponding maximum P_c measured was 0.80 psig.

In conclusion, the results suggest that the trunk drag could be reduced to zero if the CG were positioned above the CP and if the trunk flutter were suppressed.

4.F. Roll Damping.

The first portion of these tests consisted of increasing the cushion flow (configurations 1, 2, 3, and 4) to determine its effect on roll damping (tests 56, 55, 58, and 85 respectively). The damped natural frequency decreased as the flow increased ($f_d = 0.29, 0.26, 0.24,$ and 0.21 cps, respectively). The damping ratio showed no clear dependence on cushion flow rate ($\zeta = 0.057, 0.066, 0.069,$ and 0.067 , respectively).

The dynamic roll stiffness results were found to agree with the static roll stiffness data. In both cases the stiffness decreased as the trunk pressure decreased (or cushion flow increased) such that $k_\phi = 70, 53, 48,$ and 36 ft lb/deg, respectively. The roll damper coefficient showed no clear dependence on cushion flow since C_ϕ equaled $4.3, 4.4, 4.3,$ and 3.7 ft lb_f sec/deg, respectively.

The second portion of the roll damping tests involved a preliminary evaluation of the ability of the roll thrusters to increase the roll damping ratio. The thrust from both wing tip thrusters was pointed down when the aircraft was hovering with the wings level. The signal from the wing tip linear height transducer was used to control the thruster solenoids. The feedback circuit was adjusted so that the differential thrust was zero when the wing tip was level and a maximum when the wing tip was some selected distance from its equilibrium position.

Maximum differential thrusts of 22 and 34 lbs were used and the feedback control was varied to have these maximum thrust differentials occur at 13, 8, 6, and 3 inches wing tip deflection from equilibrium. With 22 lbs thrust, the highest damping ratio (0.13) occurred when maximum thrust was reached at 3 inches deflection. With 34 lbs thrust however, the highest damping (0.20) occurred when maximum differential thrust was reached at 6 inches wing tip deflection from the level position.

These damping ratios are not the optimum that could be achieved. When the right wing tip was lower than equilibrium, the trunk control was simply set to help level the wings. Therefore as the right wing was moving upwards toward equilibrium, the thruster was accelerating the wing — which increased the overshoot. A better control logic would be to have the thrusters resist the direction of motion when the wing tip is moving away from a level position, and to give zero differential thrust when the wing tip is moving towards a level position. Figure 31 shows a comparison of the damping achieved with no thrusters versus when the wing tip thrusters were used.

A sample calculation for damping ratio is given in Appendix B.

4.G. Pitch Damping.

The first four configurations were tested to determine what effect an increase in cushion flow had on the pitch damping characteristics (tests 59, 60, 61, and 86). The damped natural frequency decreased as the flow increased ($f_d = 1.05, 0.99, 0.92,$ and 0.87 cps, respectively). The damping ratio, however, showed no clear dependence ($\zeta = 0.046, 0.051, 0.038, 0.050$, respectively).

The dynamic pitch stiffness decreased as the flow increased ($k_\Theta = 1370, 1225, 1065,$ and 953 ft respectively). This result was in contrast to the static pitch stiffness which appeared to be independent of cushion flow rate. The pitch damper coefficient showed no clear dependence on flow rate ($C_\Theta = 19, 20, 14,$ and 17 ft lb sec/deg, respectively).

In summary, the pitch and the roll damping tests showed that an increase in cushion flow (and a resulting decrease in trunk pressure) caused both the frequency of oscillation and the stiffness to decrease.

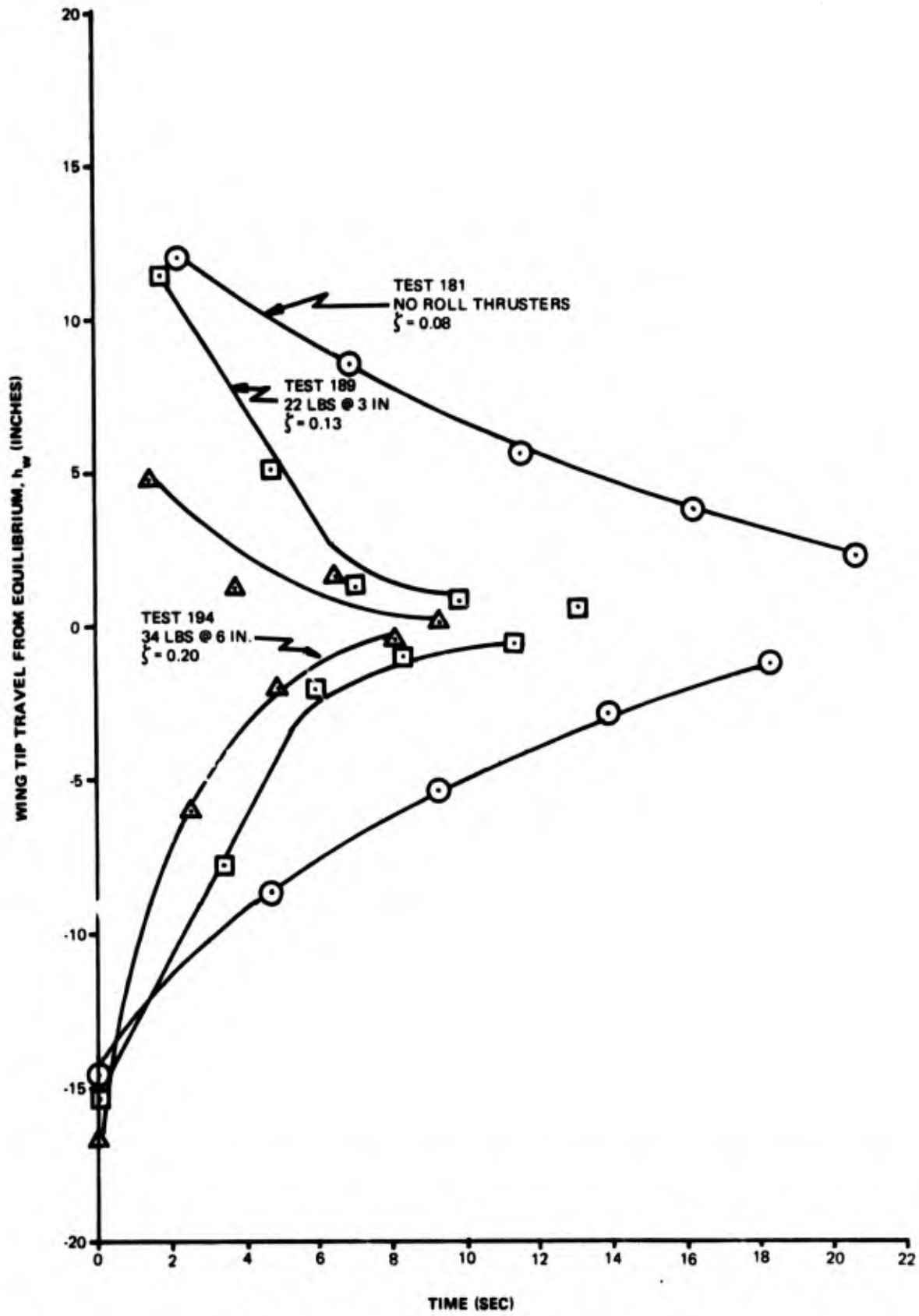


Figure 31. Roll Damping Improvement Using Thrusters.

4.H. Heave Damping Drop Tests.

A total of 28 heave damping drop tests were conducted with the aircraft CG moved forward to approximately coincide with the trunk CP. Seven different configurations were used and peak sink speeds from zero up to 8 ft/sec were tested. The sink speeds were limited to 8 ft/sec (approximately no-flare approach sink speed of Jindivik) to prevent a possible overstressing of the wings. The 550 lb wing assembly was vibrating during free fall at 4.6 cps with ± 2.9 g accelerations at the wing tip (g_w), and was stressed further by the impact. This wing vibration does not simulate the actual landing conditions since the wings will be fully loaded and not vibrating during a normal landing approach with forward speed.

The present Jindivik aircraft is designed to absorb a peak load of 11,000 lbs from the landing skid. Therefore it has been assumed that at 2470 lbs, the aircraft can tolerate a 4.5 g upward load ($g_{cg}+1$) from the ACRS. The peak loads measured near the aircraft CG varied with peak sink speed and with configuration. A summary of the peak acceleration (g_{cg}) for the 28 tests is shown in Table 9.

There were relatively small but consistent differences in peak accelerations for the seven configurations. Configurations 1, 3, and 4 all reached the same peak acceleration at 4.8 fps sink speed – independent of the amount of flow provided by the cushion ejector.

Table 9. Peak Acceleration at CG During Drop Tests (max. g_{cg} reading).

| Trunk Air | Ejector | Ejector | Ejector | Ejector | Ejector | Ejector | Direct |
|--------------------------------|--------------|--------------------------|--------------------------|----------------|-------------------------|-------------------------|-------------------------|
| Cushion Air | Vent Open | Ejector $P_{cp}=12.5$ | Ejector $P_{cp}=30.4$ | Vent Closed | Tip Fan $P_{cp}=104$ | Tip Fan $P_{cp}=104$ | Tip Fan $P_{cp}=104$ |
| Relief Valve | - | - | - | Yes | - | Yes | Yes |
| Config. No. | 1 | 3 | 4 | 6 | 7 | 8 | 9 |
| Peak Sink speed (ft/sec) | | | | | | | |
| 0.0 | | | | 0.2 | | | |
| 1.0 | | | | | | | 0.4 |
| 3.1 | | | | 0.8 | 0.9 | 0.7 | 0.5 |
| 4.1 | | | | 1.0 | 1.2 | 1.0 | |
| 4.8 | 1.5 | 1.5 | 1.5 | 1.5 | 1.6 | 1.3 | 1.1 |
| 6.0 | | | | 2.0 | 2.0 | 1.7 | 1.4 |
| 6.9 | | | | 2.1 | 2.4 | 2.0 | 1.9 |
| 7.8 | | | | | | 2.4 | 2.3 |

The use of the trunk pressure relief valve helped lower the peak loads by 20% when an ejector was used to supply the air to the trunk (configuration 7 vs. 8).

When the trunk flow was supplied with a direct air supply (configuration 9), the pressure relief valve was essential to prevent trunk overpressure. The system using direct trunk flow plus a relief valve gave lower peak loads than the use of an ejector with or without a relief valve. The ejector, however, was providing more air flow to the trunk.

With regard to minimizing peak loads, there appeared to be no clearly best system for a cushion air supply. Vent open, vent closed, ejector, and fan systems gave similar results.

A summary of the peak load-stroke data is given in Table 10. By assuming that the cushion area remained at a constant value of 2346 sq in, the % of the peak load carried by the cushion ($P_c A_c$) and the peak trunk footprint, A_t , could be estimated. For this low flow ACRS, the peak cushion load was usually only 33 to 45% of the total ACRS load. The remainder of the load was created by the trunk flattening against the landing surface. At about 8 fps sink speed, the peak trunk footprint area was approximately equal to the maximum tread area on the trunk. At sink speeds above 8 fps, the trunk loads may not increase as quickly because the footprint area would have reached its maximum value. If further trunk flattening occurred, the lightweight trunk material itself might contact the landing surface unless the trunk were protected with a larger tread area.

The peak vertical trunk load was usually 55 to 67% of the peak ACRS load. For example, at a peak sink speed of 6.9 ft/sec, the trunk load reached peak values of 4500, 5700, 4400, and 4400 lbs for configurations 6, 7, 8, and 9 respectively. The 5700 lb load for configuration 7 was unusually high and probably was caused by the fact that configuration 7 was the only one of the four that did not use a trunk pressure relief valve.

This peak trunk load can be related to the peak nose down pitching moment if the effective trunk coefficient of friction (μ_t) is known between the brake tread and the landing surface. There is however, very little information available about the effective coefficient of friction at landing because the impact is a highly non-equilibrium event which involves varying amounts of air flow "lubrication," and also because the landing surface itself can have a wide variety of characteristics — from dry concrete to mud. The pull test data showed that the breakaway trunk friction coefficient for this ACRS operating in equilibrium on a smooth plywood floor averaged 0.47 with a low-flow cushion ejector and reduced to 0.18 for a higher flow cushion fan system. The friction coefficient for the tread material (μ_m) without any air flow nozzles was 0.61 on the plywood.

Since the peak trunk upward force is identical to the peak downward load on the skid brake material, the peak horizontal drag force for a trunk load of 5700 lbs would be between 1000 and 2700 lbs if the effective trunk friction coefficient at impact was between 0.18 and 0.47. Since even the peak cushion pressure with the cushion vent open (configuration 1) reached 0.6 psig, it could be possible that the peak impact friction coefficient is low (roughly 0.2), while the equilibrium slideout coefficient (cushion vented) is two times higher (roughly 0.4). If this were true, then the peak impact drag (for $W_t = 5700$ lbs) would be about 1150 lbs and the slideout drag (for $W_t = 2500$ lbs) would be about the same (1000 lbs). The effect of aerodynamic lift with pitch angle must also be considered for a more complete analysis.

The moment arm for the horizontal brake drag about the aircraft CG (z_{cg}) is approximately 2.9 ft when the aircraft is at a hover height of 11.6 inches (Figure 38). Therefore, for a peak trunk load at impact of 5700 lbs, the effective moment arm is 2.6 ft and the peak nose down pitching moment created by ACRS drag is between 2600 and 7000 ft-lbs (for μ_t of 0.18 to 0.47 respectively).

Table 10. Summary of Heave Damping Drop Test Results
(Load - Stroke Data)

| Config. No. | Peak V_{sink} fps | Test No. | Peak Accel. a_{cg} | Peak P_t psig | Peak P_c psig | Min. h_{cg} in. | Max. Stroke Below Hover in. | Peak ACRS Load l_b | Max. Valve Stroke s_v in. | Peak A_t sq. in. | % Max. Load On Cushion |
|-------------|----------------------------|----------|-----------------------------|-----------------|-----------------|--------------------------|-----------------------------|----------------------|-----------------------------|--------------------|------------------------|
| 1 3 4 | 4.8 | 123 | 1.5 | 2.67 | 0.6 | 9.6 | 2.8 | 6250 | 0.0 | 1810 | 23 |
| | 4.8 | 122 | 1.5 | 2.46 | 1.2 | 9.6 | 2.6 | 6250 | 0.0 | 1390 | 45 |
| | 4.8 | 121 | 1.5 | 2.45 | 1.1 | 10.6 | 1.9 | 6250 | 0.0 | 1500 | 41 |
| 6 | 0.0 | 129 | 0.2 | 1.64 | 0.7 | 11.2 | 0.2 | 3000 | 0.0 | 830 | 55 |
| | 3.1 | 130 | 0.8 | 2.13 | 0.7 | 9.7 | 2.3 | 4500 | 1.02 | 1340 | 37 |
| | 4.1 | 131 | 1.0 | 1.97 | 0.8 | 8.9 | 3.0 | 5000 | 1.09 | 1580 | 38 |
| | 4.8 | 132 | 1.5 | 2.00 | 1.0 | 8.6 | 3.6 | 6250 | 1.20 | 1950 | 38 |
| | 6.0 | 133 | 2.0 | 2.30 | 1.2 | 7.1 | 4.5 | 7500 | 1.24 | 2030 | 38 |
| | 6.9 | 134 | 2.1 | 2.37 | 1.4 | 7.7 | 4.6 | 7750 | 1.41 | 1880 | 42 |
| 7 | 3.1 | 136 | 0.9 | 2.07 | 0.7 | 10.0 | 2.2 | 4750 | 0.0 | 1500 | 35 |
| | 4.1 | 137 | 1.2 | 2.16 | 0.8 | 9.7 | 2.4 | 5500 | 0.0 | 1680 | 34 |
| | 4.8 | 138 | 1.6 | 2.30 | 1.0 | 8.7 | 3.3 | 6500 | 0.0 | 1800 | 36 |
| | 6.0 | 139 | 2.0 | 2.45 | 1.1 | 8.6 | 3.7 | 7500 | 0.0 | 2010 | 34 |
| | 6.9 | 140 | 2.4 | 2.56 | 1.2 | 8.3 | 4.3 | 8500 | 0.0 | 2220 | 33 |
| 8 | 3.1 | 141 | 0.7 | 1.82 | 0.8 | 10.3 | 2.0 | 4250 | 1.00 | 1300 | 44 |
| | 4.1 | 142 | 1.0 | 1.99 | 0.9 | 9.4 | 2.5 | 5000 | 1.08 | 1450 | 42 |
| | 4.8 | 143 | 1.3 | 1.97 | 0.9 | 8.9 | 3.3 | 5750 | 1.17 | 1850 | 37 |
| | 6.0 | 144 | 1.7 | 2.23 | 1.2 | 7.1 | 4.1 | 6750 | 1.28 | 1760 | 42 |
| | 6.9 | 145 | 2.0 | 2.34 | 1.3 | 6.5 | 4.7 | 7500 | 1.35 | 1900 | 41 |
| | 7.8 | 146 | 2.4 | 2.58 | 1.3 | 6.0 | 5.6 | 8500 | 1.35 | 2110 | 36 |
| | 7.8 | 147 | 2.3 | 2.59 | 1.2 | 6.2 | 5.3 | 8250 | unk | 2100 | 34 |
| | 7.8 | 150 | 2.5 | 2.36 | 1.4 | 5.5 | 5.5 | 8750 | 1.45 | 2320 | 38 |
| 9 | 1.0 | 154 | 0.4 | 1.65 | 0.8 | 11.1 | 0.6 | 3500 | 0.0 | 980 | 54 |
| | 3.1 | 155 | 0.5 | 2.00 | 0.8 | 10.0 | 2.1 | 3750 | 1.15 | 935 | 50 |
| | 4.8 | 156 | 1.1 | 2.17 | 0.9 | 8.8 | 3.3 | 5250 | 1.28 | 1450 | 40 |
| | 6.0 | 157 | 1.4 | 2.23 | 1.1 | 8.2 | 4.0 | 6000 | 1.37 | 1530 | 43 |
| | 6.9 | 158 | 1.9 | 2.35 | 1.2 | 7.2 | 4.8 | 7250 | 1.45 | 1880 | 39 |
| | 7.8 | 159 | 2.3 | 2.41 | 1.3 | 6.9 | 5.0 | 8250 | 1.50 | 2160 | 37 |

Figure 32 shows how six of the load-stroke parameters from Table 10 vary with peak sink speed. Configuration 9 was the "softest" system while configuration 7 gave the highest peak loads. The maximum stroke used by configuration 7 was slightly shorter than for configuration 9, therefore the load-stroke efficiency was about the same for all configurations.

The peak cushion pressures were found to be approximately the same for a given sink speed - regardless of whether the air supply system used an ejector, fan, or vent open.

The cushion pressure also reached peak negative values (pressures less than ambient) on several drop tests. For example, during test 121 (configuration 4 at 4.8 fps sink speed) the cushion pressure reached -0.39 psig near the top of the first "bounce" or heave cycle and -0.20 psig near the top of the second cycle.

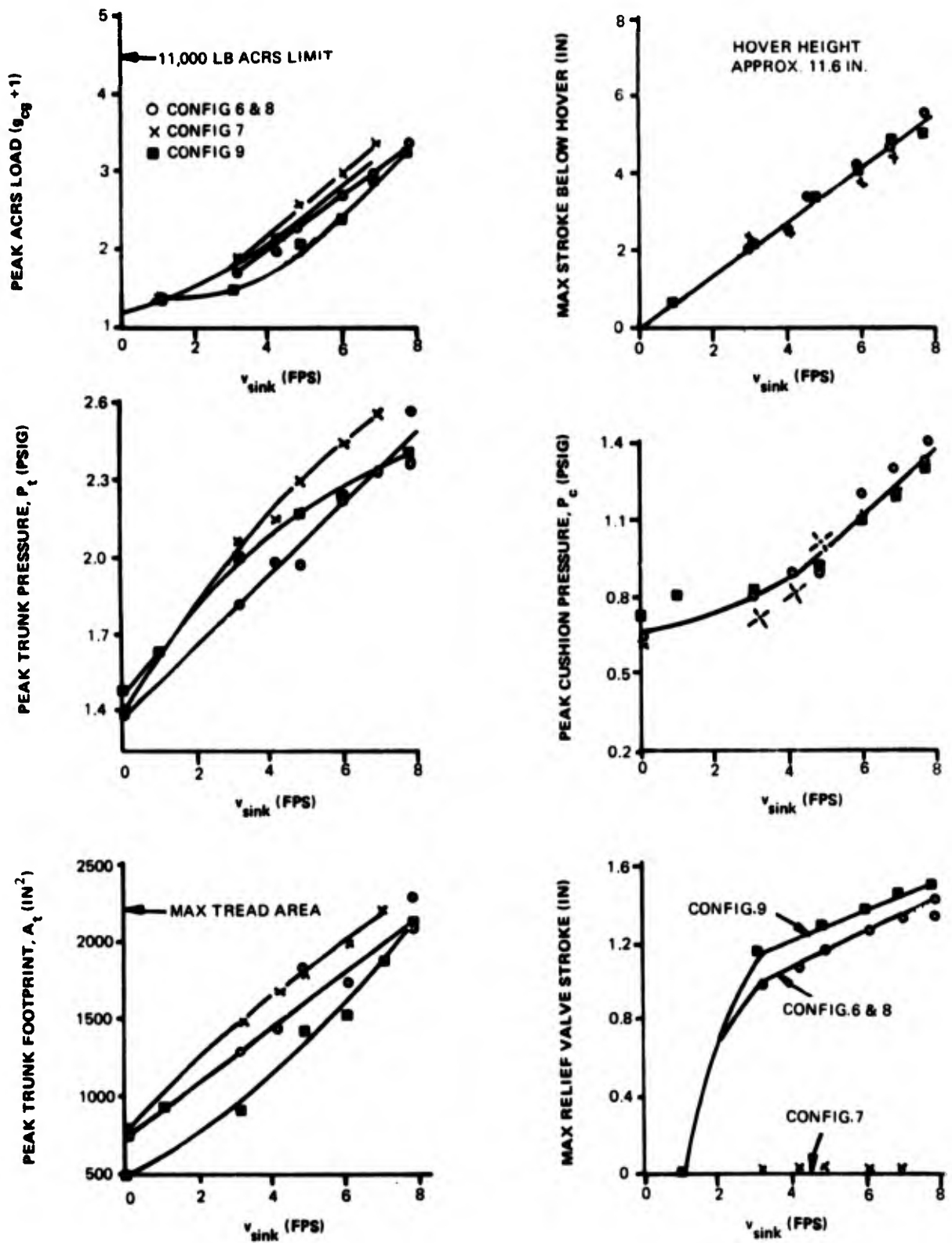


Figure 32. Peak Load-Stroke Conditions Versus Sink Speed.

The trunk pressure relief valve operated reliably and consistently for 20 drop tests. The rate at which the valve opened depended on how fast the trunk pressure increased. For direct bleed, the valve reached a one inch stroke only 0.044 sec after it cracked open (test 159); while for an identical sink speed test but with a trunk ejector, the valve reached a one inch stroke 0.06 sec after it began opening (test 146). If the trunk pressure acted uniformly over the valve orifice plate, then the valve stroke would ideally be a linear function of the trunk pressure. The drop test data consistently showed however; that the valve started opening before its design cracking pressure of 1.71 psig, and after about 0.75 inches of stroke the valve opening became less sensitive to trunk pressure (Figure 33). When the stroke goes beyond 0.75 inches, the flow through the relief valve increases rapidly and the average pressure across the valve face is less than the trunk pressure.

The shape of the load-stroke curve for these tests was found to be nearly triangular (50% efficiency). The load-stroke curve for test 146 is shown in Figure 34. The load built up for about 3.5 inches before reaching the hover height and then continued to build up until the downward motion was stopped at 5.6 inches below the hover height. At the hover height, the upward load was 3000 lbs instead of the equilibrium value of 2500 lbs. These loads are nearly the same because the cushion pressure during this drop test only reached 63% of its usually equilibrium value when at the hover height of 11.6 inches.

The peak sink speed reached during test 146 was approximately 7.6 ft/sec. The velocity was zero when the aircraft was released from a height (h_{cg}) of 24.1 inches (time, $t = 0.0$). The aircraft fell at -1 g acceleration until it entered ground effect at a height of 15.1 inches and a sink speed of 7.0 ft/sec ($t = 0.221$ sec). Once in ground effect the aircraft acceleration decreased until it passed through zero g at a height of 12.1 inches. At this time (0.259 sec) the sink speed had reached its peak of about 7.6 ft/sec. The aircraft continued to slow down, passing through a peak 2.36 g acceleration, and finally reaching zero sink speed at a height of 6.0 inches ($t = 0.378$ sec).

The total energy under the load-stroke curve is 3181 ft lbs, which is more than the 2242 ft lbs associated with the estimated 7.6 ft/sec peak speed, but less than the 3771 ft lbs associated with a total height change of 18.1 inches. This apparent loss of 590 ft lbs potential energy may be accounted for by the energy transmitted to the flexible wing assembly - which was oscillating at ± 2.8 g before impact and ± 5.2 g after impact. If the load-stroke efficiency were based upon the potential energy instead of the energy into the aircraft fuselage, then the efficiency would be nearly 60% instead of 50%.

A typical visicorder run record (for drop test no. 146) is shown in Figures 35 and 36. During the test, the visicorder paper speed was run at 0.4 in/sec. This enabled an entire drop test to be recorded in a short length. From this overall picture (Figure 35), the parameter values at release and at hover could be easily shown, as well as the damping oscillations.

After the drop test, the tape recorder was rewound and the data was played back with a paper speed of 10.0 inches per second. This record (Figure 36) allowed a close inspection of how the various parameters varied with time during the first bounce or cycle.

The heave damping characteristics were calculated from the drop test data using the same techniques used to determine the pitch and roll damping. The heave damping was found to be very good. The aircraft heave oscillation damped out in 1.5 to 3 cycles.

At the end of 1.5 to 3 cycles the frequency of oscillation was found to abruptly decrease from approximately 2 cps to less than 1 cps. This abrupt frequency reduction occurred on all 26 heave damping drop tests. An important conclusion can be drawn from this result. When the aircraft impacts the landing surface, the heave damping is very high and therefore the vertical motions of the aircraft CG are well damped within 0.75 to 1.5 seconds. The aircraft will then abruptly switch to a pitch damping motion and

- TEST 132
- TEST 134
- ◇ TEST 142
- ⊕ TEST 146
- ⊙ TEST 156
- × TEST 159

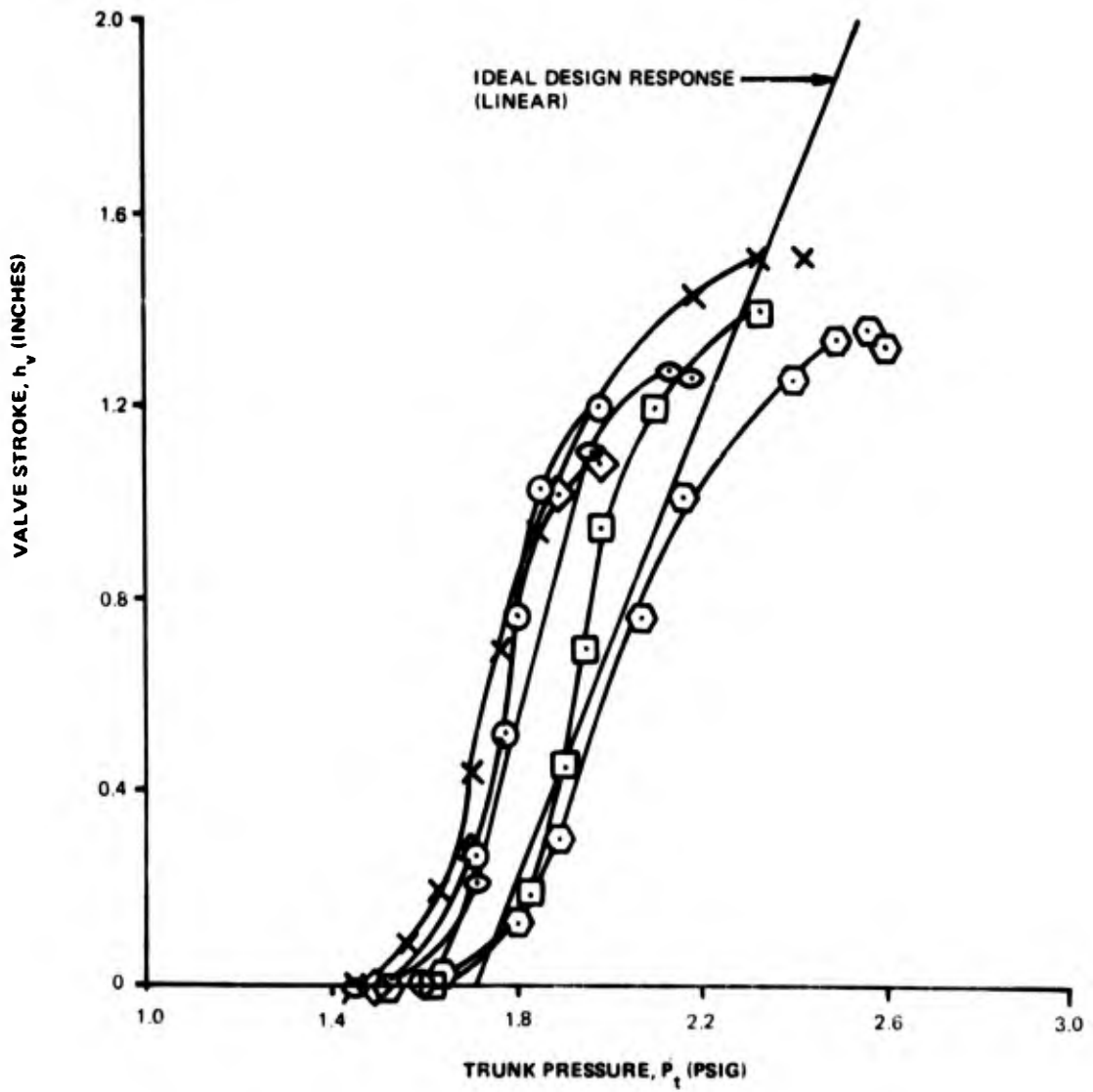


Figure 33. Pressure Relief Valve Response.

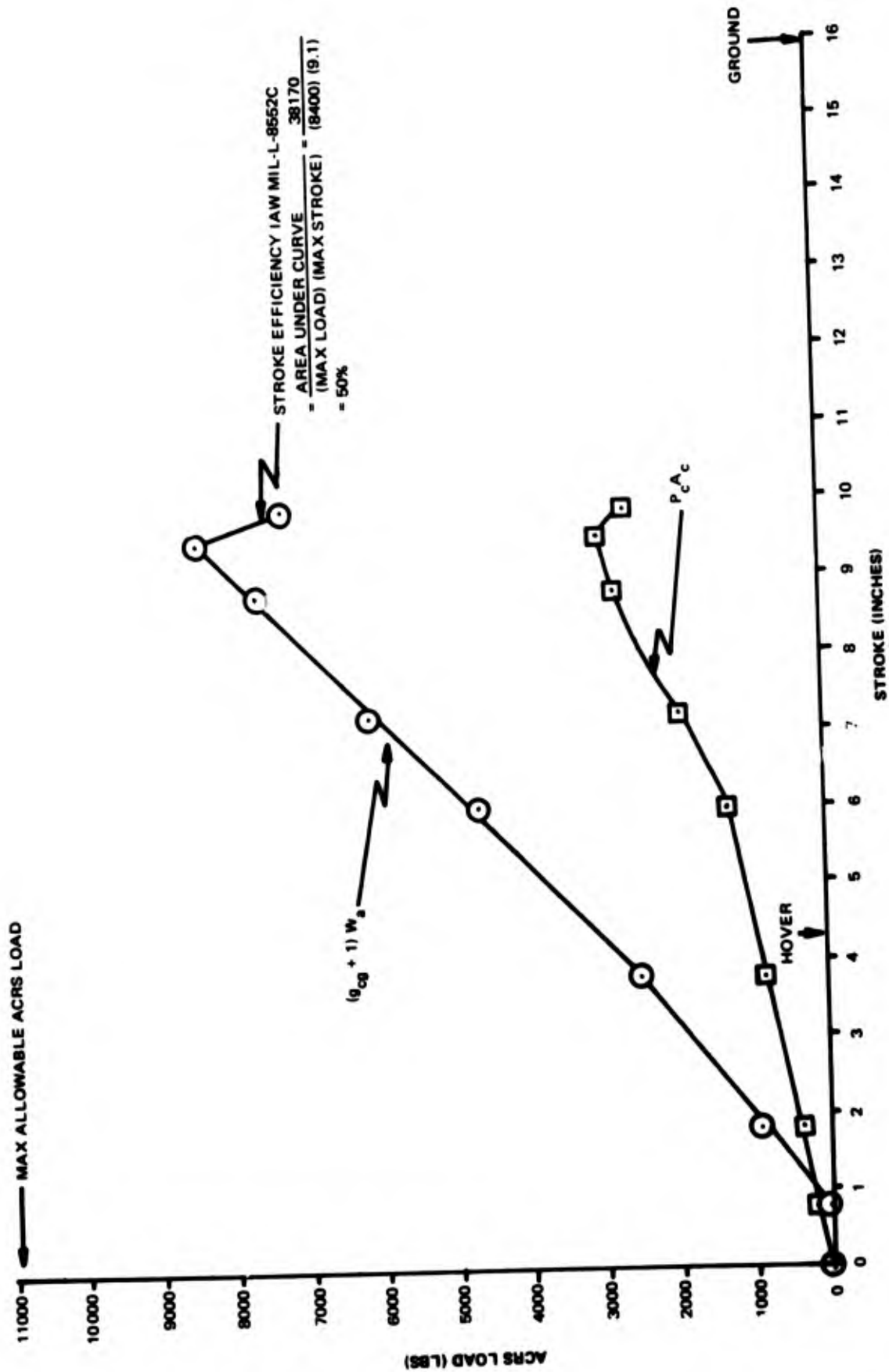


Figure 34. Load-Stroke Curve.

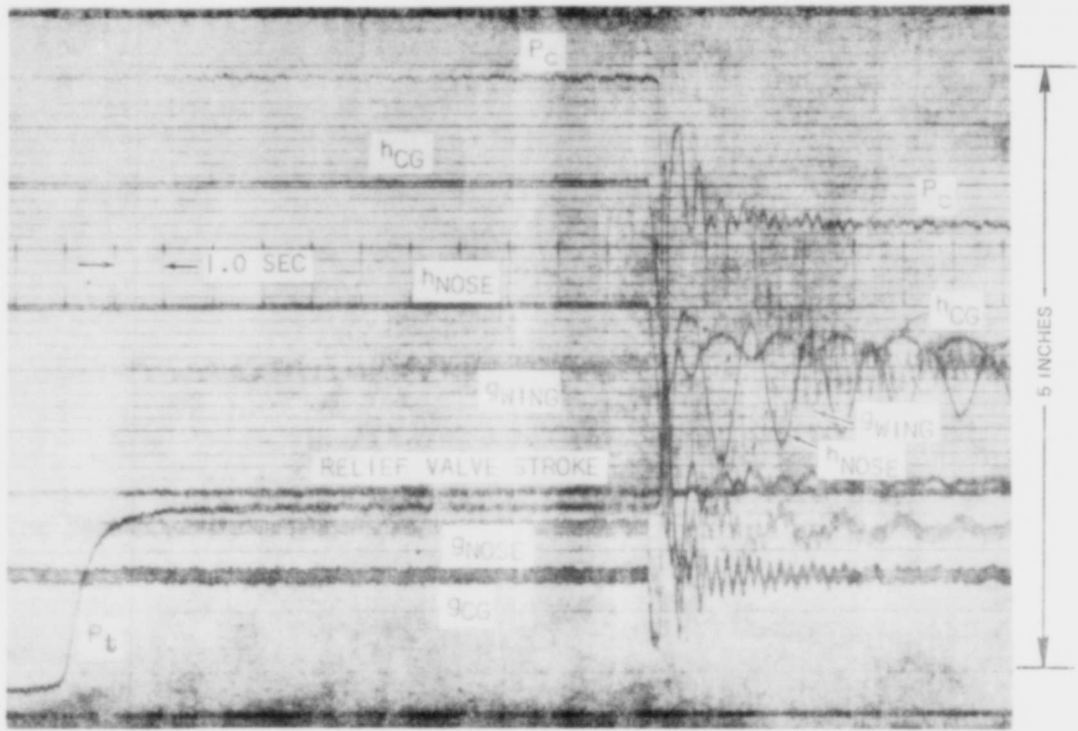


Figure 35. Drop Test Visicorder Record, 0.40 ips.

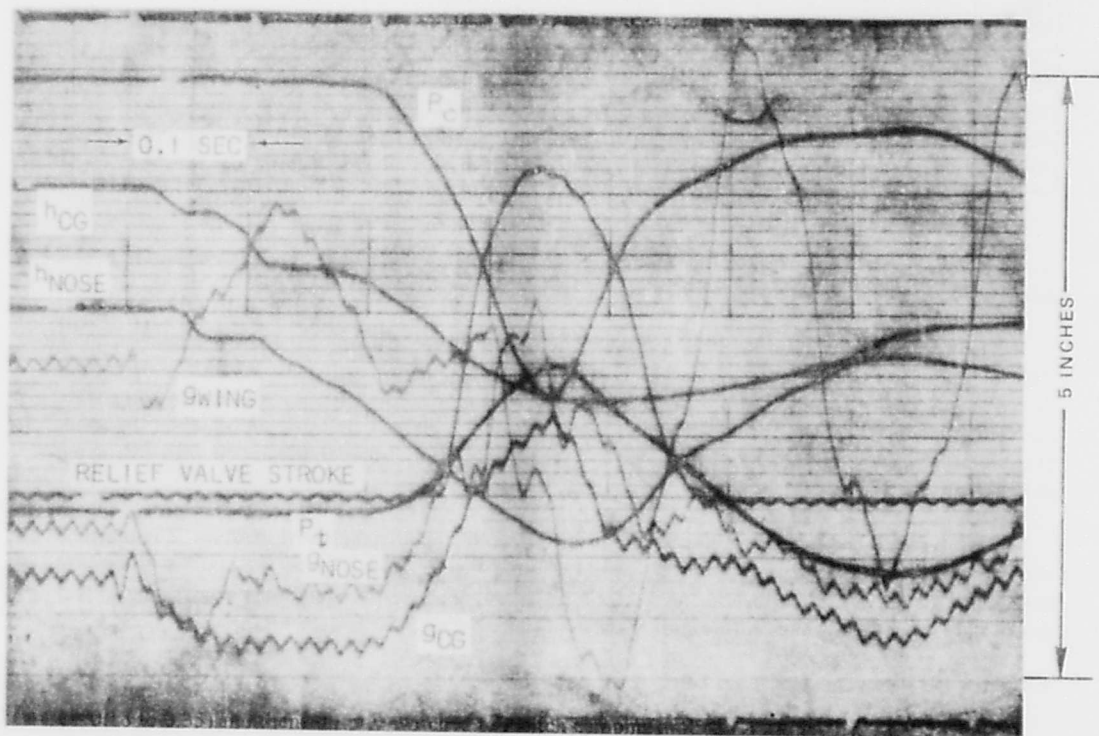


Figure 36. Drop Test Visicorder Record, 10 ips.

Table 11. Heave Damping Data.

| Test No. | Config. No. | Peak Sink Speed (fps) | Damped Natural Freq. F_d (cps) | No. of Heave Cycles Comp. | Damping Ratio ζ | Dynamic Heave Spring Coefficient k_h (lb/inch) | Heave Damper Coefficient C_h (lb sec/in) |
|----------|-------------|-----------------------|----------------------------------|---------------------------|-----------------------|--|--|
| 123 | 1 | 4.8 | 2.0 | 1.5 | 0.27 | 1100. | 46. |
| 122 | 3 | 4.8 | 2.1 | 3 | 0.18 | 1130. | 31. |
| 121 | 4 | 4.8 | 2.1 | 3 | 0.18 | 1130. | 31. |
| 132 | 6 | 4.8 | 2.2 | 1.5 | 0.35 | 1350. | 65. |
| 138 | 7 | 4.8 | 1.9 | 1.5 | 0.20 | 980. | 31. |
| 143 | 8 | 4.8 | 1.9 | 1.5 | 0.31 | 1050. | 51. |
| 156 | 9 | 4.8 | 1.9 | 1.5 | 0.27 | 1000. | 43. |
| 155 | 9 | 3.1 | 2.0 | 1.5 | 0.28 | 1150. | 49. |
| 159 | 9 | 7.8 | 1.7 | 1.5 | 0.30 | 800. | 43. |

continue the slideout and deceleration while oscillating in pitch at roughly 1 cps. The magnitude of the pitch oscillations depends on how well the pitching moments are balanced at impact.

The heave damping ratio was found to be 4 to 7 times higher than the usual pitch damping ratio of 0.05, depending on configuration. Table 11 shows how the 4 damping parameters varied with configuration for a constant peak sink speed of 4.8 fps. The effect of varying peak sink speed is also shown in the table for configuration 9. The heave damping ratio was noticeably increased (0.27 or above) when the trunk pressure relief valve was used (configurations 6, 8, and 9). The only other configuration with a damping ratio as high as 0.27 was configuration 1, which used an open vent.

The dynamic heave stiffness was found to be higher than the static heave stiffness. The dynamic stiffness however was calculated from an equation using f_d , W_a , and ζ ; while the static stiffness was determined graphically. Nevertheless, the dynamic pressures are above the equilibrium static values so that one would expect the dynamic stiffness to be higher.

4.1. Pitch and Heave Damping Drop Tests.

A total of 26 drop tests were conducted with the aircraft's CG positioned 9.0 inches aft of the CP. Configurations 1, 2, 3, and 4 were tested at sink speeds up to 6.9 ft/sec.

The peak accelerations and pressures were found to be about the same as measured during the heave damping tests. The natural damped frequency was also found to change abruptly after about 2 cycles from the high heave frequency of nearly 2 cps to the lower frequency of 0.9 cps associated with pitch.

The only major difference found between these tests and the heave damping drop tests was the extremely high pitch angle that was reached after impact due to the unbalanced moments applied. The pitch angle reached maximum values of about 9 degrees for high sink speed tests. At 6.9 fps the tail of aircraft touched the landing surface. These extreme pitch angles would cause the aircraft to bounce on landing due to the lift increase with angle of attack.

Figure 37 shows the change in nose height with time for a sink speed of 5 fps (configuration 3, test 117). The extreme pitch angle of 8.5 degrees illustrates the importance of properly balancing the pitching moments. The nose up moment produced in this laboratory test would be counteracted during an actual landing by the nose down moment created by surface drag. The trunk position (x_{cp}) must be properly selected so as to balance these moments at impact.

The problem that a designer presently faces is that no accurate data exists for the value of μ_t . μ_t was measured during these static laboratory tests and found to be between 0.13 and 0.57 on a smooth plywood floor, depending on \dot{m}_c . Nevertheless, μ_t is not known for a variety of surfaces and with a forward speed of 130 knots. Figure 38 shows that the present selection of $x_{cp} = 9$ inches will balance the impact moments if: $W_c/W_t = 0.25$, $\mu_t = 0.38$, and $y_t = 29.6$ inches.

The basic Jindivik aircraft structure was not damaged during any of the tests. The outer skin of the center fuselage under wing drop panel did buckle slightly however, due to the trunk pressure load. The panel damage would not have any effect on aircraft performance since it is covered by the trunk. The panel should however, be reinforced to prevent damaging its skin.

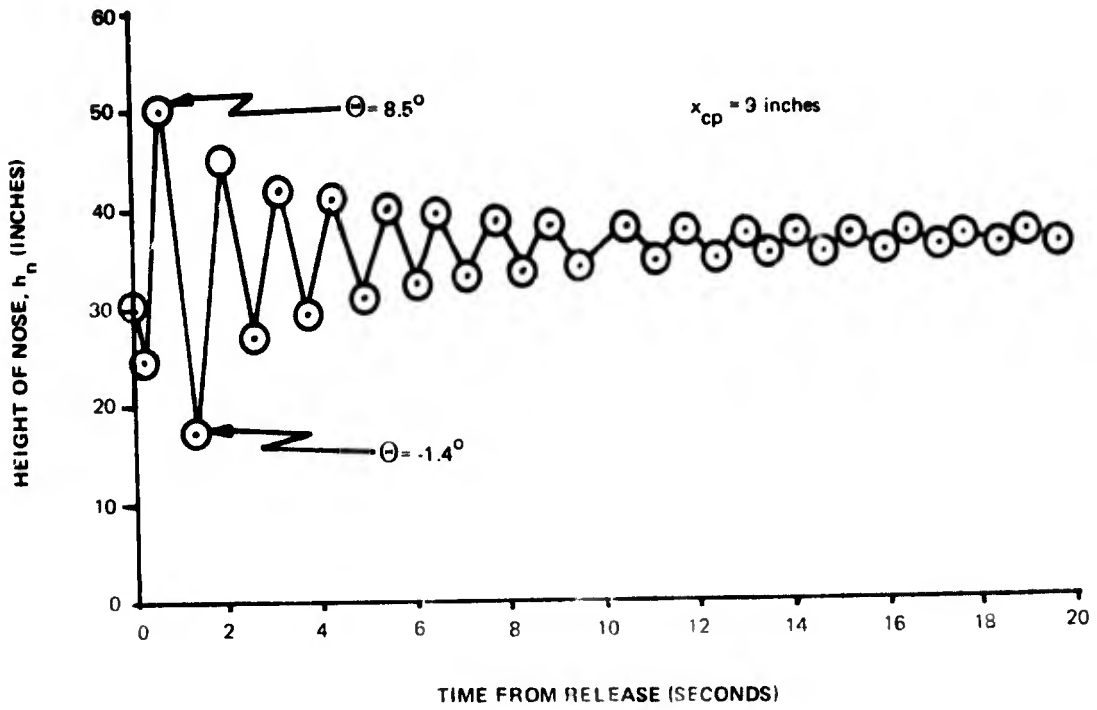
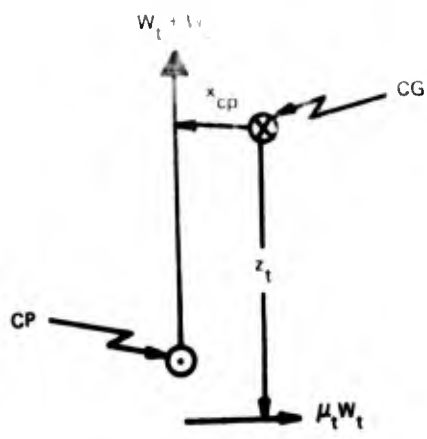


Figure 37. Combined Pitch and Heave Damping.



$$\text{FOR } \sum M_{cg} = 0, \quad x_{cp} = \frac{z_t \mu_t}{\left(1 + \frac{W}{W_t}\right)}$$

Figure 38. Balance of Moments at Impact.

5. CONCLUSIONS

5.A. Static Tests.

The ACRS is a low air flow system and the bottom of the trunk is covered with skid brake material. Different equilibrium positions are therefore possible due to the brakes being "stuck" at slightly different distances outboard from the aircraft centerline. The position depends on how the aircraft was loaded before it reached the new equilibrium condition.

Another difference between the ACRS and ACLS is the effect of P_c on P_t . As P_c decreases towards zero, the trunk pressure increases for an ACRS but decreases for an ACLS.

5.B. Pull Tests.

The brake tread material coefficient of friction (μ_m) over the plywood floor was 0.61. The trunk coefficient of friction (μ_t) was reduced by an air lubricity effect to about 0.4 when approximately 1.0 lb m/sec was supplied through holes in the tread. When about 5 lb m/sec of cushion flow was added with a fan, the added air lubricity decreased μ_t further to about 0.15. The corresponding aircraft coefficient of friction (μ_a) decreased to 0.05, or 125 lbs of drag.

The cushion flow can be reversed to create a suction pressure in the cushion and thereby substantially increase the brake drag or decrease the aircraft stopping distance. When 0.7 lb m/sec was drawn from the cushion area, a pressure of -1.2 psig was achieved and a brake drag equivalent to a 0.8 g aircraft deceleration rate was measured.

The brake drag was very sensitive to cushion flow when \dot{m}_c was negative. When flow was added to the cushion however, the trunk started to flutter and the brake drag became less sensitive to cushion flow.

5.C. Damping Tests.

The ACRS was very well damped in heave. The natural damped frequency was about 2 cps and the damping ratio was between 0.18 and 0.35 - depending on configuration. The roll damping ratio was found to be about 0.065, which is considered fair. The pitch damping was considered poor since the damping ratio was only 0.04 to 0.05.

During all the drop tests, the aircraft first went through 1.5 to 3 cycles of heave damping ($f_d = 2$ cps, $\zeta = 0.18$ to 0.35) and then abruptly switched to a pitch damping motion ($f_d = 0.9$ cps, $\zeta = 0.04$).

5.D. Load-Stroke Response.

The shape of the load-stroke curve was found to be nearly triangular. The stroke efficiency was usually 50 to 60%. The higher efficiency was calculated if potential energy was used instead of the aircraft CG acceleration readings.

At the no-flare Jindivik sink speed of 7.8 fps, the ACRS usually reached 73% of its peak allowable load of 11,000 lbs (3.3 g load versus 4.5 g allowable). The effect of wing lift would be to further reduce this peak ACRS load. At 7.8 fps, the stroke reached 44% of maximum stroke (approximately 5 inches below hover height).

The dynamic heave stiffness was found to be from 30 to 60% higher than the static heave stiffness. The dynamic pitch stiffness was found to be zero to 40% higher than the static stiffness. The dynamic and static roll stiffnesses were found to be the same, because the trunk and cushion pressures remained at equilibrium and only a small amount of energy was input to the system.

The cushion load, W_c , has been defined as the product of cushion pressure and area ($P_c A_c$), although these parameters are difficult to predict. The peak cushion load for this ACRS was estimated to be only 23 to 55% of the total cushion and trunk load (versus over 90% for an ACLS). On several drop tests the cushion load was negative (acted downward) at the top of the first two heave cycles following impact. Peak downward loads were found to be about 900 lbs or 0.4 g.

5.E. Cushion Flow Effects.

The amount of cushion flow added to the small ACRS trunk flow was found to have only a minor effect on peak impact loads. The dynamic pitch stiffness and the roll stiffness were found to decrease, however, as the cushion flow is increased. The amount of cushion flow had a large effect on brake drag for negative flows, but much less effect for high flow rates which caused the trunk to flutter. In general, a large cushion flow rate was found to have no clear advantages for an ACRS.

5.F. Configuration Effects.

The trunk air can be supplied satisfactorily from either an ejector or a combination of direct bleed plus a trunk pressure relief valve. The cushion air is only used to decrease trunk drag for taxi and this is most efficiently supplied by a fan rather than an ejector. The use of a trunk pressure relief valve was found to be beneficial in improving heave damping and limiting the peak loads at impact. The relief valve is required if the trunk is supplied with direct bleed air, but it is optional if the trunk air is supplied from an ejector.

5.G. Test Data Summary.

A brief summary of the test results is given in Table 12. Dynamic response results can be modeled by using equivalent spring and damper coefficients for the air cushion system.

Table 12. Summary of Test Results.

| Parameter | Range of Measured Values |
|---|--|
| hover P_t | 1.39–1.93 psig |
| hover P_c | 0.00–0.76 psig |
| hover h_{cg} | 10.5–12.7 inches |
| hover \dot{m}_t | 0.8–1.3 lbm/sec. |
| hover \dot{m}_c | <0–1.3 lb m/sec. |
| hover brake drag, F_{pull} | 122–1950 lbf |
| hover yaw stiffness, k_ψ | not measured |
| roll stiffness k_ϕ (static & dynamic) | 36–70 $\frac{\text{ft-lb}}{\text{deg.}}$ |
| roll natural damped frequency, $f_{d\phi}$ | 0.21–0.29 cps. |
| roll damping ratio, ζ_ϕ | 0.057–0.069 |
| roll damper coefficient, C_ϕ | 3.7–4.4 $\frac{\text{ft-lb-sec}}{\text{deg.}}$ |
| pitch static stiffness, k_Θ | 980 $\frac{\text{ft-lb}}{\text{deg.}}$ |
| pitch dynamic stiffness, k_Θ | 953–1370 $\frac{\text{ft-lb}}{\text{deg.}}$ |
| pitch natural damped frequency, $f_{d\phi}$ | 0.87–1.05 cps |
| pitch damping ratio, ζ_Θ | 0.038–0.051 |
| pitch damper coefficient, C_Θ | 17–20 $\frac{\text{ft-lb-sec}}{\text{deg.}}$ |
| heave static stiffness, k_h | 725–870 lb/inch |
| heave dynamic stiffness, k_h | 800–1350 lb/inch |
| heave natural damped frequency, f_{dh} | 1.7–2.2 cps |
| heave damping ratio, ζ_h | 0.18–0.35 |
| heave damper coefficient, C_h | 31.–65. lb-sec/inch |
| load-stroke efficiency | 50% |
| peak acceleration at 7.8 fps, g_{cg} | 2.3–2.5g |
| minimum height at 7.8 fps, h_{cg} | 5.5–6.9 inches |

6. RECOMMENDATIONS

A. Since the roll stiffness of the ACRS is low, wing tip skids are needed for roll protection. Wing tip roll thrusters can be useful to increase roll damping and stiffness, but extra bleed air plus long ducting is needed. Therefore, instead of using a "roll to yaw" ground control, examine the effectiveness of a direct yaw control using a jet engine tailpipe flow deflector which operates on the same sidewall pressure control principle as the wing tip roll thruster.

B. Further examine the effectiveness of "suction braking" to dramatically reduce aircraft stopping distance.

C. Since the pitch damping of the present ACRS design is low, carefully examine the effect of trunk location versus aircraft CG location. Additional work is needed on novel configurations to improve pitch damping. One possibility would be a two compartment, fore and aft, "figure eight" trunk shape which uses suction braking in the aft compartment.

D. The trunk brake tread wear during ground taxi and later during landing tests should be carefully observed to insure that an adequate area has been provided.

E. The best ACRS cushion air supply configuration appears to be one which uses no added cushion flow during landing and slideout, but instead uses a vented cushion area. This configuration results in the least variety of impact responses for various landing surfaces, higher stiffness and damping, and the shortest aircraft stopping distance with the simplest configuration. For taxi on the ACRS, a fan appears best to supply the cushion air needed to reduce the brake drag. If suction braking is incorporated, however, then the best device may be a two-way ejector instead of a fan. It may be important to develop ways to reduce ACRS trunk flutter during taxi in order to improve system efficiency.

F. The minimum air flow required for an adequate ACRS landing system may be zero. The tests have shown that an order of magnitude reduction over the airflow used for an ACLS appears to give a very adequate landing-only system. The further reduction from about 1. lb m/sec towards zero will require using low friction tread material in the forward portion of the trunk and verifying the control effectiveness and system dynamics with forward speed braking tests on a fully equipped aircraft.

7. REFERENCE MATERIAL

LIST OF REFERENCES

1. "Recovery of Unmanned Aircraft, ASD Technology Needs", TN-ASD-4-72-526, 19 Dec 1972.
2. Digges, K. H. and Vaughan, J. C., "Drone Launch and Recovery Using Air Cushion Systems", AFFDL/FEM Briefing Brochure, April 1973.
3. Ryken, J. M., "A Study of an Air Cushion Landing System for Recovery of Unmanned Aircraft", AFFDL-TR-72-87, July 1972. (AD 758789)
4. Sinfield, L. S., "RPV ACLS Applications Study", AFSC Contract F33615-73-C-4140, Teledyne Ryan Aeronautical TR ASD/XR 73-22, 15 Dec 73. Secret.
5. Gardner, L. H. and Milns, P., "Air Cushion Landing System Applications Study", AFSC Contract F33615-73-C-4169, Boeing TR ASD/XR 73-21, Jan 74. Secret.
6. Vaughan, J. C., "The Jindivik Program to Develop Air Cushion Technology for Drones - A progress report". Paper presented at the 16th meeting of TTCP Sub-Group H-TP-1, Targets and Drones, 24-25 Sep 73, U.S. Army Missile Command, Huntsville, Ala.
7. McCudden, H. B., et al, "Conceptual Design of an Air Cushion Landing System for an Unmanned Aircraft", AFFDL-TR-72-155, 3 January 1973.
8. Moten, J. M., "Cost Effectiveness Study of the Jindivik MK.303A Target", prepared for CINC PAC FLT, 4 Aug 1967.
9. Ryken, J. M., "Design of an Air Cushion Recovery System for the Jindivik Drone Aircraft", AFFDL-TR-74-38, March 1974.
10. Rogers, J. R., "Two-Dimensional Air Cushion Landing System Peripheral Jet Configuration Study", AFFDL-TR-73-5, November 1973.
11. Carreras, E. M., "Static Performance of a Cushion Fed Air Cushion Landing System", AFIT Thesis, GAW/AE/74-1, Dec 73 (AFFDL-TM-74-56-FEM).
12. Vaughan, J. C., et al, "Static Drop Tests of a Quarter Scale Model of the CC-115 Aircraft Equipped with an Air Cushion Landing System", AFFDL-TM-72-01-FEM, Sep 1972.
13. Rodrigues, A., "Drop and Static Tests on a Tenth Scale Model of an Air Cushion Landing System (ACLS)", AFFDL-TR-73-46, Sep 1973.
14. Parker, P. M., "Landing Simulation of a 1/10 Scale Jindivik Drone Equipped with an Air Cushion Landing System", AFIT Thesis, GAM/AE/73A-15, Nov 72 (AFFDL-TM-74-58-FEM).
15. Digges, K. H., "Theory of an Air Cushion Landing System for Aircraft", AFFDL-TR-71-50, Jun 1971.
16. Vaughan, J. C., "Performance of Jet Ejectors", ASD/XR 72-5, 15 Feb 1972. (AD 759671)
17. Kundstadt, E., "Study of Reverse Flow Characteristics of a Tip Fan and an Ejector", AFFDL-TR-73-73, Sep 1973.
18. Vaughan, J. C., "The Jindivik Drone Program to Demonstrate Air Cushion Launch and Recovery", paper presented at First Conference on ACLS, Miami Beach, Florida, December 12-14, 1972, Proceedings published by UTSI, March 1973.
19. Bauer, F. C., "Air Cushion Landing System; Drop Dynamics Theory (Mechanical)", AFIT Thesis, GAM/AE/73A-1, Dec 73. (AFFDL-TM-74-57-FEM)
20. Vaughan, J. C. and Steiger, J. T., "Vertical Energy Absorption Analysis of an Air Cushion Landing System", AFFDL-TM-72-03-FEM, August 1972.
21. Stuart, J.L., "An Experimentally Based Prediction of the Static Performance in the Vertical Direction of an Air-Cushion Landing System". AFFDL-TM-74-55-FEM, March 74.

APPENDIX A

TEST CHECKLIST

CHECKLIST FOR STATIC TESTS

1. Turn on INSTRUMENTATION & VISICORDERS (Allow 20 Min Warm-up)
 2. Close TRUNK & CUSHION BALL VALVES.
 3. Check AIR CART SUPPLY PRESSURE. If below 2000 PSIG, RECHARGE. Don't run BELOW 1000 PSIG.
 4. Check all INSTRUMENTATION, LEVEL AIRCRAFT, CALIBRATE, CLOSE CALIBRATION LINES & ZIPPERS.
 5. Close DOORS TO HIGH BAY. Post with signs "DO NOT ENTER, TEST UNDERWAY".
 6. Check CABLE SUPPORT. Check SAFETY MECHANISM & DROP PIN. (RED FLAG DOWN)
 7. Everyone put on EAR PROTECTION (if required)
 8. Open MAIN BALL VALVE SLOWLY. 500 PSIG RELIEF VALVE MAY POP. Adjust REDUCER VALVE TO GIVE 375 ± 50 PSIG ON TRUNK & CUSHION SUPPLY LINE PRESSURE GAGES.
 9. Open N₂ BOTTLE VALVE. SET CONTROL PRESSURE TO 200 PSIG.
 10. Remove JACKS & LOWER AIRCRAFT TO WING TIP HEIGHT = _____ IN.
Level AIRCRAFT. RECALIBRATE HEIGHTS. RUN VISICORDERS.
 11. Fill-in DATA SHEET & TEST LOG BOOK.
 - 12A. Set TRUNK LINE PRESSURE TO _____ PSIG using GROVE LOADER.
 - 12B. Set CUSHION LINE PRESSURE TO _____ PSIG using GROVE LOADER.
 13. Write RUN NUMBER on VISICORDER, PAPERS, RECORD TAPE COUNTER.
 14. TURN ON RECORDER.
 15. Turn on VISICORDERS AT 0.4 IPS.
 16. Open TRUNK & CUSHION BALL VALVES SLOWLY (START RUN TIME).
 - 17A. MEASURE HEIGHTS AND RECORD DATA (Need 20 sec. RUN TIME for complete SCAN VALVE).
 - 17B. ADJUST CONDITIONS (if req'd) HEAVE, PITCH, ROLL, GIVE PRESSURE, ETC.
 18. CLOSE TRUNK & CUSHION BALL VALVES, SLOWLY to prevent chain loads (Keep Air Cart Pressure \geq 1000 PSIG).
 19. Turn Off VISICORDER.
 20. Turn off RECORDER. Record tape counter.
 21. Record & Reduce Data & Prepare for next test. Record Comments.
- AT END OF TESTS FOR DAY:
22. Close MAIN BALL VALVE. UNPOST SIGNS ON DOORS.
 23. Close NITROGEN BOTTLE VALVE and GROVE LOADERS, BLEED CONTROL LINE.
 24. Put AIRCRAFT ON JACKS.

CHECKLIST FOR DROP TESTS

- 1-13. Same as for static tests.
14. Check to insure DC POWER, "HOT" SWITCH, and RELEASE SWITCH ARE ALL OFF.
15. Remove SAFETY LATCH LOCK PIN. PULL SAFETY MECHANISM OUT (red flag out). Insert safety latch lock pin.
16. Turn on RECORDER.
17. Turn on VISICORDERS at 0.4 ips. Let run for 10 seconds.
18. Open TRUNK BALL VALVE slowly. Allow P_1 to reach equilibrium.
19. Turn DC Power Supply Switch on, turn "Hot Switch" on. Insure that red light is on and aircraft is ready to drop.
20. Turn off VISICORDER. Set to 10 ips paper speed.
21. Open CUSHION BALL VALVE.
- 22A. Turn on VISICORDER at 10 ips.
- 22B. Release Aircraft (let oscillations dampen out).
23. Turn Off VISICORDER.
24. Close TRUNK BALL VALVES SLOWLY TO PREVENT SMASHING AIRCRAFT TO GROUND.
25. Turn off RECORDER. Record tape counter.
26. Turn off "HOT SWITCH"
27. Lower hoist. Attach cable to aircraft. Remove latch pin, and attach safety latch mechanism (red flag down). Reinsert latch pin. Raise Aircraft off floor.
28. Record & Reduce Data & Prepare for next test. Record comments, carefully. Note maximum g's.

AT END OF TESTS FOR DAY:

29. Close MAIN BALL VALVE. UNPOST SIGNS ON DOORS.
30. Close NITROGEN BOTTLE VALVE and GROVE LOADERS, BLEED CONTROL LINE.
31. Put AIRCRAFT ON JACKS.

APPENDIX B

SAMPLE CALCULATION FOR DAMPING DATA

(PITCH TEST NO. 59)

| Counter i | Measured Data | | Calculated Data | | |
|--------------|---------------|-------------------|-------------------|-----------------------|-----------------------|
| | Time (sec) | h_n (inches) | h_i (inches) | h_{i+2} (inches) | $\frac{h_i}{h_{i+2}}$ |
| 1 | 0.000 | 26.1 | - 7.4 | - 5.4 | 1.370 |
| 2 | 0.625 | 41.0 | +7.5 | +5.3 | 1.415 |
| 3 | 1.000 | 28.1 | - 5.4 | - 4.3 | 1.256 |
| 4 | 1.525 | 38.8 | +5.3 | +4.0 | 1.325 |
| 5 | 1.975 | 29.2 | - 4.3 | - 3.0 | 1.433 |
| 6 | 2.475 | 37.5 | +4.0 | +3.1 | 1.290 |
| 7 | 2.975 | 30.5 | - 3.0 | - 2.2 | 1.364 |
| 8 | 3.425 | 36.6 | +3.1 | +2.0 | 1.550 |
| 9 | 3.925 | 31.3 | - 2.2 | - 1.5 | 1.467 |
| 10 | 4.300 | 35.5 | +2.0 | +2.0 | 1.000 |
| 11 | 4.875 | 32.0 | - 1.5 | - 1.2 | 1.250 |
| 12 | 5.275 | 35.5 | +2.0 | | |
| 13 | 5.725 | 32.3 | - 1.2 | | |

natural damped frequency, $f_d = \frac{6 \text{ cycles}}{5.725 \text{ sec}} = 1.048 \text{ ips.}$

$\sum_{i=1}^{12} h_{ni} = 402.1$ need to use an even number of points to get the correct average.

average $h_n = 402.1/12 = 33.5$

$h_i = h_{ni} - \text{average } h_n$

$h_{i+2} = h_{ni+2} - \text{average } h_n$

$\sum_{i=1}^{12} (h_i/h_{i+2}) = 14.72$

average $(h_i/h_{i+2}) = 1.338$

$d = \ln(\text{average } (h_i/h_{i+2})) = 0.291$

damping ratio, $\zeta_{\Theta} = d / \sqrt{4\pi^2 + \phi^2} = 0.04619$

dynamic pitch stiffness, $k_{\Theta} = \frac{0.689 f_d^2 I_{yy}}{(1 - \zeta^2) g_c} = 1370 \text{ ft lb/deg.}$

pitch damper coefficient, $C_{\Theta} = \zeta k_{\Theta} \sqrt{1 - \zeta^2} / \pi f_d = 19 \text{ ft lb sec/deg.}$

LIST OF SYMBOLS AND ABBREVIATIONS

- A** = area (sq in). Used for: A_b (brake contact), A_c (cushion footprint), A_n (total trunk nozzle exit area), A_t (trunk footprint), and A_v (pressure relief valve vent).
- ACLS** = air cushion landing system
- ACRS** = air cushion recovery system
- ACTS** = air cushion takeoff system
- C** = damper coefficient. Used for report the dynamic damping characteristics for heave (C_h , lb_f sec/in), pitch (C_Θ ft lb_f sec/deg) and roll (C_ϕ ft lb_f sec/deg).
- C_d** = discharge coefficient of an orifice.
- CF** = location of the center of force, W_t exerted upward by the trunk footprint.
- CG** = location of the aircraft's center of gravity.
- CP** = location of the center of pressure, P_c , for the cushion area.
- F** = jet thrust (F_j) or forward pulling force, F_{pull} (lb_f).
- FS** = fuselage station (inches), measured from Jindivik nose.
- f_φ** = damped natural frequency (cps).
- g** = acceleration (dimensionless "g's", normalized by g_c). Three vertical accelerometers on the aircraft measured: g_{cg} (center of gravity), g_n (nose), and g_w (starboard wing tip). g is also a dimensionless force term, normalized by the aircraft weight.
- g_c** = constant of proportionality in Newton's second law (32.174 ft lb_m/lb_f sec²).
- h** = height (in). Three linear transducers on the aircraft measured the height above the floor for: h_{fus} (bottom of center fuselage, slightly offset from CG), h_n (nose), and h_w (starboard wing tip). h_{fus} was then connected to give h_{cg} , the fuselage clearance directly below the CG.
- I** = moment of inertia (slug ft²). Three aircraft inertias are: I_{xx} (fuselage axis), I_{yy} (wing axis), and I_{zz} (vertical axis). Each axis passes through the aircraft CG.
- IGE** = in ground effect. Condition where the air cushion system is close enough to the ground that the pressures or flow rates are effected.
- k** = Spring coefficient. Used to report the static and dynamic characteristics for heave (k_h , lb_f/in), pitch (k_Θ ft lb_f/deg), and roll (k_ϕ ft lb_f/deg).
- L** = aerodynamic lift or lift hook load (lb_f).

- l = length of a moment arm (in).
- \dot{m} = flow rate (lb_m/sec). Used for the weight flow rate: entering the cushion (\dot{m}_c), leaving the trunk through the tread nozzles (\dot{m}_t), or the sum of the two flows (\dot{m}_{ct}). Also used for the primary (\dot{m}_p) or secondary (\dot{m}_s) flow rates for an ejector or tip turbine fan.
- OGE = out of ground effect. Condition where the air cushion system is far enough above the ground that the pressures and flow rates are not influenced.
- P = pressure (lb_f/in^2). Used for gage pressures for: cushion (P_c) and trunk (P_t). Also used for ambient absolute pressure (P_a).
- t = time (sec).
- V = volume (ft^3).
- v = speed (ft/sec).
- W = weight (lb_m) or force (lb_f). Used for aircraft weight (W_a), cushion force (W_c), trunk force (W_t), and combined cushion and trunk force (W_{ct}).
- x, y, z = distance parallel to x, y, z axis; respectively (in). Forward, starboard, and down from the CG are positive directions.
- ζ (zeta) = damping ratio. Used for heave (ζ_h), pitch (ζ_Θ), and roll (ζ_ϕ).
- Θ, ϕ, Ψ = aircraft pitch, roll, and yaw angle, respectively (deg). Angles measured about $y, x,$ and z axis; respectively. Right-hand coordinates.
- μ = coefficient of friction. A ratio of the horizontal friction drag divided by the vertical weight on the material (μ_m) or on the ACRS trunk (μ_t), or divided by the aircraft weight (μ_a).
- ρ = density (lb_m/ft^3).

SUBSCRIPTS

a = aircraft
a = ambient conditions
b = brakes
c = cushion
cg = center of gravity
cp = center of pressure
ct = combined cushion and trunk
h = heave
j = jet
m = material
n = nose
n = trunk nozzles
p = primary air
pull = pulling force
s = secondary air
sink = aircraft sink speed condition at impact
t = trunk
tan = trunk ground tangent line
v = vent valve
w = wing
 Θ = pitch
 ϕ = roll
 Ψ = yaw